Redesign of Grand Rapids' Field Pole Lifting Device

Final Design Report

Manitoba Hydro

Group 13

Submitted to: Jared Bunkowsky

Advisor: William C DeGagne

Date: November 30, 2015

Tyler Shaw _____

Jack Wiebe _____

Anton Sigurdson _____

Travis Zygarlicki _____

Table of Contents

List of Figures

List of Tables

Executive Summary

The purpose of this project is to analyze the existing field pole lifting device at Manitoba Hydro's Grand Rapids Generating Station, as well as design a solution to improve the safety and ease of use of the bottom clamp of the device. Our final design addresses the safety risks, through FEMA analysis, to provide a safer design, while mitigating the risk of the design. This report delivers detailed drawings, hand calculations of our design, CAD models of the assembly and FEA modeling validating that the design meets all constraints and limitations.

The final design meets all category five needs and metrics, provided by the client, including a total weight of 35 lbs, a total of two workers for installation and operation, and all sizing constraints. The design also decreases the total set up time and installation time because of its decreased weight.

The design meets the minimum 1/3 yield criterion with maximum stresses of 22633 psi and 21408 psi for the tusk and distributed loading, respectively. The maximum crack lengths the design can experience in the stiffeners and tusks locations are 0.788 in and 0.315 in, respectively. These crack lengths can easily be detected before they reach their critical lengths and cause failure. The design can also handle an infinite number of load cycles.

The design is to be made out of with six different 70WT steel waterjet parts and welded into one assembly to ensure maximum simplicity, accuracy and precision, while minimizing the overall cost of the device. The design's total cost is estimated to be $3280.

1. Introduction

The overall objective of this project is to analyze the current field pole lifting device at Manitoba Hydro's Grand Rapids Generating Station and to design a new bottom clamp that is safer and easier to use than the current design. Field poles weigh 2715 lbs each and are situated within the rotor of a hydroelectric turbine. The lifting device currently in use contains both a top and bottom clamp, which are connected by steel rods. The overhead crane in the dam's powerhouse lifts this assembly. The bottom clamp must be lifted overhead and connected to the two rods with an extended bolt. This operation is difficult, time-consuming and inherently dangerous.

To meet the objectives, the problem is defined by quantifiable target specifications that meet the client's needs. The needs of the client are developed and prioritized based on the lifting device's incident history, operational procedure, and the client's requests. Target specifications quantifying these needs with ideal and marginal values, and track if our design is meeting the client's needs. Constraints and limitations developed from standards, codes and client information further refine the set target specifications values.

To test the viability of our design, hand calculations, finite element analysis (FEA), fatigue analysis, brittle fracture analysis and failure mode and effects analysis (FMEA) are performed to ensure the safety and reliability of our design. Final specifications are compared to the original target specifications. We are able to verify that we have met all of the client's needs, while maintaining safety and reliability, using this method.

1.1. Background

Manitoba Hydro's Grand Rapids Station uses hydraulic turbine generators to produce electricity by using a spinning magnet called a rotor. The rotor's magnetic field causes magnetic induction on coiled wires in the stator to produce electricity. Between the rotor and stator there are field poles, which are used to excite the generator and amplify the rotor's magnetic field so the generator is able to produce power. Figure 1 shows an overall cross section of a hydroelectric dam and the location of the stator and rotor in relation to the turbine. The field poles are located in between the rotor and stator, as shown in Figure 2. The poles weigh approximately 2715 lbs and there are 30 poles in each generator.

One field pole from each rotor is removed yearly, which allows the crew to perform efficiency tests of the generator. Each generator at Grand Rapids also experiences full maintenance every 20 years. To remove the field poles, a standard lifting device is used, as in Figure 3. The lifting device will be used at least 4 times per year, and every 5 years it will be used for a unit overhaul equating to 60 uses (30 poles removed and 30 poles installed).

Figure 1: Cross sectional view of hydroelectric dam with an emphasis on the rotor and stator. [1]

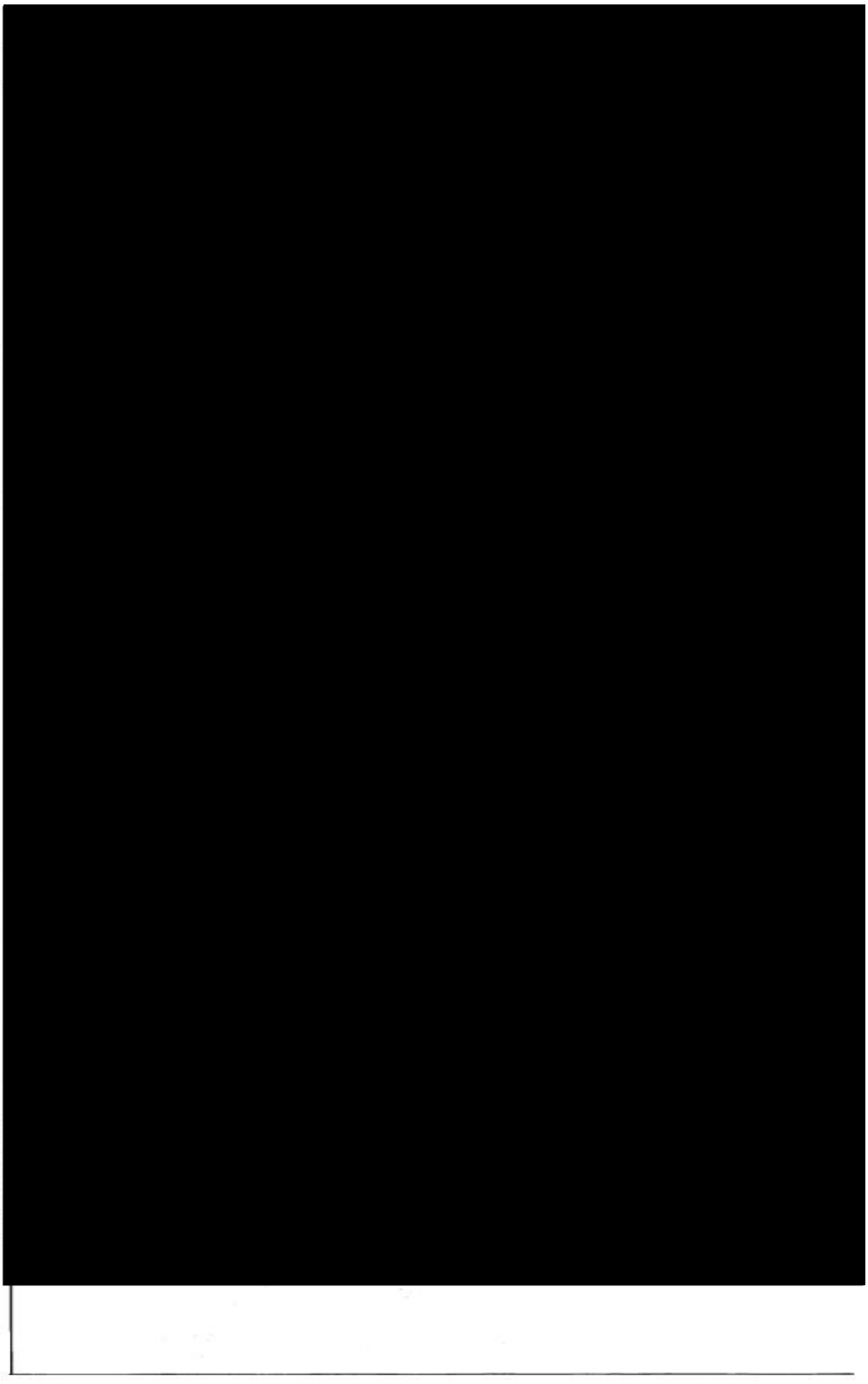

Figure 2: Cross sectional view of the generator at Grand Rapids station. The rotor and stator are directly above the turbine shaft. In between the rotor and stator is the field pole location. This section is referenced in Figure 1 [1].

To remove the poles, wedges that align the poles on the rotor must first be removed. A crew of three men then use a lifting device that attaches to the overhead crane at the generating station. The device consists of an overhead clamp, a bottom clamp, and two steel rods that connect the clamps, as shown in Figure 3.

Figure 3: The component drawing of the lifting assembly (left) and the assembly including the field pole (right) [2].

As shown in Figure 4, the crew slots the rods in between the poles, being careful that they do not strike the rods against the pole or rotor. Once the rods are through the gap, the crew members attach the bottom clamp under the rotor on a platform deck. The pole is then lifted with the overhead crane and set on a piece of plywood for transportation.

Figure 4: The crane and lifting device removing a field pole from the rotor [3].

There have been safety incidents with the lifting device because of its maneuverability and the weight of the individual pieces during operation. Currently, the bottom piece weighs approximately 70 lbs. The tight quarters and poor access to the bottom of the field pole do not allow safe installation of the bottom clamp, as shown in Figure 5. Due to these factors, the operating procedure calls for a three member crew to install the bottom clamp. Manitoba Hydro needs the device to be more accessible and easier to install during only the installation of the bottom clamp.

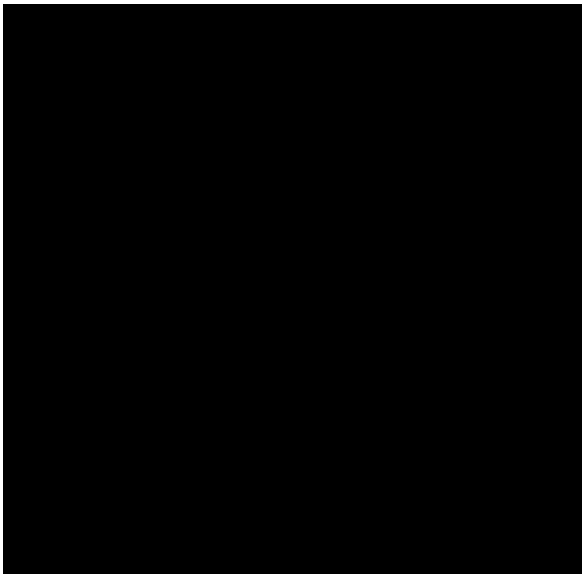

Figure 5: Three man crew setting up lifting device from under the rotor [3].

1.2. Purpose Statement and Objectives

The purpose of this project is to analyze the existing field pole lifting device at Grand Rapids Generating Station and design an innovative way to improve the ease of use and safe handling of the bottom clamp during transportation and operation. The new lifting device must also meet all of Manitoba Hydro's best practices and standards.

The project objectives are as follows:

1. Generate need statements that define what the customer requires for the new design
2. Create target specifications that define customer needs in quantifiable terms
3. Create basic concept generation based on meeting the ideal values generated from the target specifications
4. Develop a specific concept established from weighted decision matrices
5. Compute basic hand calculations to justify FEA model(s) of the selected concept
6. Create CAD model(s) that accurately represent the design, assembly, and operation of the selected concept
7. Create FEA model(s) that accurately represent the loading conditions of the CAD model designed of the selected concept
8. Compare the final design and the target specifications, to ensure the design meets set target specifications and the client's needs

1.3. Target Specifications

The first step in achieving these goals is identifying the target specifications for the lifting device. This section includes a list of needs based on our client meeting, the relative importance of each need, and client approval of the list. A list of metrics is developed from those needs. In order to set clear goals for the project, each metric is assigned a marginal and ideal value. Since the design will only be competing with the existing device, the properties of the existing device are used as a benchmark. However, these metrics can be applied to any other future design in order to directly compare proposals.

1.3.1. Needs Statement

The following table shows the device needs based on the meeting with our client. The main concerns are the bottom clamp's weight and its ease of use. The customer needs are ranked in order of relative importance, with 5 indicating the highest importance and 1 indicating the lowest.

TABLE I: STATEMENT OF NEEDS

#	Need	Importance
1	The lifting device is light weight.	5
2	The lifting device is simple to setup and use.	5
3	The lifting device is strong enough to support the weight of the poles.	5
4	The lifting device is safe to use.	5
5	The lifting device is reusable.	4
6	The lifting device is easily maintained	3
7	The lifting device does not damage the surroundings during use.	3
8	The lifting device is maneuverable.	2
9	The lifting device is low cost.	1
10	The lifting device is aesthetically pleasing.	1
11	The lifting device is adaptable.	1

1.3.2. Specification Table

After these priorities were confirmed by the client, a list of metrics and units is created and importance values are assigned, with 5 being most important and 1 being least important. Metrics allow us to

evaluate designs based on measurable criteria. Each metric corresponds to one or more needs. This relationship is displayed graphically in the house of quality, presented in section 4.3. To create the specification table, marginal and ideal values are assigned to each metric.

TABLE II: SPECIFICATION TABLE INCLUDING UNITS, THEIR RELATIVE IMPORTANCE, MARGINAL BENCHMARK VALUES AND IDEAL TARGET SPECIFICATIONS

Metric #	Need #	Metric	Units	Imp.	Marginal Value	Ideal Value
1	1, 7, 8, 9	Total weight	lbs	5	70	35
2	2, 7, 11	Number of parts in design	# of parts	2	6	4
3	2, 4, 8	Number of workers to install	# of people	5	3	2
4	4, 5	Cycles to failure	Cycles	4	500	unlimited
5	3, 4	Strength under loading	Factor of safety	3	3	3
6	2, 7, 8	Device setup time	Minutes	5	10	2-3
7	9	Unit manufacture cost	CAD	1	5000	2000
8	10	Aesthetics	Subjective	1	1	2
9	1, 7, 8, 11	Minimum width poles	in	5	5	1/2
10	11	Field poles sizes	# of applicable stations	1	1	>1
11	2, 7, 6	Assembly/disassembly time	Minutes	3	5	4
12	1, 7, 8, 11	Minimum width of top and bottom clamps	in	5	7.5	5
13	4, 6	Corrosion resistance	MPY (mils penetration per year)	3	0.2	0.1
14	1, 3, 8	Material density	$\mathrm{kg/m^3}$	4	7750	<7750

Since there are no other designs with which to compare, the marginal values are based on the existing lifting device. Strength and fatigue requirements are from a Manitoba Hydro stress analysis standard

that outlines FEA and design requirements and explicitly mentions a lifting device [4]. The material density refers to that of AISI 1025 steel, the material of the current device.

1.3.3. Constraints and Limitations

To simplify the design of the lifting device, a number of constraints and limitations are applicable based on the background information provided by the client. These constraints and limitations are based on a number of factors, including the timeline that has been set for this project, physical constraints that must be made in the design, specific requirements that the client has requested, and standards required by the both client and the Manitoba Government.

The constraints for this project are as follows:

1. The lower clamp must be re-engineered from the original model as per the client's request
2. The design must have a 1/3 yield criterion, based on Manitoba Hydro's internal stress analysis standard [4]
3. FEA, CAD model, operation guidelines and engineering drawings must be designed according to Manitoba Hydro's best practices
4. The CAD model must be made in AutoDesk Inventor, and the FEA model must be made in ANSYS Workbench
5. The design must meet all of Manitoba Hydro's internal standards as well as Manitoba's Workplace Safety and Health Regulation, M.R. 217, specifically pertaining to applicable portions of ASME BTH-1, Below-the-Hook Lifting Device Design [5]
6. The bottom clamp must be rounded on the outside edge, as per the clients request, to help with loading the field poles
7. Lifting rods must be at maximum 4 in in diameter to allow the device to fit in the air gaps between the field poles (field measurement provided by the client)
8. The bottom clamp must not extend more than 21 3/8 in beyond the sides of the field pole to allow the field pole to be removed [3]
9. The distance between the top and bottom clamps must be at least 74 in to fit the field pole in the lifting device [3]
10. The 3/8 in air gap between the field pole and stator must be maintained during the lifting device's operation
11. The cost of the lifting device should be approximately $5000 to manufacture, including labor and material costs, as specified by the client

12. The design must account for both vertical lifting and laying down, using rounded edges, of the field poles
13. By Manitoba's Workplace Safety and Health Regulation, M.R. 217 all below the hook lifting devices must be painted yellow

The design constraints are all as per the client's requests, as per the physical limitations of removing the electrical poles or as per the relevant Manitoba Standards or Client Standards. All constraints pertaining to measurements can be found on the drawings specified in Appendix 8. It must be noted that the 1/3 yield criterion, as well as the minimum dimensions, directly impact the total weight and the strength of the device.

The limitations for this project are as follows:

1. All design measurements are based on old design drawings provided by the client
2. All functionality of the device is based on pictures provided by the client
3. The project timeline is limited by the length of the university's fall semester

Since the design will not be prototyped by the conclusion of this project, the design's structural integrity will only be tested by FEA. The operation and assembly times will not be tested before the end of this project.

2. Analysis of Existing Device

The existing design was modelled in AutoDesk Inventor CAD software. This model creates a benchmark for improvement as well as a better understanding of the constraints and functionality of the lifting device as a whole. The following figure illustrates the entire assembly with inset views of the top clamp, the top assembly and the bottom clamp.

Figure 6: Full assembly of existing lifting device. Inset, clockwise from left: The top clamp; the top clamp assembly with the lifting hook attached by pin; and the bottom clamp

3. Design and Safety Standards

As a crown corporation, Manitoba Hydro follows Manitoban and Canadian safety standards, in particular the Workplace Health and Safety Act (WHS), CSA standards, and their own internal standards. Both external standards reference the ASME B30 standard, which applies to cranes and other related equipment.

The subsection of the B30 standard applicable to this device is B30-20, Below-The-Hook Lifting Devices. Within this volume we are concerned with chapter 20-1, Structural and Mechanical Lifting Devices. Our design is classified as a supporting lifter. This standard, however, deals primarily with maintenance, testing, and use. These procedures fall outside of the scope of this report, which is concerned with design alone, but it is good background knowledge.

ASME also has a standard for below-the-hook lifting device design: BTH-1. This standard applies to this report and is used as a guideline for the final design. This standard includes design criteria for structural members under certain loading conditions as well as design guidelines for components such as bolts and welds. It also covers structural analysis such as fatigue and basic FEA procedures. Our final design exceeds the BTH-1 requirements.

In addition to overarching standards, Manitoba Hydro has some internal standards. The most applicable to us is the Mechanical Stress Analysis Standard, which gives a guideline for stress, fatigue, fastener, and weld analysis. It also covers FEA and even has a section on lifting devices. The information within agrees with BTH-1 for the most part but has information specific to Manitoba Hydro.

Weld dimensions are discussed in both BTH-1 and the internal standard in terms of weld thickness. Another Hydro document provides a guideline for using FEA to analyze weld performance [6]. The ASME and Hydro codes both reference CSA W59-03, which gives weld thicknesses based on member thicknesses.

4. Final Design

The final specifications for the design have been determined through a rigorous design process. While the overall geometry of the part is the same as the existing device, the dimensions have been optimized to distribute stress more efficiently. The material has been selected to keep the stress below the allowable limit, and the device loading scenarios have been identified and analysed with hand calculations.

4.1. Design Features

The plate, stiffener and tusk dimensions were all changed to better carry stress through the part. Figure 7 and Figure 8 show the parts that were optimized to achieve a light and reliable design. Not shown in the figures is the rubber pad that attaches to the plate. This pad serves to protect the field pole from the clamp's hard surface. For the final dimensions, see the detailed drawings in Appendix 8.

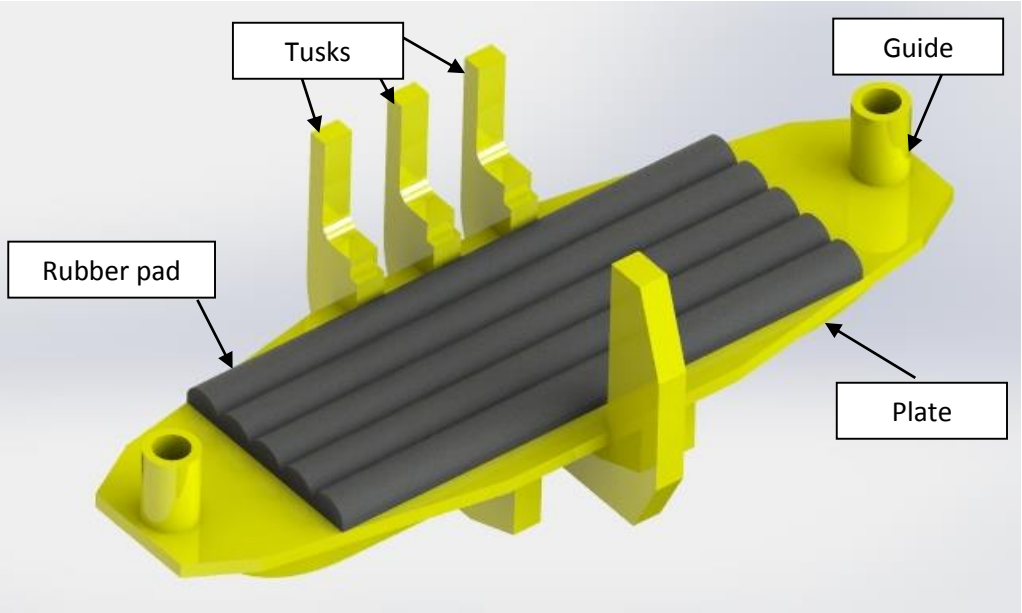

Figure 7: Final design of the bottom clamp, isometric view.

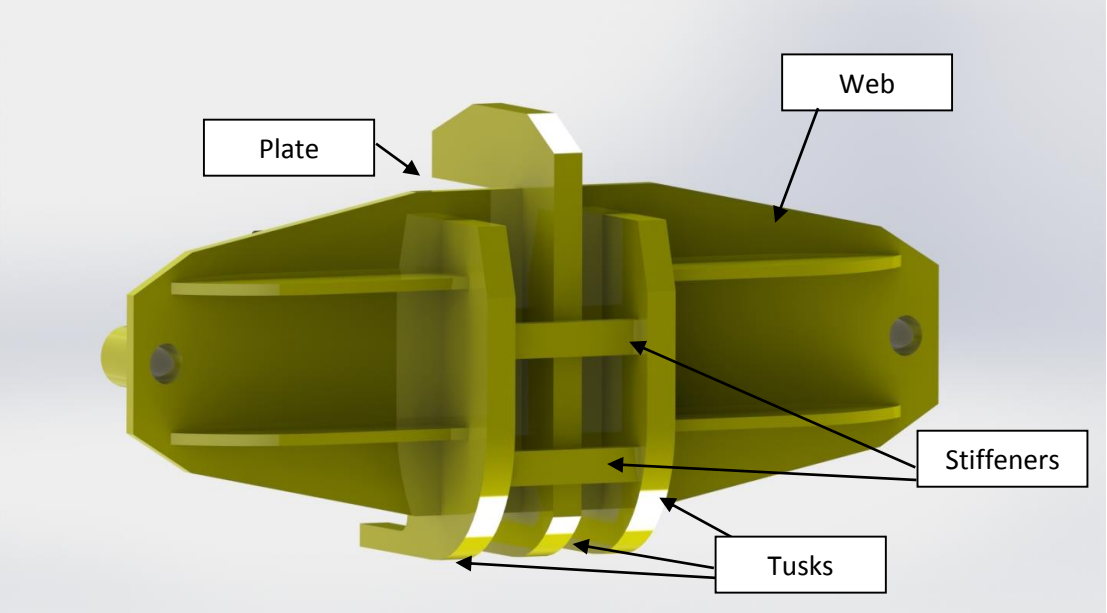

Figure 8: Final design of the bottom clamp, bottom view.

4.2. Dimension Optimization

Based on the FEA performed on the selected final design, it was clear that stress was not as evenly distributed as we would like. The numerical results indicate areas where material can be removed. These areas include the corners of the plate, the stiffeners, and the thicknesses of the webs and tusks. The member thicknesses need to stay constant throughout the member and at a stock thickness to maintain ease of manufacturability.

The two important loading cases to optimize for are the distributive load case, where the entire part is in bending, and the concentrated fork case, where the weight is carried by the tusks. The geometries are too complicated to solve and optimize analytically, so the insights and the chosen dimensions are solved for numerically using a simplified analysis. The final dimensions will be validated with a rigorous numerical analysis.

4.2.1. Plate

The thickness of the plate is appropriate near the rod holes but the other areas of the plate see little stress. The thickness of the plate cannot be reduced, in order to maintain uniform thickness and therefore manufacturability. The corners of the plate, though, are unnecessary, so the new plate design has a football shape. The exact shape was dictated by the desire to keep the same plate width at the tusks and to avoid the webs, which are important to help reduce the stress near the rod holes.

4.2.2. Stiffeners

The FEA showed that the stress was low in the stiffeners, and the analytical hand calculations prescribe very small stiffeners. However, with the removed material weakening the part, the clamp bends more when loaded. This results in higher stress in the stiffeners, which are pulled apart by the outside tusks while being pushed down by the middle tusk. This effect was not included in the analytical calculation, and results in significantly higher stresses than analytically predicted. Even with this added effect, the stresses remain relatively low, so a stiffener thickness of 3/8" is used. In this loading scenario, the stiffeners would most likely fail at the welds, where the moment is highest, or if a crack is present.

4.2.3. Webs

Both the hand calculations and the FEA show that the webs are thicker than necessary. To save weight, the thickness is reduced to 1/4". The depth to thickness ratio is 6, which is lower than the maximum for members in bending, so the webs will not buckle. The webs keep their original length and space between each other so they remain effective near the rod holes.

4.2.4. Tusks

The FEA results show that the tusks of concept design 2 are inadequate. However, the tusk dimensions of the multi-component concept worked very well, so the optimized design uses its ¾" thickness. As well, the length of the tusk below the plate was reduced. To make the assembly easier to tip over when the field pole is laid down, the chamfer on the bottom of the tusks is replaced by a quarter circle. This feature was specifically requested by the client.

4.3. Material Selection for Final Design

The material selection process was performed for a previous report and is included in Appendix 1. The process consisted of research of material properties followed by a decision matrix to evaluate them. The result was to use AISI 4130 or AISI 4340 steel. However, after consulting Manitoba Hydro, these materials were deemed too difficult to weld, and the company suggested using a grade of steel from the CSA G40.21 standard.

The steels in this standard are characterized by a number, indicating its yield strength in ksi, and one or two letters, indicating its particular properties.

TABLE III describes the types of steel based on the lettering system, while TABLE IV shows the availability of each steel grade and type.

TABLE III: AVAILABLE STEEL TYPES PER CSA G40.21 [7]

G40.21 Types	Description
Type W	Weldable Steel
Type WT	Weldable Notch Tough Steel (low temperature)
Type R	Atmospheric Corrosion Resistant Steel
Type A	Atmospheric Corrosion Resistant Weldable Steel
Type AT	Atmospheric Corrosion Resistant Weldable Notch Tough Steel
Type Q	Quenched and Tempered Low Alloy Steel Plate Steel
Type QT	Quenched and Tempered Low Alloy Notch Tough Steel Plate

TABLE IV: STEEL GRADES, TYPES AND STRENGTHS PER CSA G40.21 [7]

	Yield Strength							
Type	**38**	**44**	**50**	**55**	**60**	**70**	**80**	**100**
W	38W	44W	50W	55W	60W	70W	80W	-
WT	38WT	44WT	50WT	55WT	60WT	70WT	80WT	-
R			50R					
A			50A		60A	70A	80A	
AT			50AT		60AT	70AT	80AT	
Q								100Q
QT								100QT

This project calls for a material with good weld characteristics and good impact properties. A similar steel to the ones previously recommended is 70WT. Its density and strength are similar to 4130 and 4340 but it has much better weld and impact properties, so the final design uses 70WT steel.

The current upper and lower clamps of the field pole lifting device also have a rubber pad located within the field pole's lifting footprint. This pad ensures the field pole is fully in contact with each clamp and that the field pole will not slide on either of the clamps. The current device uses a pad which is secured to each clamp with tape, as shown in Figure 9. At the client's request we have selected a skirtboard rubber with a durometer hardness of 65-75. The rubber is designed for abrasion resistant applications and is easily bonded to steel materials [8]. The rubber is to be bonded to the top and bottom clamps

with a Neoprene High Performance Rubber & Gasket Adhesive 1300L, designed for high stress applications [9].

Figure 9: Current lower clamp showing current rubber pad and mounting [3].

4.4. Loading Scenarios

To ensure the bottom clamp meets the strength constraint, hand calculations and FEA modelling must be completed. Hand calculations are necessary to ensure that FEA solutions provide reasonable results. The three loading scenarios that the bottom clamp will experience are:

1. Vertical distributed loading of the plate, experienced during field pole removal
2. Vertical loading of the rounded edges, experienced while the pole is being laid down
3. Bending loading of the tusks, experienced while the pole is being laid down

These scenarios dictate the loading and boundary conditions of both the hand calculations and the FEA.

4.4.1. Distributed Loading

The simplest loading the lifting device can experience under vertical loading is a perfect distribution of the weight of the pole across the bottom clamp.

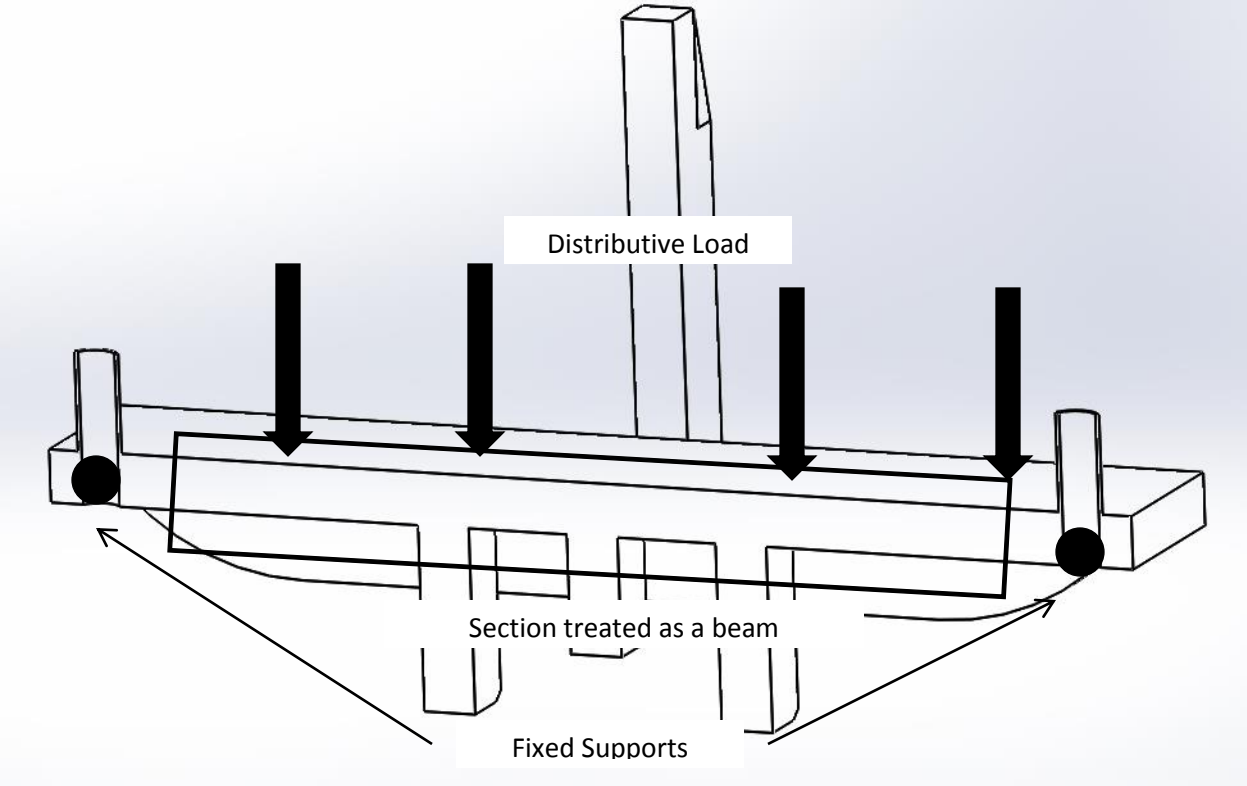

Figure 10: Cross section of view of the bottom clamp and the simplified loading scenario.

To simulate this loading, the clamp is modeled as a fixed beam with a perfectly distributed load. This is an accurate representation of the loading happening in the middle of the device because the poles are symmetric and always supported near the middle of the device. The ends of the beam are considered fixed because the screws that support them resist both angle deformation and deflection.

4.4.2. Compression Loading

When the poles are set down, the full weight of the pole runs through the edges of the tusks to the ground, as shown in Figure 11 below. The stresses in the tusks are much higher than in the middle of the clamp.

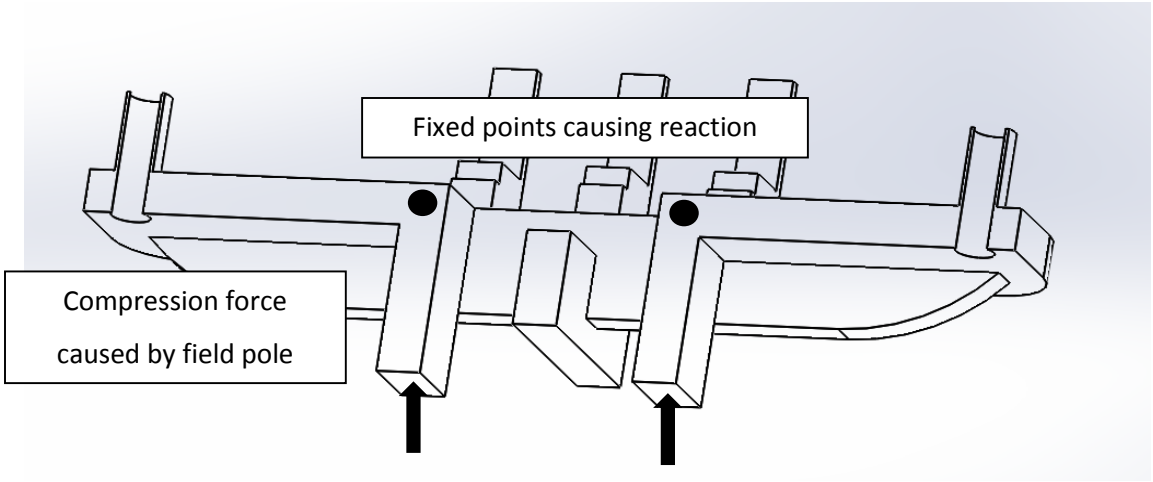

Figure 11: Simplified loading of the bottom clamp during storage of the field pole.

To simplify this loading for hand calculations, the load is considered to be a compressive load that is equally divided among the tusks. The webs and stiffeners prevent the edges from buckling.

4.4.3. Tusk Loading

Analyzing the stress concentration of the tusks on the bottom clamp during pole storage is the third loading scenario. When the poles are laid down, half the weight of the pole is distributed through the tusks, as in Figure 12 below, with the top clamp supporting the other half of the weight. The stresses in the tusk fillets are the highest of any loading scenario.

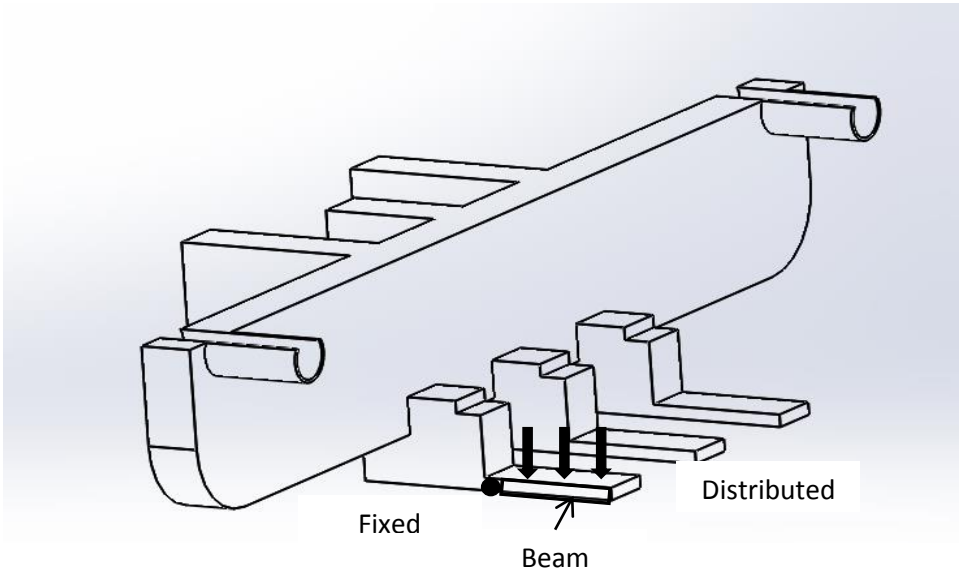

Figure 12: Cross section view of bottom clamp with simplified loading.

To simplify this loading for hand calculations, the forks are considered to be cantilever beams. The load is considered to be a distributive load on the thin portion of the fork. The weight of the pole is equally divided among the forks on the top and bottom clamp. The left side of the beam is considered fixed and the left side's deflection angle is zero. These boundary and loading conditions are chosen as a worst-case scenario, since the weight of the field pole may not be concentrated on the thin portion of the tusks.

4.5. Hand Calculation Results

The full hand calculations and the methodology are found in Appendix 2 but the results are tabulated below, along with the associated yield criterion. Case 1 is bending of the entire device, split between each cross-section type, while case 2 is plate bending at the rod holes. Case 3 is a crushing force during round edge loading and case 4 is tusk bending.

TABLE V: SUMMARY OF CALCULATED STRESS IN MATERIAL REMOVAL DESIGN

Case #	Loading Scenario	Component	σ_{max} (ksi)	Yield Criterion
1a	Distributed loading	Middle plate (worst case) stiffeners	3.23	1/20
1b		Middle plate (worst case) pi-beam	2.88	1/25
2		Middle plate (hole)	20.4	1/4
3	Round edge loading	Rounded edges	0.517	1/135
4	Tusk loading	Horizontal forks	18.3	1/4

These results show that the stress is close to ideal in some areas, but very small in others. This implies that there are geometries that are overdesigned, and that more cut outs at these points could yield even more weight savings. These results are not accurate enough, however, to justify the design, so FEA is necessary.

5. FEA Methodology

Obtaining accurate results using FEA is highly dependent on using an appropriate method. This section covers the methods and procedures to create the finite element models and to obtain the results for the various loading scenarios. The steps to build the model include the construction and element selection of the model, meshing, identifying boundary conditions, and applying loads.

5.1. Construction

The model was constructed using Autodesk inventor. The fillets produced by welding, which are integral to reducing stress concentrations, are excluded from this model. The analysis of the welds is included in Section 8.1. The CAD model was saved as a STEP file and imported to ANSYS Workbench for FEA. By using this design and analysis software, the model was constructed such that features such as bracket geometry, mesh density, element shape, load, and plate sizing are all controlled by a handful of parameters. This allows for the model to be quickly changed from testing different geometries with elastic material properties to plastic material properties or even fracture analysis.

The model was constructed using SOLID186 elements. These are basic hexahedron elements, depicted in Figure 13, totalling 20 nodes each with three degrees of freedom. The SOLID186 element was chosen because its ability to map mesh geometries such that the mesh densities could easily be controlled. This element has degrees of freedom in the X, Y, and Z directions, but SOLID elements in ANSYS do not have rotational degrees of freedom.

Figure 13: SOLID186 Hexahedral Element [10]

SOLID186 elements have specific material properties, explained in TABLE VI. For our analysis, we want an isotropic homogeneous linear elastic material, thus we defined EX=EY=EZ, NUXY=NUYZ=NUXZ. Additionally, the effects of temperature, thermal expansion, and damping are not within the scope of our project and thus were not defined. SOLID186 elements have several special features, namely plasticity, hyperelasticity, viscoelasticity, viscoplasticity, creep, stress stiffening, large deflection, large strain, initial stress import, automatic selection of element technology, birth, and death. Most of these special features are coded into the design but are suppressed for this analysis, making it simple to expand the scope of the analysis in the future.

TABLE VI: SOLID186 ELEMENT PROPERTIES [10]

Symbol	Element Property	Symbol	Element Property
EX	Modulus of Elasticity in X	ALPX	Thermal Expansion coefficient in X
EY	Modulus of Elasticity in Y	ALPY	Thermal Expansion coefficient in Y
EZ	Modulus of Elasticity in Z	ALPZ	Thermal Expansion coefficient in Z
NUXY	Poisson's ratio in XY	DENS	Density
NUYZ	Poisson's ratio in YZ	GXY	Shear Modulus in XY
NUXZ	Poisson's ratio in XZ	GYZ	Shear Modulus in YZ
DAMP	Damping Ratio	GXZ	Shear Modulus in XZ

During meshing, ANSYS is allowed to use the tetrahedral SOLID187 elements where needed. These elements are essentially the same element as the SOLID186 elements, but with half the number of degrees of freedom and a different shape.

5.2. Mesh Density

Creating an appropriate mesh for the analysis is important to minimize computing time while maintaining accuracy. A high-density mesh has more nodes, leading to better results, but a fine mesh is not helpful at areas with less stress or simpler geometry. The mesh used in the analysis was created using both a mapped and unmapped meshing code. This code allows ANSYS to create the mesh while controlling the mesh density in areas of interest. The mesh density is controlled using the Smart Size (SMRTSIZE) command for the unmapped sections and a line element size (LESIZE) command for the mapped sections.

The unmapped sections are refined enough to converge geometries that have no stress concentrations, while the LESIZE command increases the amount of elements in the model as well as increasing the mesh density around the concentrations of the design. The mesh density for testing was iterated through the LESIZE command around areas with stress concentrations to prove that the results converge. The studies did not converge directly next to the 90 degree corners, but this result is expected at this unrealistic geometry. Rather, the convergence was proven away from the concentrations, as the stress values were found to be independent of the meshed grid and number of degrees of freedom.

The effect of the LESIZE command can be seen in Figure 14, which shows the mesh refinement on a web stiffener. The area where the web meets the tusk has the highest stress of any area that needs to be welded. The LESIZE command controls the linear elements on the thin edge of the web, increasing the density near the tusk.

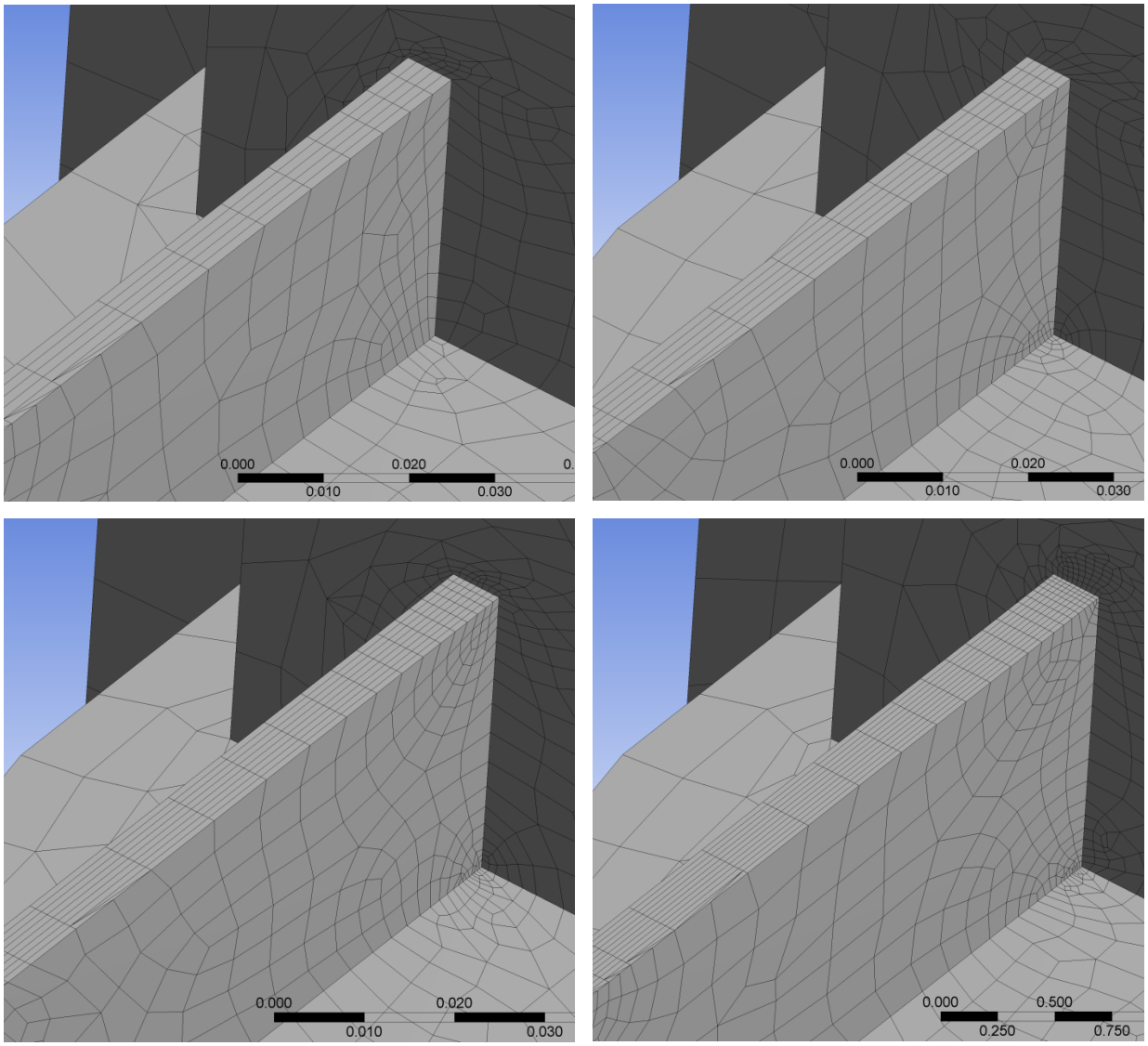

Figure 14: Mesh density LESIZE code refinement

5.3. Boundary Conditions and Constraint Equations

The boundary conditions utilized for the FEA depend on the loading scenario being analyzed. The three distinct loading scenarios are defined in section 4.4. In this section, these loading scenarios are broken down into the necessary boundary conditions, constraint equations, and loads.

5.3.1. Distributed Loading

The boundary conditions must mimic the actual real world conditions as closely as possible. To achieve this, surfaces are added to the bottom of the clamp where the nuts are located when the lifting device is assembled. These surfaces, shown in Figure 15, are then fixed to mimic the nuts supporting the weight of the field pole. While this is not completely realistic, since it assumes the clamping rods and nuts are completely rigid, it will give a conservative structural response. The redistribution of the stress from the lower clamp to the clamping rods themselves will only lower the maximum stress experienced in the lower clamp. As well, the fixed constraints will produce stress concentrations surrounding these locations. In addition to the fixed supports at the nuts, the holes that the clamping rods are run through are fixed from moving in the radial direction but free to move in both the axial and tangential directions. This corresponds physically to the holes being held in place by the clamping rods, but free to both spin and slide up or down the clamping rods.

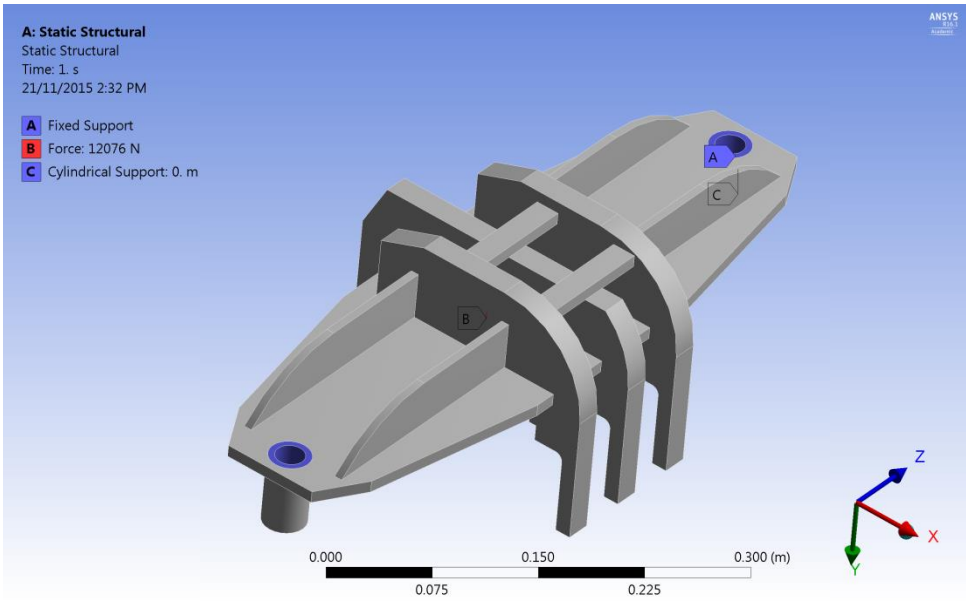

Figure 15: Fixed and cylindrical boundary conditions, distributed load case

5.3.2. Compression Loading

To simulate the crushing load applied by lowering the field pole onto the floor, a single, fixed boundary condition is applied to the underside of the clamp. This fixed boundary condition, shown in Figure 16, will simulate the clamp being lowered onto the power house floor and will be applied to any surface that contacts the floor as the pole is lowered.

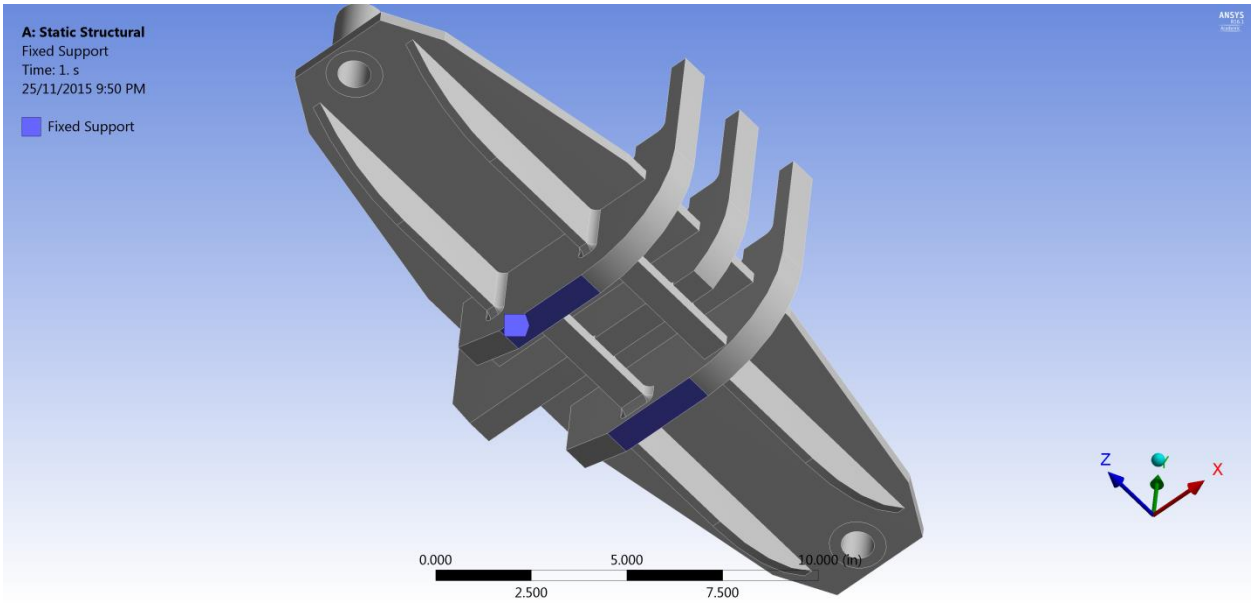

Figure 16: Round edge case boundary conditions

5.3.3. Tusk Loading

Once lowered onto the powerhouse floor, the field pole is lowered down from vertical to lie horizontally. During this operation, the thin portions of the tusks on the front side of the clamp are loaded with roughly half of the field pole's weight. To simulate the boundary conditions for this loading scenario, the tusk curvature on which the clamp is rotated is mated to a fixed plate. This is then represented by a frictionless contact patch between the contacting parts. Additionally, the circular tubes on either side of the lifting device are constrained using a cylindrical support, which allows rotation. The area the nut contacts the underside of the lifting device has a frictionless support applied to it in order to simulate the effect the nut and clamping rod. The angle that the teeth make with the ground is iterated between 45 and 5 degrees to find the worst case loading scenario, as further discussed in section 6.3. Figure 17 and Figure 18 shows the contact patch as well as the area contacted by the nut.

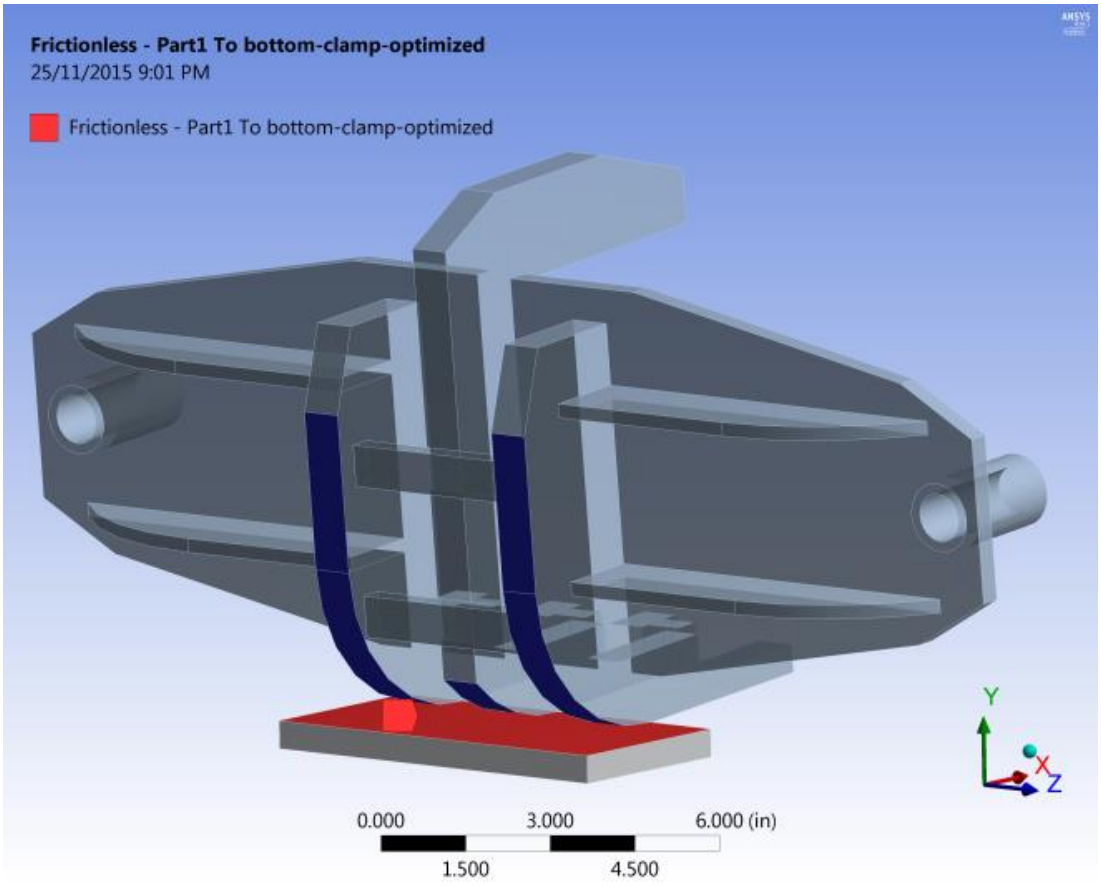

Figure 17: Tusk loading boundary conditions

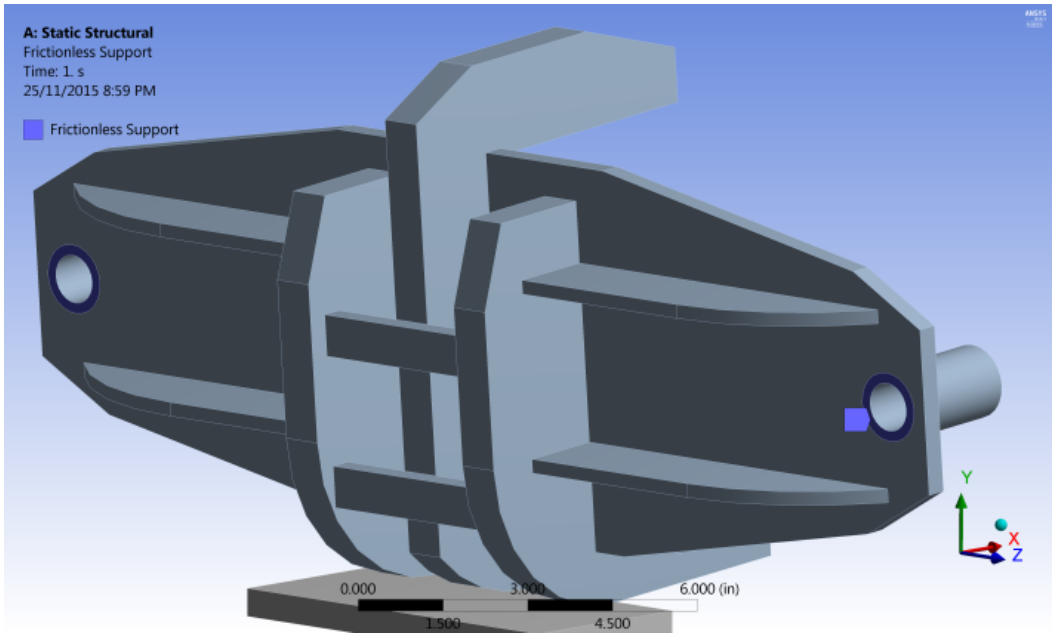

Figure 18: Frictionless guide boundary conditions

5.4. Loading

The model was loaded either on the plate, for scenarios one and two, and on the tusks for case three.

5.4.1. Distributive and Compression Loading

For the first two loading scenarios, the load is applied to the plate through the rubber pad. The entirety of the field poles weight is distributed over the surface by applying a 2715lbsf load to the area, as seen in Figure 19.

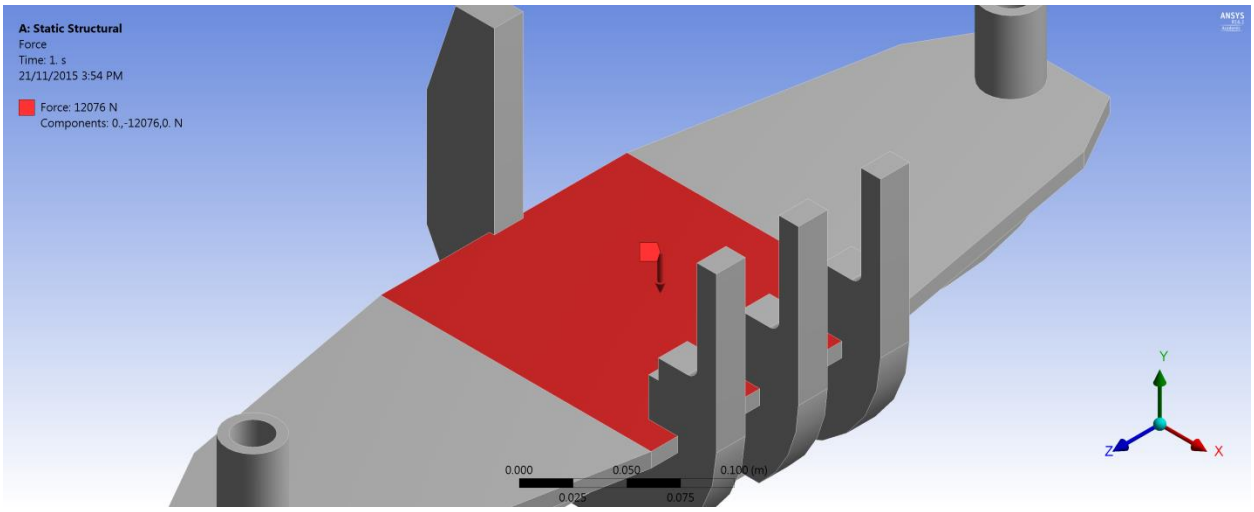

Figure 19: Plate loading scenario

5.4.2. Tusk Loading

For the third loading scenario, half of the weight of the field pole is distributed over the three faces of the tusks. This is achieved by applying force of 1357lbsf to the three tusk faces, as seen in Figure 20.

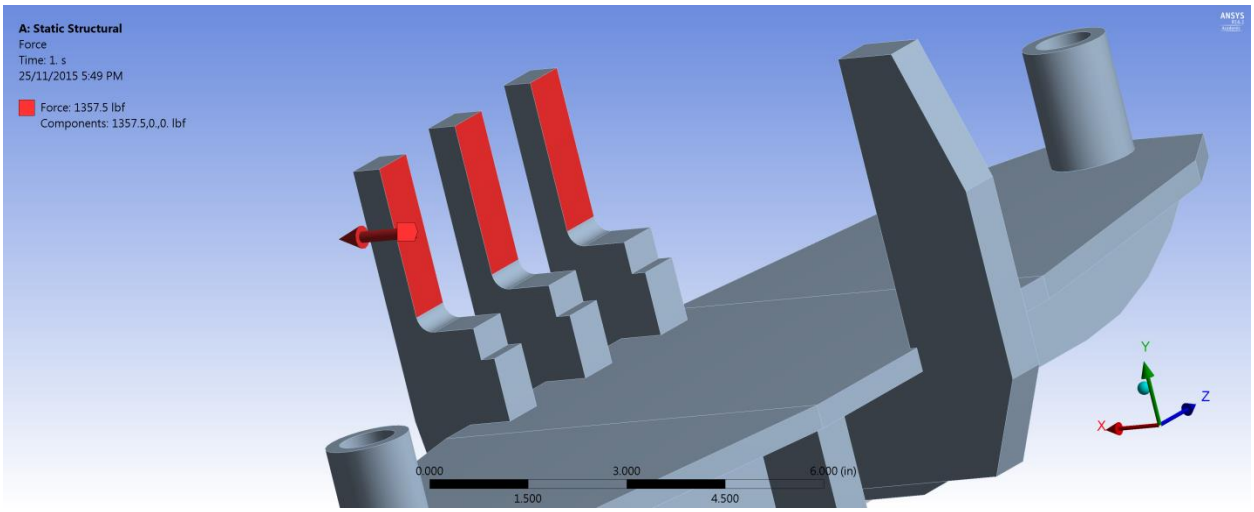

Figure 20: Tooth loading scenario

6. FEA Results

With the model meshed and the loads and boundary conditions applied, the results can be computed. This section shows the results of the analysis, focussing on convergence and the location of maximum stress for each loading scenario. Some areas do not converge, due to stress concentrations and the lack of fillets in the model, but points sufficiently close to the sharp corners do converge. The stress contour plots also give insight into how the load is transferred through the design.

6.1. Distributed Loading Scenario

The Von Mises stress contour plots for the top and the bottom of the model are shown in Figure 21 and Figure 22, respectively, and the deflection contour plot is shown in Figure 23.

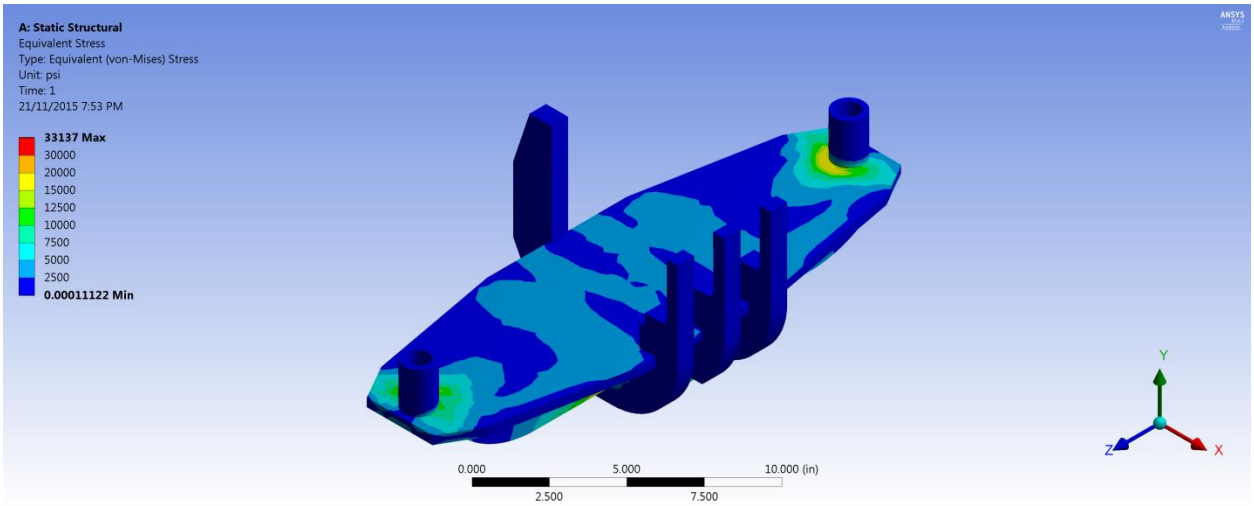

Figure 21: Von Mises stress contour plot (top)

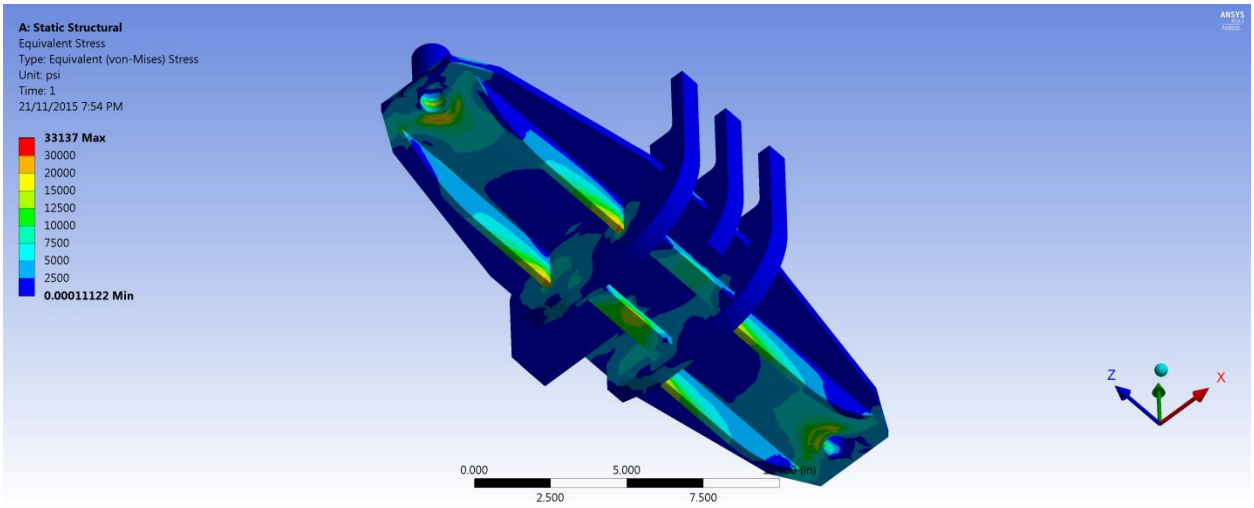

Figure 22: Von Mises stress contour plot (bottom)

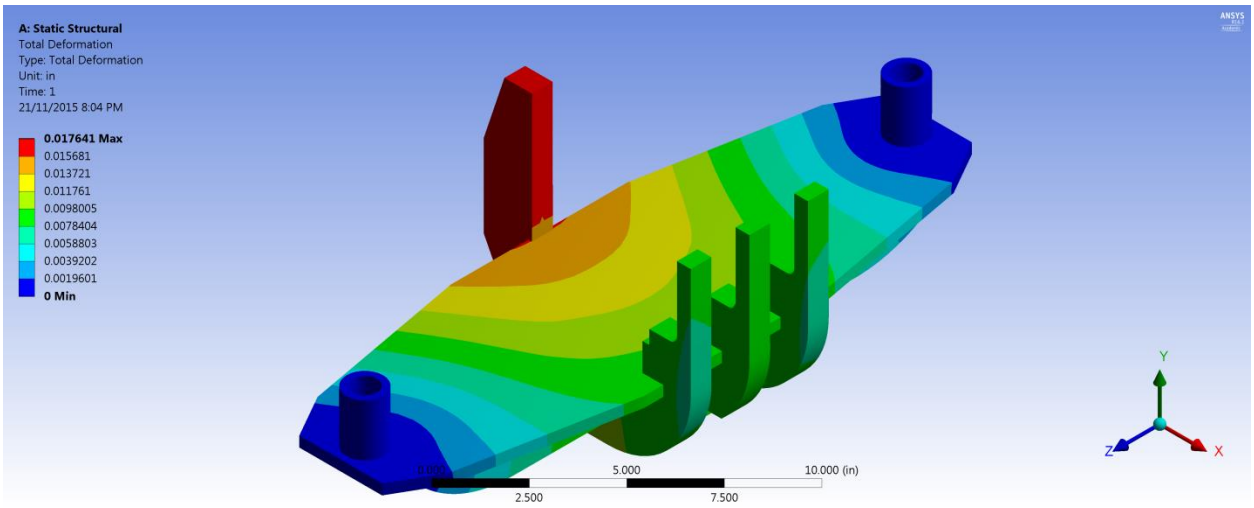

Figure 23: Deflection contour plot

Figures 20 and 21 show that stress is a maximum where the web stiffeners meet the tusks, so the stresses were further investigated at this location. The mesh density is controlled by LESIZE as iterations are performed and the stress recorded linearly away from the concentration point. These linear stress distributions are plotted in TABLE VII and TABLE VIII along with the corresponding degrees of freedom associated with each iteration.

TABLE VII: LINEARIZED VON MISES STRESS DISTRIBUTION ABOUT MAX CONCENTRATION (A)

Degrees of freedom	Linear Stress Distribution
103134	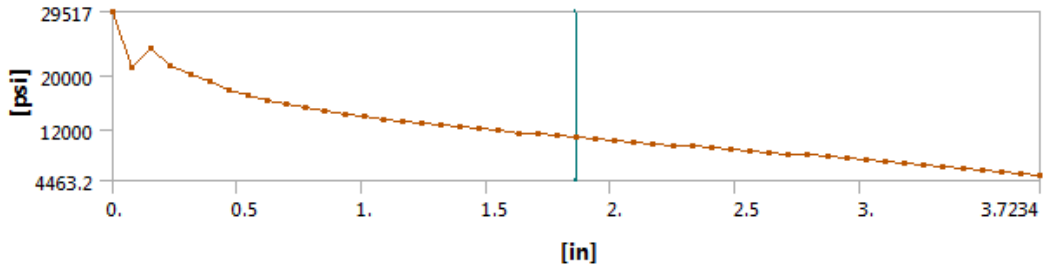
135015	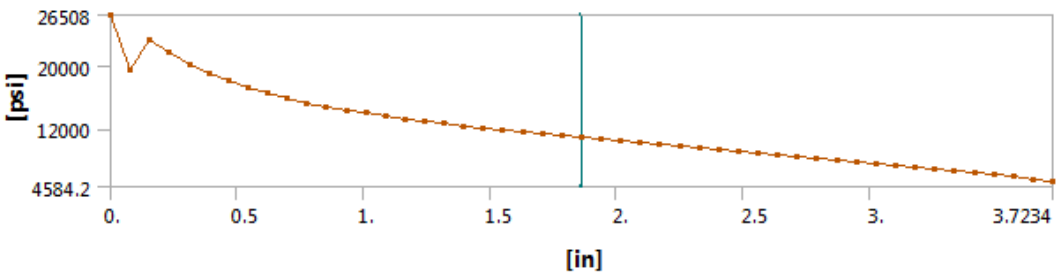
174726	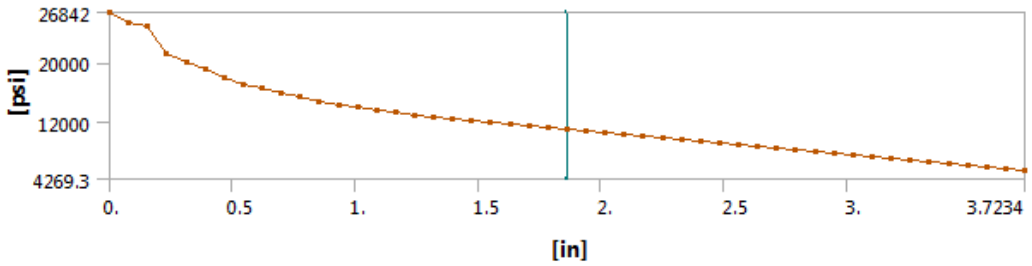
197430	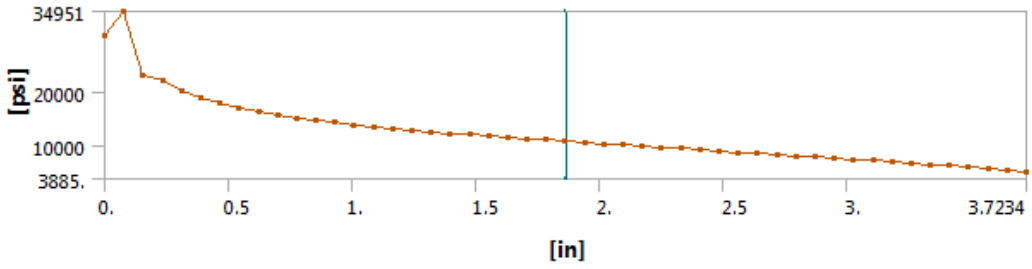

TABLE VIII: LINEARIZED VON MISES STRESS DISTRIBUTION ABOUT MAX CONCENTRATION (B)

Degrees of Freedom	Linear Stress Distribution
222675	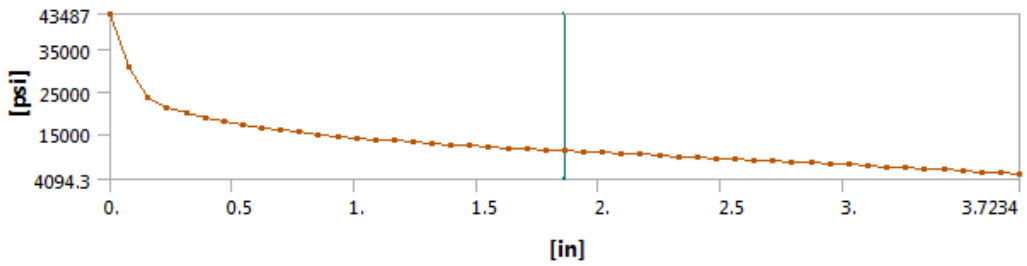
247251	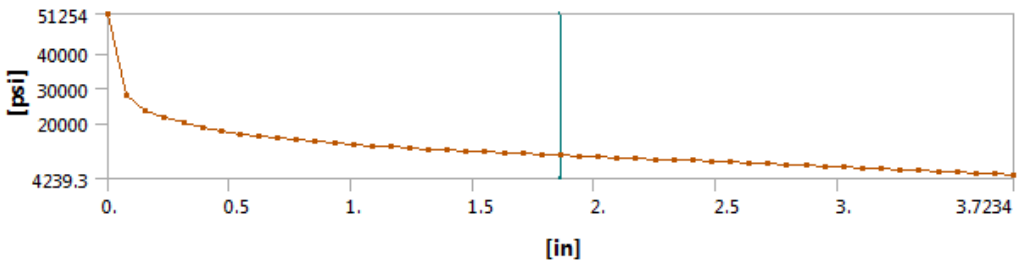
286830	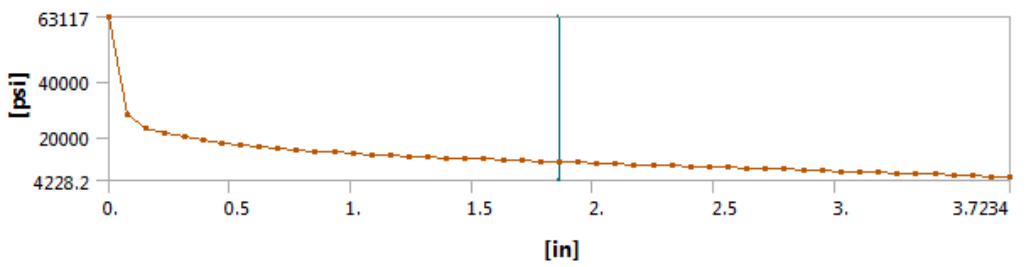

From TABLE VII and TABLE VIII it can be seen that the stress does not converge right at the tip of the 90 degree corner as would be expected, but by adding a sufficient amount of elements close to the concentration point, a convergence is proven very close to the 90 degree corner. The maximum stress found in this converged section is just under 30ksi. This stress is over our allowable stress. However when fillet welds are taken into account, the points where the computed stress is higher than the allowable stress are within the weld leg distance. Weld dimensions are addressed in detail in section 8.1.2, but the weld size at this point is ¼". TABLE VIII shows that ¼" away from the concentration, the stress becomes less than the maximum allowable value.

6.2. Compression Loading Scenario

Figure 24 shows that this scenario converges. The compression loading scenario is more than satisfactory, as the tusks can easily withstand the load and buckling will not occur. The Von Mises stress contour plots for the top and the bottom of the model are presented in Figure 25 and Figure 26.

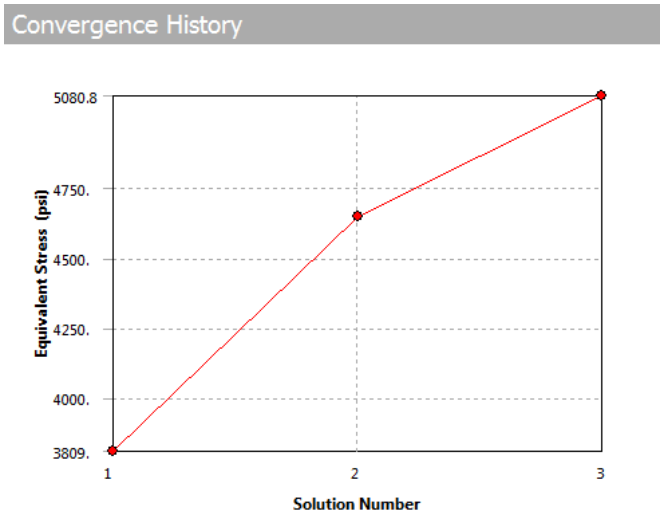

	Equivalent Stress (psi)	Change (%)	Nodes	Elements
1	3809.		8134	4162
2	4647.8	19.837	30038	18190
3	5080.8	8.9033	79404	52479

Figure 24: Compression loading scenario convergence plot

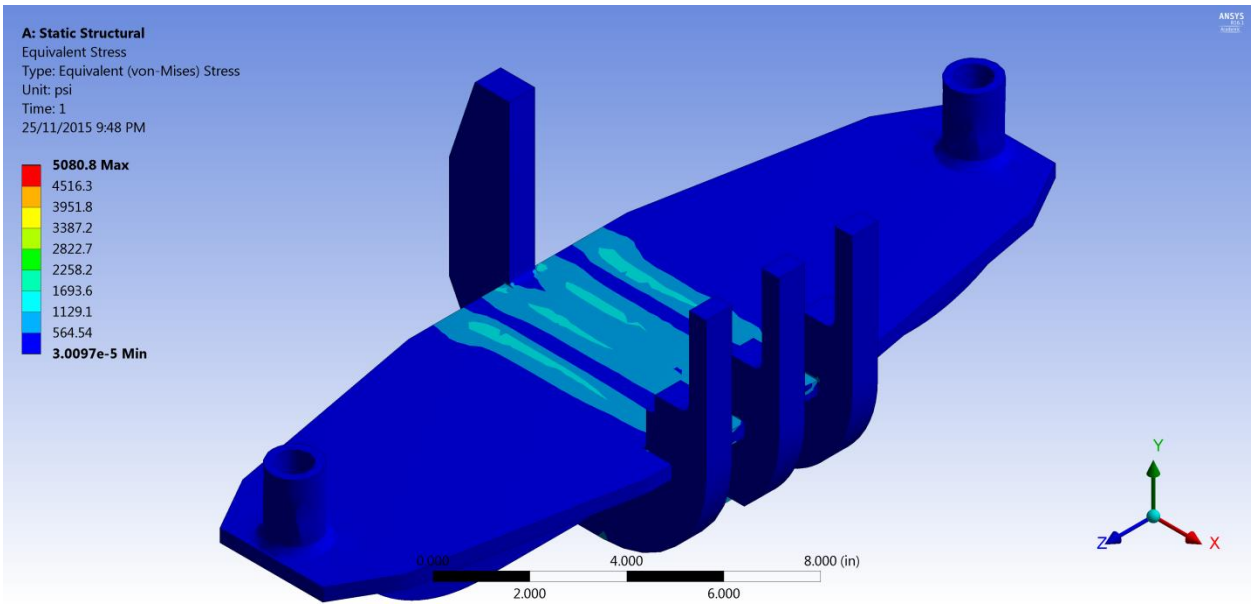

Figure 25: Compression loading scenario Von Mises contour plot (top)

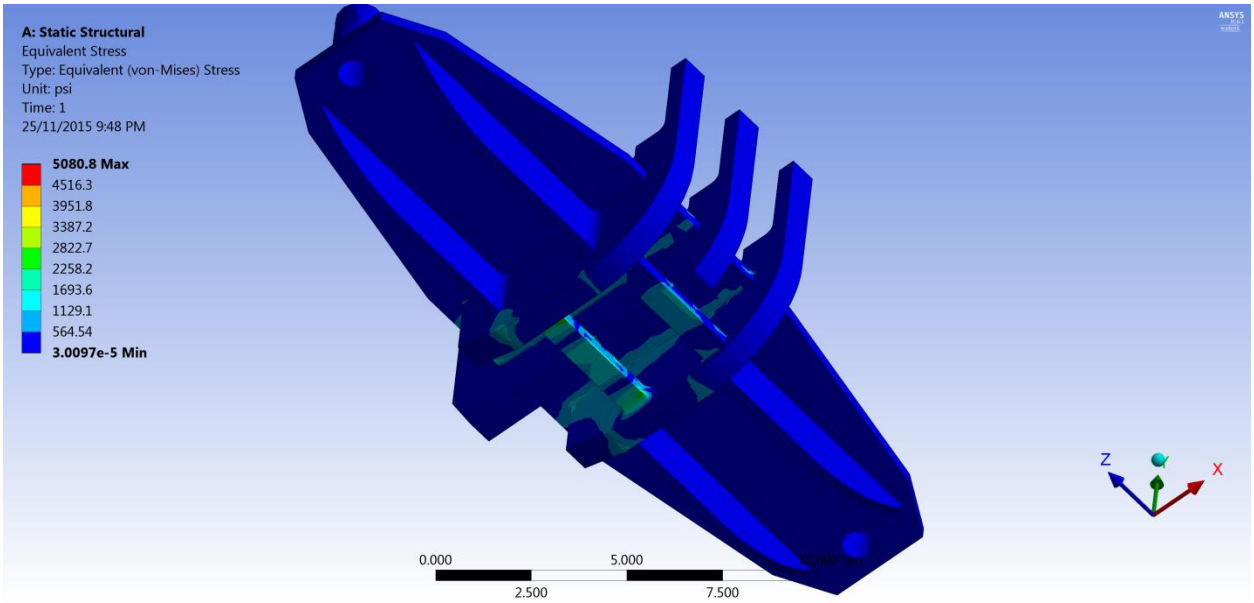

Figure 26: Compression loading scenario Von Mises contour plot (bottom)

The maximum stress is just over 5 ksi, well below the maximum allowable level. The deflections are shown below:

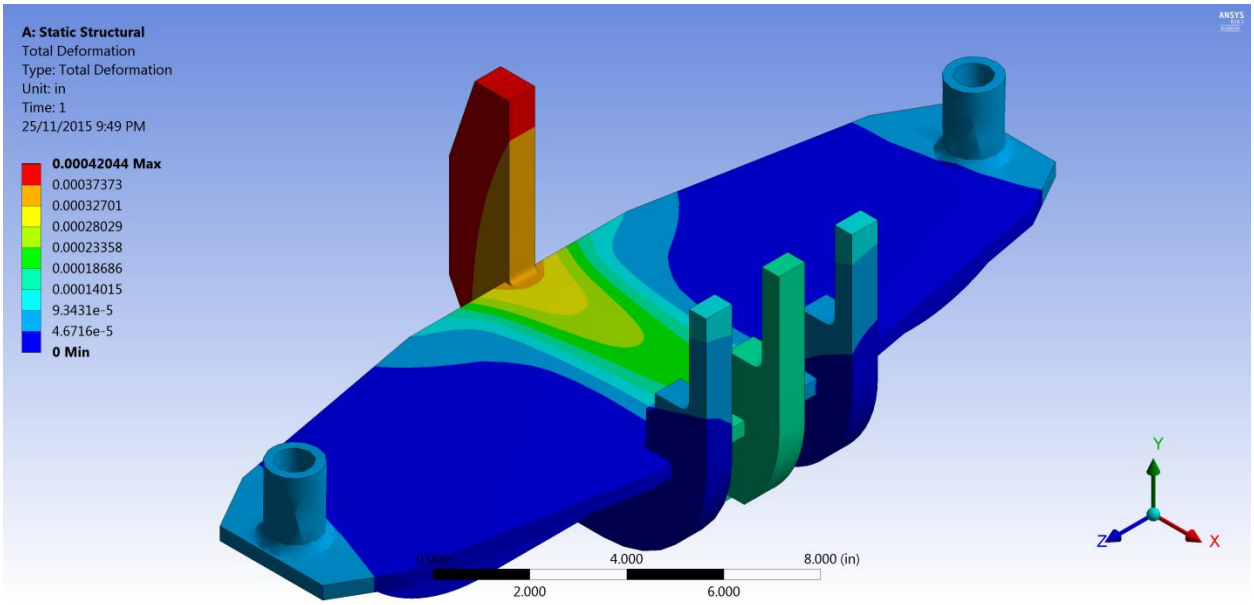

Figure 27: Compression loading scenario deflection contour plot

6.3. Tusk Loading Scenario

Convergence is proven for the analysis in Figure 28.

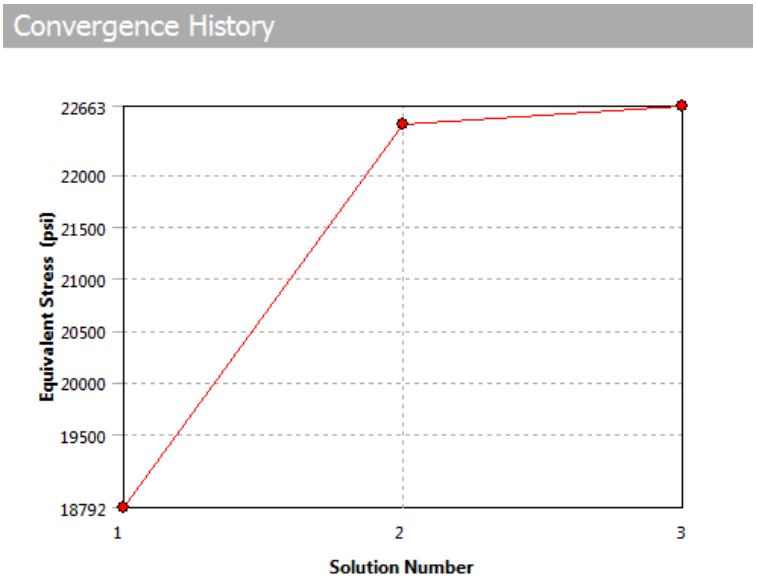

	Equivalent Stress (psi)	Change (%)	Nodes	Elements
1	18792		16456	7565
2	22486	17.896	49966	29686
3	22663	0.78495	142020	92236

Figure 28: Tooth loading scenario convergence plot

The Von Mises stress contour plots for the top and the bottom of the model are presented in Figure 29, Figure 30 and Figure 31, while the deflection contour plot is shown in Figure 32. The highest stress in this scenario occurs at the filleted corner of the tusks. While the stress remains below the maximum allowable value, the result is also very dependent on the real-world loading of the tusks. If some of the weight of the pole is transferred onto the thicker portion of the tusks, the stress in the fillet will drop significantly.

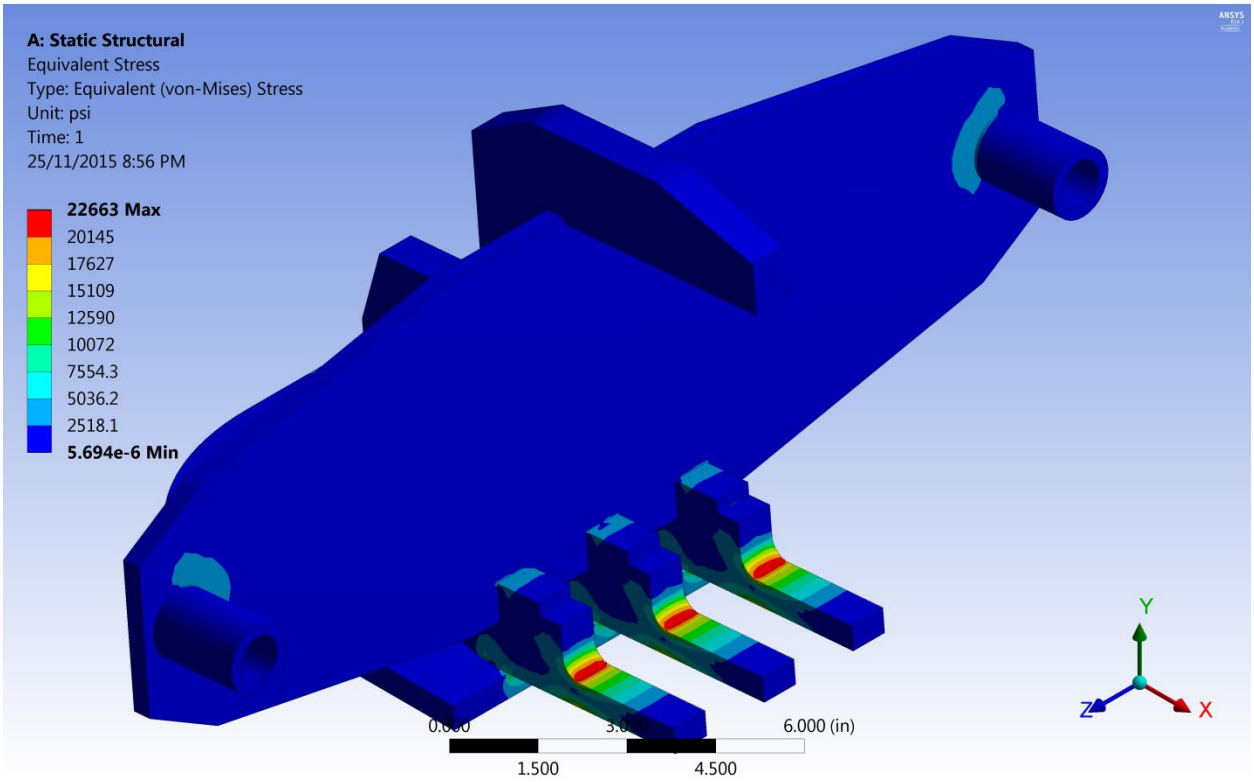

Figure 29: Compression loading scenario Von Mises contour plot (top)

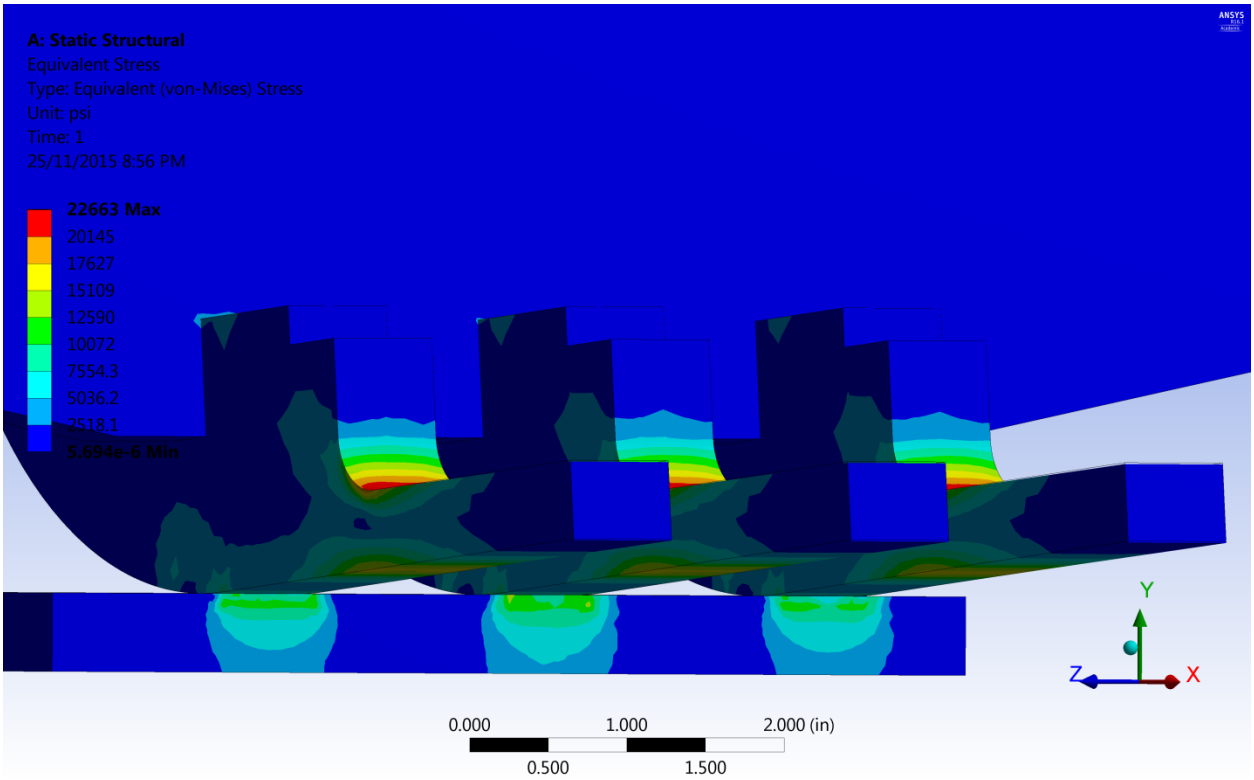

Figure 30: Compression loading scenario Von Mises contour plot (front)

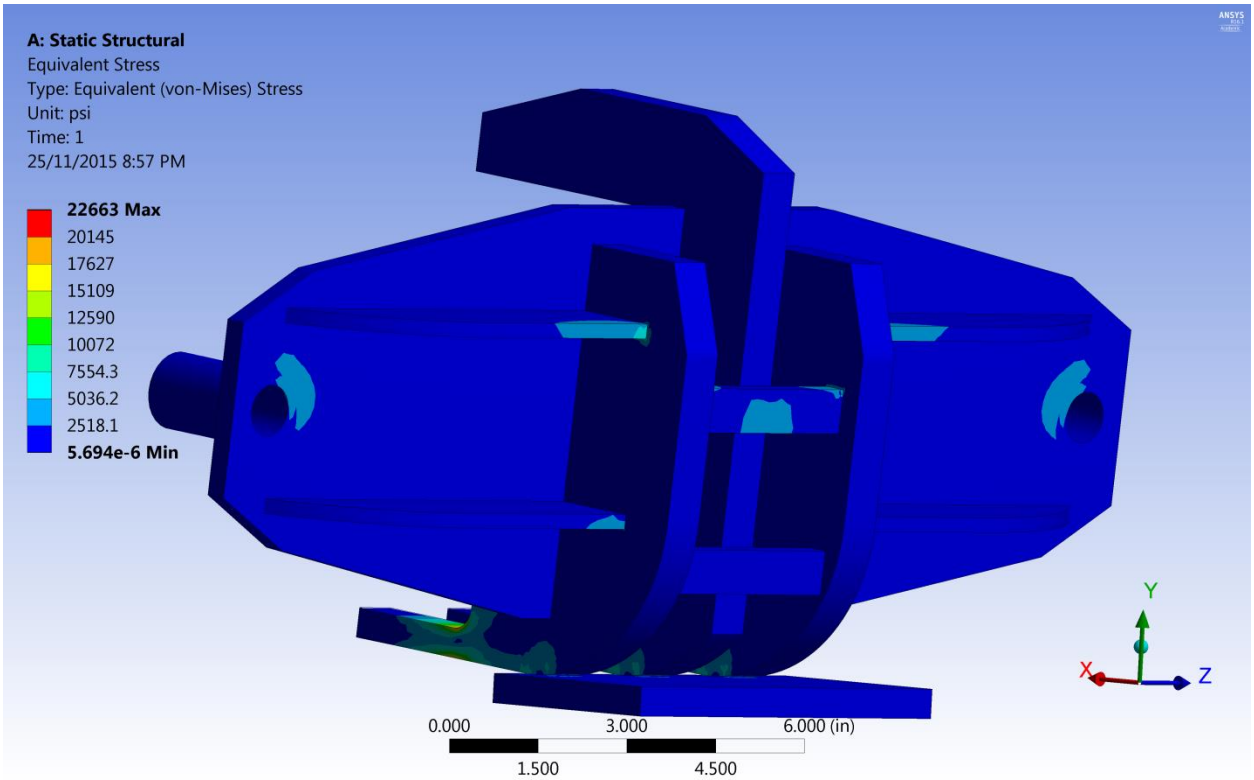

Figure 31: Compression loading scenario Von Mises contour plot (bottom)

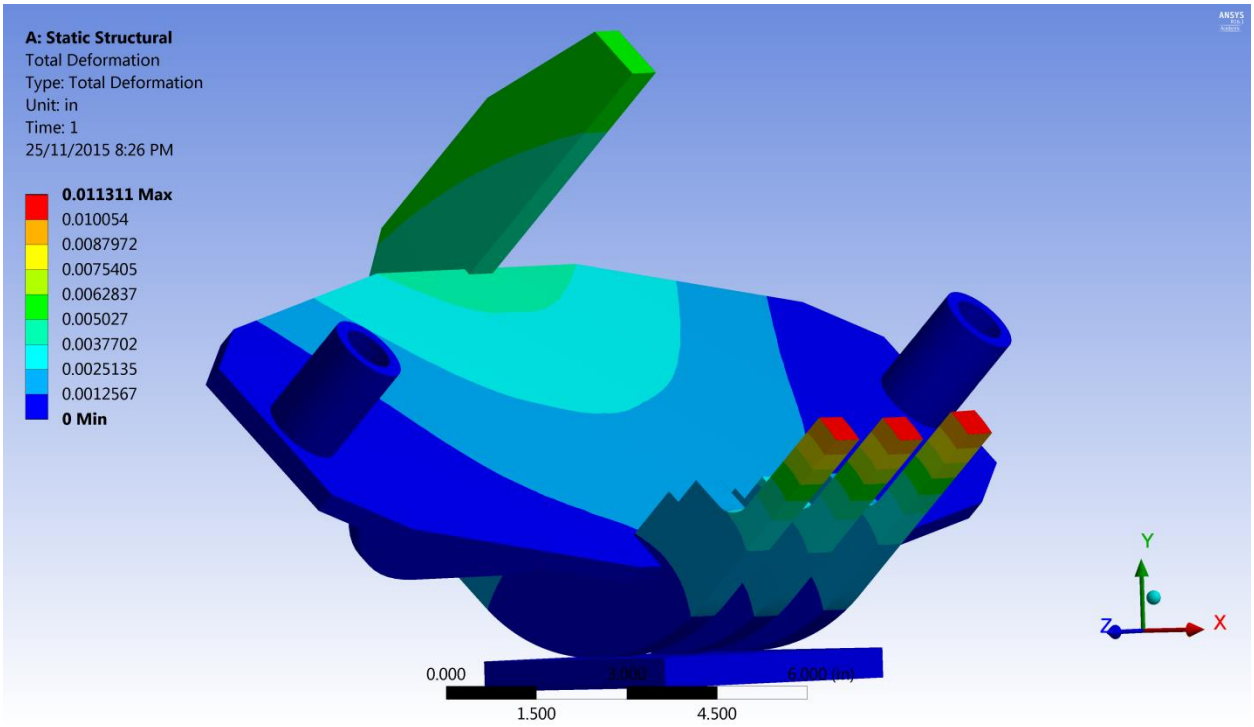

Figure 32: Compression loading scenario deflection contour plot (bottom)

6.4. Summary of FEA Results

The FEA results show that the stress remains below the maximum allowable value to ensure the yield criterion is met. The exception occurs in the distributed load case where the web meets the tusk, but this result only occurs because weld dimensions are neglected in the FEA model. Using weld dimensions of .24 in we can ensure the stresses meet the 1/3 yield criterion. The compression case has very low stress. The tusk loading scenario has stress close to the allowable limit, which occurs at the tusk fillet, but it is within the yield criterion limit and represents the worst-case loading scenario. TABLE IX shows the loading scenarios and their corresponding yield criteria.

TABLE IX: SUMMARY OF FEA RESULTS AND THEIR CORRESPONDING YIELD CRITERIA.

Loading	Maximum Stress (psi)	Yield Stress (psi)	Yield Criteria
Distributive Loading (.25 in fillets)	21408	70000	31/100
Compression	5080	70000	7/100
Tusk Loading	22633	70000	32/100

7. Alternate Failure Modes

Fracture and fatigue are modes that cause a design to fail at stresses below the yield strength of the material. Fracture failure is the study of how materials fail with the presence of a crack. For fracture, a general solution is used to test both distributive and teeth loading conditions. Based on this general solution, the largest allowable stable crack size can be predicted. Fatigue occurs due to weakening of the material caused by porosity growth. Fatigue failure can be used to predict the number of cycles a design can experience before failure.

7.1. Fracture Analysis

The full analysis methodology is presented in Appendix 7 but an overview of the procedure and the results are presented in this section. This analysis simplifies the cross-section of the clamp to be a T-beam. When considering the location of potential fracture, the area that experiences the maximum amount of tensile stress is inspected. in this case it will be at the bottom of the stiffeners.

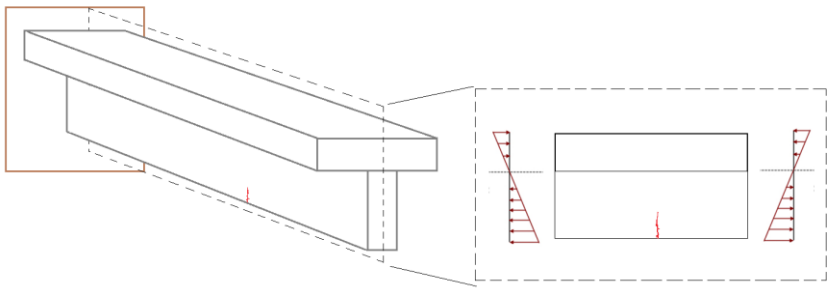

Figure 33: Stiffener simplification and crack positioning

For this crack geometry, there is both an axial tensile stress and a bending stress. By superposition, the mode 1 fracture effects of each are analysed separately and then combined. The stress intensity factors for both stresses are shown in the following two figures:

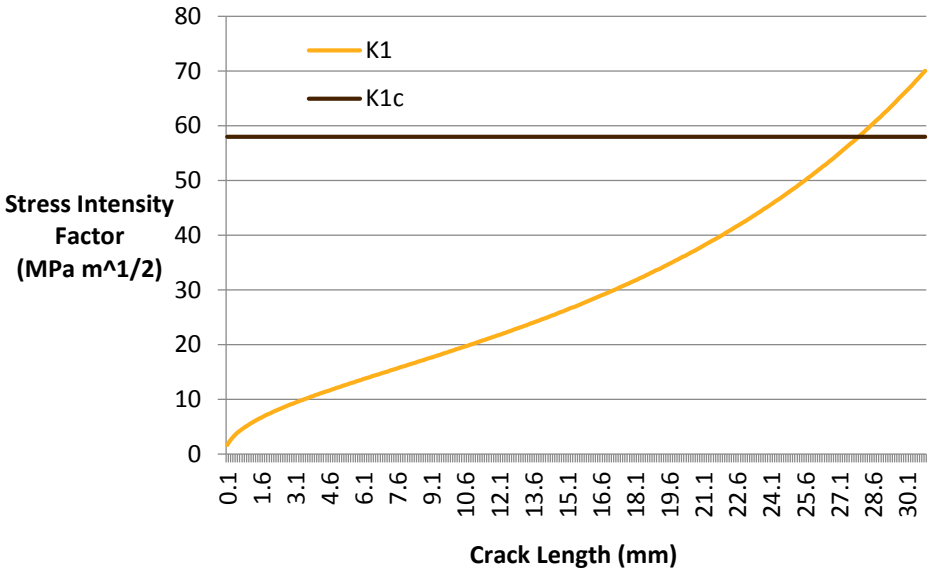

Figure 34: Stress intensity for varying crack length for tensional loading

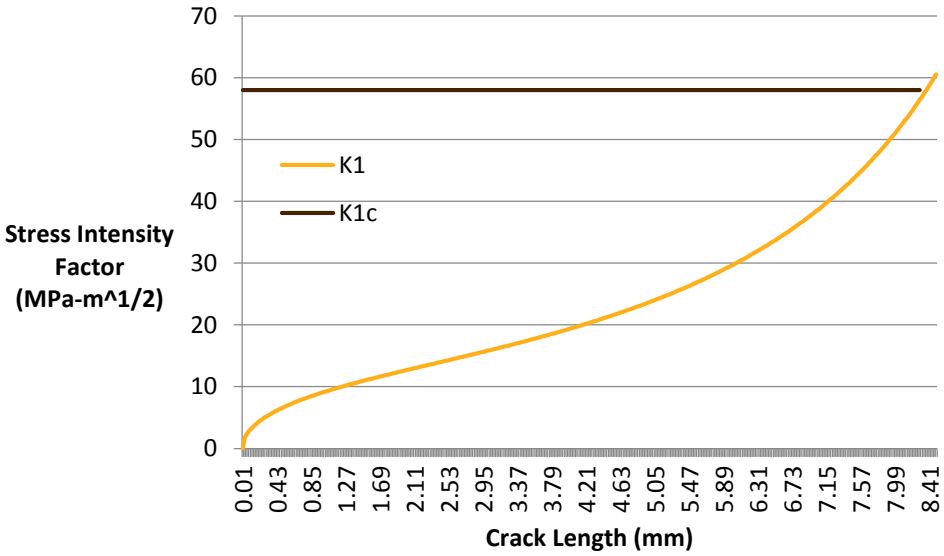

Figure 35: Stress intensity for varying crack length for bending loading

By adding the results from both loading orientations, the stress intensity factor for mode 1 fracture can be found for this fracture case, as shown in Figure 36.

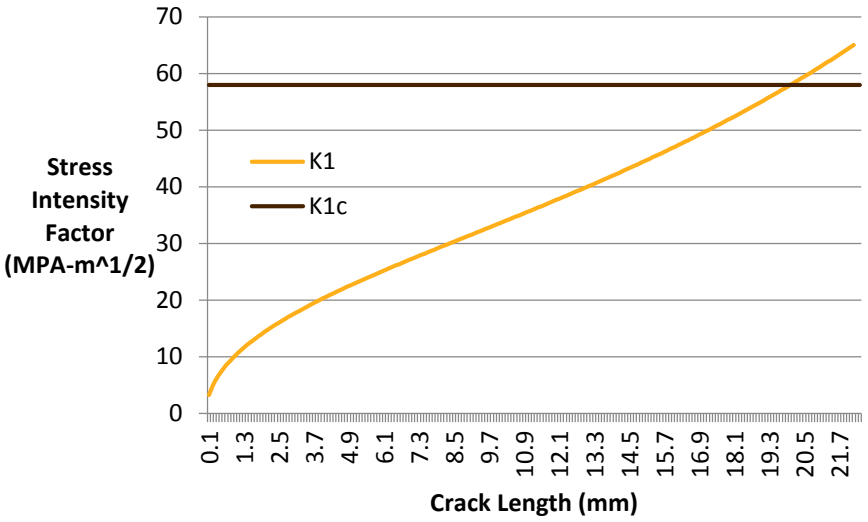

Figure 36: Stress intensity for varying crack length for tensional and bending loading

From this analysis, the critical crack length found in the stiffeners is 20 mm, or 0.788 in, propagating directly into the bottom of the stiffener. This critical crack length is substantially larger than the minimum visible crack length of 1 mm, or 0.04 in.

The same analysis is performed for the teeth as analyzed previously. The teeth geometry will see only the bending load, and as such the 155 MPa bending stress is used as the stress. Following the same methodology as the above discussion, the stress intensity is graphed against crack length and fracture toughness of the material. The results are presented in Figure 37.

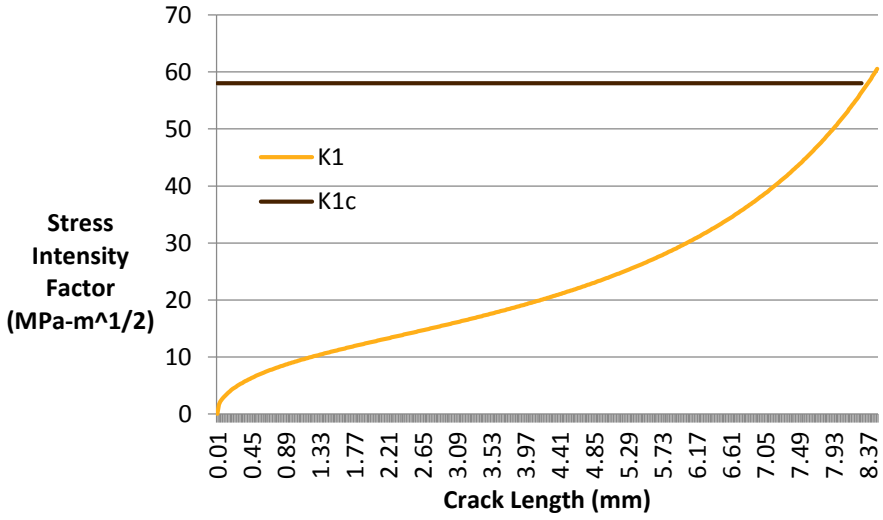

Figure 37: Stress intensity for varying crack length for tusk

It can be seen from Figure 37 that the critical crack length in the teeth is 8 mm, or 0.315 in, which exceeds our minimum visible crack length.

7.2. Fatigue Analysis

Another failure mechanism that must be considered is fatigue failure. Fatigue is the evolution of damage at the micro-structural level that ultimately leads to the formation of cracks and failure. It is important to account for since it causes materials to fail well below their yield strength.

Fatigue analysis can be broken into two types of failure: low cycle and high cycle. The failure region that lies between 10^0 and 10^3 cycles is defined as the low cycle region, where failure occurs at a relatively low number of cycles. A key characteristic of the low cycle region is that the stress amplitude is mostly between the yield strength (S_y) and ultimate strength (S_u) [11]. This mode of failure will not occur in this design, since the maximum stress is far less than the yield strength.

The high cycle failure is located between 10^3 and 10^6 cycles for steels. In the high cycle region, the stress amplitude should only cause elastic deformation of the part. Fatigue failure will occur because of crack initiation and propagation. This type of failure can affect our design if the clamp undergoes enough load cycles. Figure 38 is the S/N curve for CSA g40.21 60W steel and shows the high and low cycle regions.

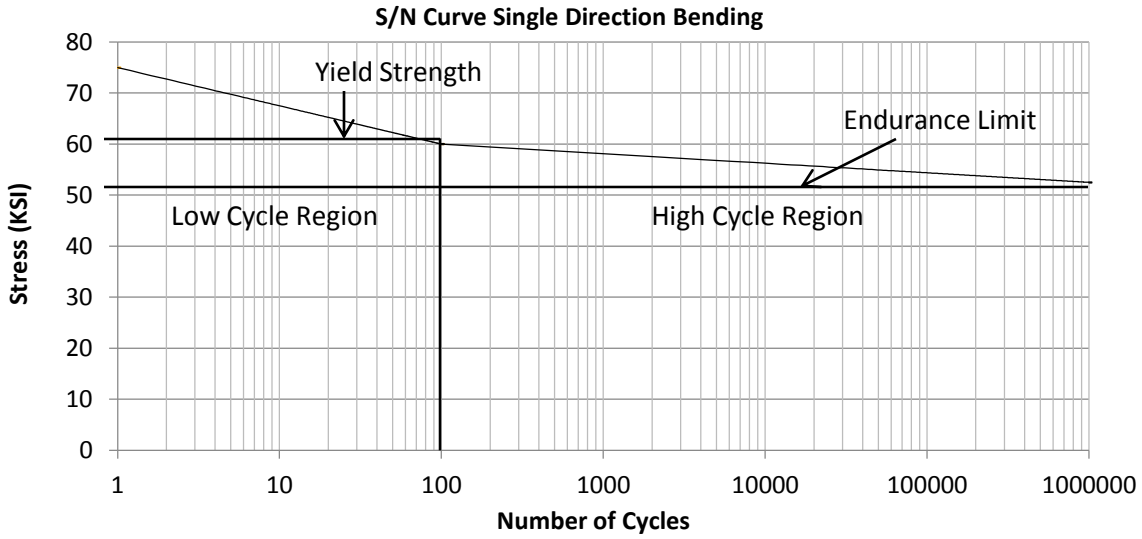

Figure 38: S/N curve for single amplitude loading [11].

By modifying the endurance limit, a new modified S/N curve can be found

$$S_e = K_{reliabilty} \cdot K_{surface} \cdot K_{size} \cdot K_{load} \cdot S_e' \quad \text{Eq. 19 [11]}$$

$K_{reliabilty}$ is the reliability factor, $K_{surface}$ is the surface factor, K_{size} is a sizing factor, K_{load} is the load factor and S_e' is the pristine stress limit at a given number of cycles. This particular model uses a reliability factor of .81, corresponding to 99% certainty; a surface finish factor of 0.65, corresponding to hot rolled steel; a size factor of 0.95, corresponding to where 95% of the stress concentration occurs on a .375 plate; a load factor of 1.4, corresponding to singular directional loading; and a pristine S/N limit of 37.5 KSI [11].The actual endurance limit S_e is as follows:

$$S_e = K_{reliabilty} \cdot K_{surface} \cdot K_{size} \cdot K_{load} \cdot S_e' = .81 * .65 * 1.4 * .95 * 37.5 = 26.25 \text{ KSI}$$

Since the actual endurance limit is larger than the 1/3 yield criteria, fatigue failure will not occur, independent of how many cycles the device is used. Figure 39 shows the modified S/N curve and the maximum stress allowed with respect to the endurance limit.

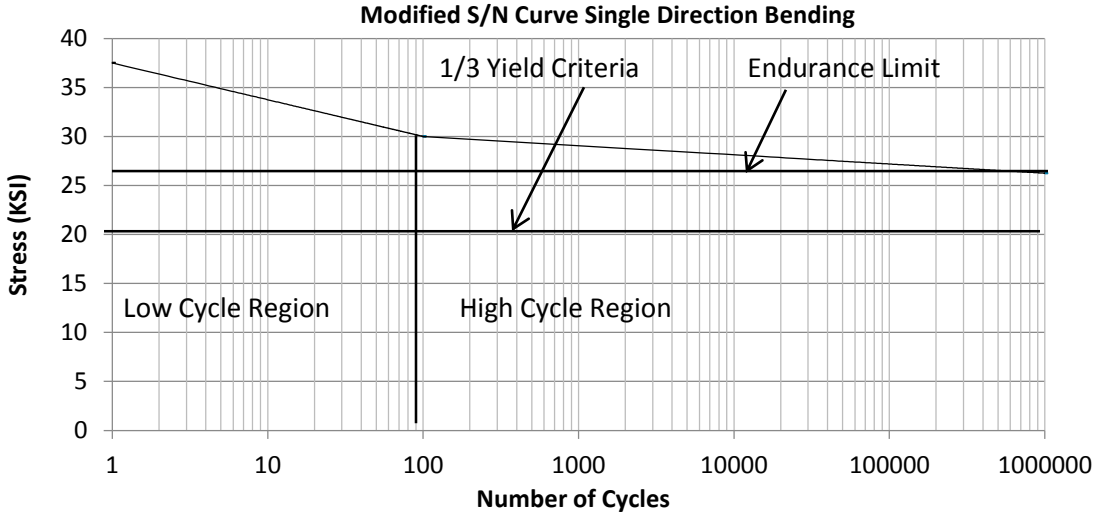

Figure 39: Modified S/N curve of flat plate undergoing single directional loading.

Since the stress falls below the endurance limit, fatigue failure will not occur.

8. Manufacturability

Manufacturability is a key aspect to the final design to ensure that the design can be easily built. To make the device as simple as possible to manufacture, the fabrication of each separate part and the general weld assembly of the final design are considered. These parameters affect the total manufacturing cost. Manitoba Hydro has specified that Wallin Industries will be manufacturing the device. Wallin's applicable machining capacity includes CNC machines, lathes, waterjet cutting, welding, and drilling. Based on the complexity and required precision, all plate pieces are cut by waterjet, all round bars are lathed, and all assemblies are welded together. Figure 40 shows the different manufacturing methods of each of the parts on the overall welded assembly.

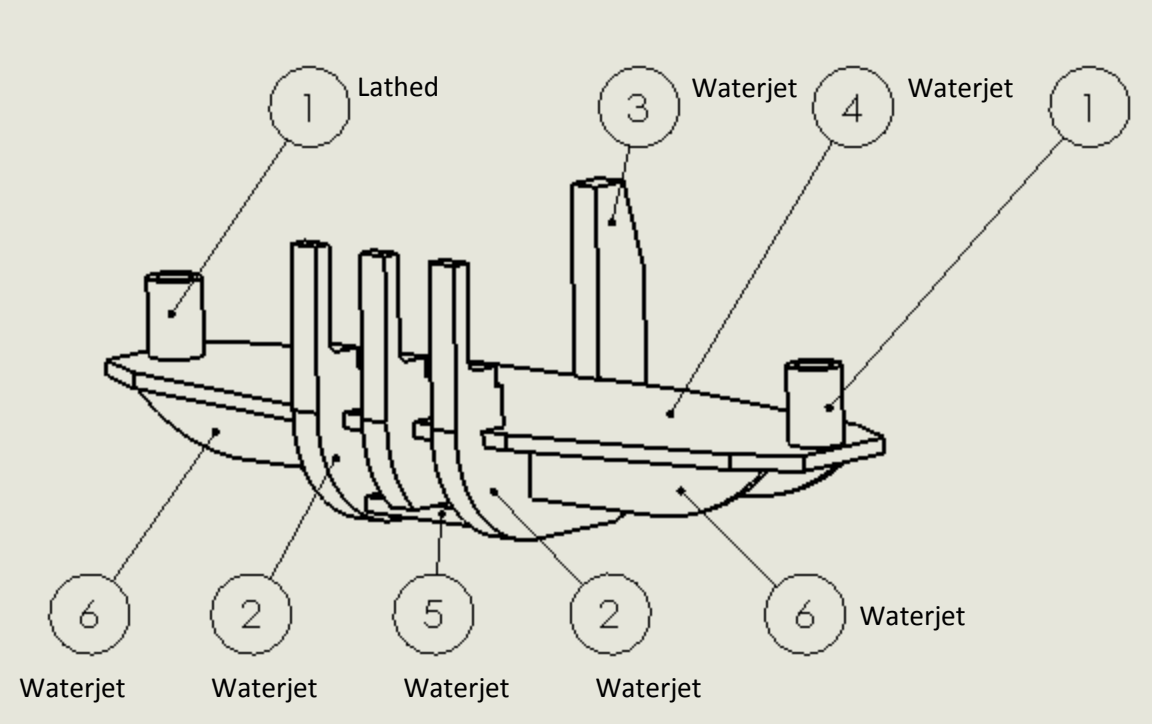

Figure 40: Welding assembly with fabrication methods.

8.1. Welding Specifications

Welds are an important factor in the design of a part since they are positioned where the highest stresses tend to occur. To design the welds for this part, the Canadian CSA W59-03 standard is used to get preliminary minimum weld sizes and FEA is used to ensure that the stresses are acceptable.

8.1.1. CSA Standard

The CSA standard has a table outlining the minimum allowable fillet weld size based on the thicknesses of the parts joined. The BTH-1 standard has the same information and references the CSA standard. The table is reproduced below:

TABLE X: MINIMUM FILLET WELD SIZE, BASED ON MATERIAL THICKNESS [11]

Material Thickness, t, of thicker part joined (in)	**Minimum fillet weld size (in)**
t ≤ ¼	1/8
¼ ≤t ≤ ½	3/16
½ ≤t ≤ ¾	1/4
¾ ≤t	5/16

8.1.2. Finite Element Analysis Method

Manitoba Hydro has an internal standard that outlines how to use ANSYS FEA to determine the necessary weld size. A mesh is applied to the corner, with the mesh size about half of the expected weld size. The stress is then probed two elements away to find σ_{avg} and inserted into the following formula [6]:

$$Weld_{throat} = \frac{\sigma_{avg} Width_{rib} Strength_{red}}{2 * (S_y/3)}$$

S_y is the yield strength and $Strength_{red}$ is the fatigue strength reduction factor. Since failure in fatigue is not going to occur, the value is unity.

This analysis will focus on the weld between the web stiffener and the tusk. This location is where the stress is highest, so if the standard's prescribed values are acceptable here, they will be acceptable at the other welds as well. The stress as a function of distance is shown in the next table:

TABLE XI: COMPUTED STRESS AT VARYING DISTANCES FROM SHARP CORNER

Distance (in)	Stress (psi)
0	63852
7.76E-02	28063
0.15514	23331
0.23271	21408
0.31028	20008
0.38785	18828
0.46542	17857
0.543	17046
0.62057	16370

Since the tusk is ¾" thick, the expected weld size is ¼". Looking at the value of 0.233" in the table, the stress is already lower than the allowable stress, implying that this size of weld will be adequate. The node distances arise from the LESIZE mapping command. If the mesh size was half the expected width, the stress two nodes away would be around the value at 0.233":

$$Weld_{throat} = \frac{\sigma_{avg} Width_{rib} Strength_{red}}{2 * (S_y/3)}$$

$$Weld_{throat} = \frac{(21408)(0.25)(1)}{2 * [(70000)/3]}$$

$$Weld_{throat} = 0.11\ in$$

This value is lower than the size required by the standard. This result makes sense, since it is expected that a standard provides a safe value. Since the standard's weld size works well at this joint, which has the highest stress concentration, it will be sufficient at the other joints as well.

8.2. Cost

Costing of the bottom clamp of the device is a very simple process. There are three factors that influence cost of this design. They are as follows:

1. Material Cost:

Material is the total cost to purchase the 70WT steel to be used for the individual parts, including delivery costs.

2. Waterjet Time:

The time it takes to waterjet a part, including the setup and removal time.

3. Lathe Time:

The time it takes to machine a circular part, including the setup and removal time.

4. Weld Time:

The time it takes to weld an assembly, including the setup and removal time of any parts that are welded in the assembly.

All parts in the cost baseline estimate detail these four costs. For accuracy and reliability all plates are to be waterjet from standard plate sizes of CSA G40.21 70 WT steel. The guides (Part 1) are to be lathed. Waterjet times are estimated on a length of cut basis [12] and welding times are estimated on a volume of weld basis [13]. Waterjet costs and welding costs have been estimated to be $90 [12] and $70 [13] per hour, respectively. Both the waterjet and welding cost include any labour involved. Lathe cost times have been estimated 70 $/hr and include any labour involved. The rubber and paint costs are approximate estimates based on price and application time. Based on these estimates the following cost baseline is shown in Figure 41.

Bottom Clamp Cost Baseline					
Part 1 X 2 (Guides)		Time	Cost		
	Material		$25		
	Lathe Machining	1.00	$70		
			$95	X2	$240
Part 2 (Central Tusk)					
	Material		$100		
	Waterjet Cutting	2.00	$180		
			$280	X1	$280
Part 3 X 2 (Side Tusks)					
	Material		$80		
	Waterjet Cutting	2.00	$180		
			$260	X2	$520
Part 4 (Plate)					
	Material		$100		
	Waterjet Cutting	2.00	$180		
			$280	X1	$280
Part 5 X 4 (Webs)					
	Material		$25		
	Waterjet Cutting	0.50	$45		
			$70	X4	280
Part 6 X 2 (Stiffeners)					
	Material		$10		
	Waterjet Cutting	0.25	$23		
			$33	X2	$65
Assembly					
	Material (Rubber)		$50		
	Installation (Rubber)		$25		
	Material (Paint)		$40		
	Installation (Paint)		$200		
	Clean up cost	2.00	$180		
	Welding	16.00	$1,120		
			$1,615	X1	$1,615
				Cost Baseline	$3,280

Figure 41: Cost baseline of final design

The cost estimate is aggregable with the marginal value of $5000. Even though the cost of the device exceeds the ideal value of $2000, it is not a primary concern of the client.

9. Risk Assessment

To properly determine risk response while installing and transporting the bottom clamp, a Failure Mode and Effect Analysis (FMEA) must be performed. FMEAs are structured approaches to identify which products will fail. Using a structured FMEA can determine the risk associated with the design and if that risk is acceptable. To determine if the new bottom clamp is safe, FMEAs have been performed on both the old and new designs.

Using previous experience from the client and analysis of the old device, five failure modes are analyzed for both designs. They are as follows:

1. Dropping the clamp during transportation
2. Dropping the clamp during installation
3. Failure during loading of the field pole
4. Failure during compression of the bottom clamp during removal
5. Failure during bending of tusks during loading

The FMEA decomposes each failure mode into potential effects, potential causes, and current controls. FMEA associates a risk number with each of the categories and multiplies them to get a Risk Priority Number (RPN) for each failure mode. TABLE XII illustrates the FMEA for the old design.

TABLE XII: FMEA OF OLD DESIGN

Component	Potential Failure Mode	Potential Effect	Severity	Potential Causes	Freq.	Current Controls	Detection	RPN	Action Recommendations
Bottom Clamp	Dropped during Transportation	1. Crushed fingers 2. Broken bones 3. Damage to device 4. Damage to surroundings	5	1. Object is heavy to lift, 2. Object is awkward to lift 3. Distance to travel is too long	5	1. PPE of crew members	5	125	1.Decrease weight component while maintaining strength and reliability 2. Improve operating procedure or transportation method
	Dropped during Installation	1. Crushed fingers 2. Broken bones 3. Damage to device 4. Damage to surroundings	5	1. Object is heavy to lift 2. Object is awkward to lift 3. Installation Time is too long	5	1. PPE of crew members, 2. Procedure calls for 3 crew members to install	3	75	1. Decrease weight of component while maintaining strength and reliability
	Failure during operation 1	1. Death if in the line of fire 2. Significant damage to surroundings including field pole and generator	10	1. Object does not meet yield criteria 2. Object was not installed correctly 3.Object had corrosion 4. fatigue damage 5. failure from crack damage	1	1. PPE of crew members, 2. Procedure calls for 3 crew members to install with specific installation procedure. 3. Has been tested hundreds of times 4. Paint to defend against corrosion of the device 5. Stamped engineering drawing verifying the yield criteria	1	10	None; risks do not effect end user
	Failure during operation 2	1. Death if in the line of fire 2. Significant damage to field pole	10	1. Object does not meet yield criteria 2. Object was not installed correctly 3.Object had corrosion 4. fatigue damage 5. failure from crack damage	1	1. PPE of crew members, 2. Procedure calls for 3 crew members to install with specific installation procedure. 3. Has been tested hundreds of times 4. Paint to defend against corrosion of the device 5.Stamped engineering drawing verifying the yield criteria	1	10	None; risks do not effect end user
	Failure during operation 3	1. Death if in the line of fire 2. Significant damage to field pole	10	1. Object does not meet yield criteria, 2. Object was not installed correctly, 3.Object had corrosion, 4. fatigue damage 5. failure from crack damage	1	1. PPE of crew members, 2. Procedure calls for 3 crew members to install with specific installation procedure. 3. Has been tested hundreds of times 4. Paint to defend against corrosion of the device 5.Stamped engineering drawing verifying the yield criteria	1	10	None; risks do not effect end user

Using the above FMEA, risk priority numbers of 125 and 75 were found. These risk numbers have been deemed too large and must be mitigated. The driving factor for both of these cases was that the frequency of an incident and proper controls are not sufficient. The severity, frequency and detection numbers are determined by the following charts. These charts are separated from rankings of 1-10, with 1 being advantageous and 10 being undesired.

Severity of Effect		***Ranking***
Minor	Unreasonable to expect that the minor nature of this failure would cause any substantial effect on system performance or on a subsequent process or service operation. Customer unlikely to either notice or care about the failure.	**1**
Low	Low severity ranking due to nature of failure causing only a slight customer annoyance. Customer will probably notice only a minor degradation of the service performance, or a slight impact on a subsequent action; i.e., some quick, minor rework.	**2**
Moderate	Failure causes some customer dissatisfaction. Customer is made uncomfortable or is annoyed by the failure. Customer will experience some very noticeable inconvenience or performance degradation. May cause either delay due to rework or irreversible damage.	**4,5,6**
High	High degree of customer dissatisfaction due to the negative impact of the failure such as an innacurate payroll run, loss of vital data or an inoperable convenience system (i.e., computer crashes). Does *not* involve safety or noncompliance to government regulations. May cause serious disruption to subsequent processing; may require major rework or loss to customer and/or create significant financial hardship.	**7,8**
Very High	Failure mode involves serious personal safety hazards, potential for civil litigation or noncompliance with government regulations.	**9,10**

Figure 42: FMEA risk severity chart [14]

Probability of Failure	Ranking	Possible Failure Rates
Remote: Failure is unlikely. No failures ever associated with almost identical processes.	**1**	<1 in 20,000
Very Low: Process is in Statistical Control. Only isolated failures associated with almost identical processes.	**2**	1 in 20,000
Low: Process is in Statistical Control. Isolated failures associated with similar processes.	**3**	1 in 4,000
Moderate: Generally associated with processes similar to previous processes which have experienced occasional failures, but not in major proportions. Process is in Statistical Control.	**4** **5** **6**	1 in 1,000 1 in 400 1 in 80
High: Generally associated with processes similar to previous processes that have often failed. Process is not in Statistical Control.	**7** **8**	1 in 40 1 in 20
Very High: Failure is almost inevitable.	**9** **10**	1 in 8 1 in 2

Figure 43: FMEA risk frequency chart [14]

Likelihood of Detection		Ranking
Very High	Current controls will almost certainly prevent the failure (process automatically prevents most failures)	1,2
High	Current controls have a good chance of detecting the failure.	3,4
Moderate	Current controls may detect the failure.	5,6
Low	Current controls have a poor chance of detecting the failure.	7,8
Very Low	Current controls probably will not detect the failure.	9
Absolute Certainty of Non-Detection	Current controls will not or cannot detect the failure.	10

Figure 44: FMEA risk detection chart [14]

These charts are relatively standardized and have guided the selection of the FMEA numbers. To properly mitigate the key risks, the new design is lighter in weight while maintaining the strength and reliability of the existing device. It must be noted that even though we have potential death in the case of operating failure, the precautions in place ensure the likelihood is low, so the risks are at an acceptable level. TABLE XIII shows the FMEA for the new design.

TABLE XIII: FMEA OF NEW DESIGN

Component	Potential Failure Mode	Potential Effect	Severity	Potential Causes	Freq.	Current Controls	Detection	RPN	Action Recommendations
Bottom Clamp	Dropped during transportation	1. Crushed fingers 2. Broken bones 3. Damage to device 4. Damage to surroundings	4	1. Distance to travel is too long	2	1. PPE of crew members	5	40	None; Risk Frequency and Damage are negligible
	Dropped during installation	1. Crushed fingers 2. Broken bones 3. Damage to device 4. Damage to surroundings	4	1. Installation time is too long	2	1. PPE of crew members 2. Procedure calls for 2 crew members to install	3	24	None; Risk Frequency and Damage are negligible
	Failure during operation 1	1. Death if in the line of fire 2. Significant damage to surroundings including field pole and generator	10	1. Object does not meet yield criteria 2. Object was not installed correctly 3.Object had corrosion 4. fatigue damage 5. failure from crack damage	1	1. PPE of crew members 2. Procedure calls for 2 crew members to install with specific installation procedure (same as original design) 3. Paint to defend against corrosion of the device 5.Yield criteria validated through FEA testing 6. Fracture failure evaluated through FEA testing 7. Fatigue analysis	4	40	None; risks do not effect end user
	Failure during operation 2	1. Death if in the line of fire 2. Significant damage to field pole	10	1. Object does not meet yield criteria 2. Object was not installed correctly 3.Object had corrosion 4. fatigue damage 5. failure from crack damage	1	1. PPE of crew members 2. Procedure calls for 2 crew members to install with specific installation procedure (same as original design) 3. Paint to defend against corrosion of the device 5.Yield criteria validated through FEA testing 6. Fracture failure evaluated through FEA testing 7. Fatigue analysis	4	40	None; risks do not effect end user
	Failure during operation 3	1. Death if in the line of fire 2. Significant damage to field pole	10	1. Object does not meet yield criteria 2. Object was not installed correctly 3.Object had corrosion 4. fatigue damage 5. failure from crack damage	1	1. PPE of crew members 2. Procedure calls for 2 crew members to install with specific installation procedure (same as original design) 3. Paint to defend against corrosion of the device 5.Yield criteria validated through FEA testing 6. Fracture failure evaluated through FEA testing 7. Fatigue analysis	4	40	None; risks do not effect end user

TABLE XIII shows how both the transportation and operation of the new bottom clamp have a reduced risk compared to the original design. The new design targets the frequency and severity of transportation and installation failure, and using a lighter device decreases the associated risk priority numbers to 40 and 24, respectively. The risk priority numbers have increased for the three operation failure modes, because the new controls are less effective than the original design. Since the new design has not been field tested, there is a greater potential for failure compared to the original design. However, there are many other controls that have been put into place in this report to ensure that the device will not fail. Therefore, this risk is considered negligible because of the analysis, so the new design is safer than the existing device.

Using an FMEA ensures that the client's need of the bottom clamp being safer in operation is fulfilled. By mitigating the transportation and installation risks, while not excessively increasing the risk of failure during operation, the risk is not an immediate safety concern.

10. Final Specifications

With the design presented and the analysis validated, the final specifications are compared to the target specifications to verify that our design meets the customer's needs. TABLE XIV shows the marginal, ideal and actual values of the final design.

TABLE XIV: FINAL SPECIFICATIONS

Metric #	Metric	Units	Imp	Marginal value	Ideal value	Actual value
1	Total weight	lbs	5	70	35	35
2	Number of parts in design	# of parts	2	6	4	6
3	Number of workers to install	# of people	5	3	2	2
4	Cycles to failure	Cycles	4	500 cycles	∞	∞
5	Strength under loading	Factor of safety	3	3	3	3
6	Device setup time	Minutes	5	10	2-3	6 est.
7	Unit manufacture cost	CAD	1	5000	2000	3280
8	Aesthetics	Subjective	1	1	2	2
9	Minimum width poles	in	5	1/2	1/2	1/2
10	Field poles sizes	# of applicable stations	1	1	1	1
11	Assembly/disassembly time	Minutes	3	5	4	4 est.
12	Minimum width of top and bottom clamps	in	5	7.5	7.5	7.5
13	Corrosion resistance	MPY (mils penetration per year)	3	0.2	0.1	0.1
14	Material density	$\mathrm{kg/m^3}$	4	7750	<7750	<7750

All highlighted values are values that we did not meet, when we originally submitted our proposal to the client. All category 5 levels that are achievable, based on the constraints and limitations have been met. The set up and assembly times could not be commented on because a prototype has not been made. That being said, since the device is much lighter than the original, we can assume that both of those

times will be less than the marginal values of the original design. For purposes of manufacturability, the number of different parts in the design is the same as the original design. There would be no advantages of attempting to decrease the number of parts as they are all waterjet cut or lathed. There are no subassemblies in the original or current design, meaning the simplicity of the device cannot be improved. Finally the cost of the final design is a little higher than ideal value. The cost overage is acceptable as confirmed by the client.

11. Summary

The purpose of this project is to analyze the existing field pole lifting device at Manitoba Hydro's Grand Rapids Generating Station as well as to design a solution to improve the safety and ease of use of the device. Our final design has addressed the safety risks, through FEMA analysis, to provide a safer design, while mitigating the risk of the design. Manitoba Hydro has received detailed drawings, hand calculations of our design, CAD models of the part and FEA showing that the design meets all constraints and limitations.

This report dealt with all aspects of the design process. The report first provides background information about the problem and gives the purpose statement and the project objectives. The report outlined the project by listing the needs and the target specifications, the project and deliverables schedule, and presented the group's research. This research included comparisons of materials and all applicable industry standards. This section also developed the basis for hand calculations later used to provide a starting point for FEA models.

With this background supplying the context, the report turned to concept generation, to which TRIZ was applied to preliminary designs. These ideas were screened using decision matrices and were combined into three concept designs. The final design was chosen because of its simplicity and ability to meet all of the client's needs.

The final design met all category five needs and metrics including a total weight of 35 lbs, a total of two workers for installation and operation, and all sizing requirements. It is not possible to tell if it will meet the assembly and installation times, because a prototype has not yet been developed. The design is to be made out of six different waterjet cut parts and welded into one assembly to ensure maximum simplicity, accuracy, and precision, while minimizing the overall cost of the device.

The design has been validated using hand calculations and FEA analysis to ensure the 1/3 yield criterion, fracture analysis to determine the maximum crack length in high-stress areas, and fatigue analysis to ensure unlimited usage.

12. Works Cited

[1] Manitoba Hydro, "Producing Electricity," [Online]. Available: https://www.hydro.mb.ca/corporate/facilities/gi_producing_electricity.shtml. [Accessed 18 September 2015].

[2] Manitoba Hydro, "Power House Rotor Pole Lifting/ Handle, 1-00112-DC-76730-0004," unpublished.

[3] J. Bunkowsky, "Rotor Pole Removal Powerpoint," unpublished.

[4] Manitoba Hydro, "Mechnical Stress Analysis Standard Revsion 00," December 2, 2013. Unpublished.

[5] ASME, "Below-The-Hook Lifting Device Design," 2014.

[6] Manitoba Hydro, "Weld Design Using FEA," Unpublished.

[7] "CSA G41.21," Portland Bold & Mfg. Co., 2015. [Online]. Available: http://www.portlandbolt.com/technical/specifications/csa-g40-21/. [Accessed 11 November 2015].

[8] Rubber Cal inc., "Skirtboard - SBR Rubber - 70A," 2014. [Online]. Available: http://www.rubbercal.com/industrial-rubber/rubber-shock-absorbers/skirtboard-sbr-rubber-70a.html. [Accessed 15 November 2015].

[9] 3M, "3M Neoprene High Performance Rubber & Gasket Adhesives 1300, 1300L," March 2015. [Online]. Available: http://multimedia.3m.com/mws/media/66251O/neoprene-hi-perf-rubber-gasket-adh-1300-1300l.pdf. [Accessed 15 November 2015].

[10] ANSYS, "Release Documentation for ANSYS," 1 September 2015. [Online]. Available: http://www.ansys.com/Products/Simulation+Technology/Fluid+Dynamics/Specialized+Products/ANSYS+Polyflow/Features/Online+Help+&+Documentation. [Accessed 12 Octorber 2015].

[11] R. L. Mott, Machine Elements in Mechanical Design Fourth Edition, Colmbus: Pearson Prentice hall, 2004.

[12] ESAB Welding and Cutting Products, "ESAB Waterjet Knowledge centre," 6 August 2013. [Online]. Available: http://www.esabna.com/us/en/education/blog/how-much-does-waterjet-cutting-cost.cfm. [Accessed 15 November 2015].

[13] ESAB Welding and Cutting Products, Basic Welding Filler Metal Technology, 2000.

[14] V. Campbell, "Risk Assessment and Mitigation: Failure Modes and Effect Analysis (FMEA)," Winnipeg, 2015.

[15] Manitoba Hydro, "Powerhouse Rotor Pole Lifting Device As-Built Asembly & Details, 1-00112-DE-76730-0003," unpublished.

[16] Manitoba Hydro, "Cross-Sectional View General Arragement, 1-00112-DE-40000-0004".

[17] "3000 Series Wrought Alloys," 31 January 2003. [Online]. Available: http://app.knovel.com/web/view/pdf/show.v/rcid:kpMMPDSMM1/cid:kt003INR1P/viewerType:pdf/root_slug:metallic-materials-properties-3/url_slug:3000-series-wrought-alloys?cid=kt003INR1P&&issue_id=kt003INPI2&b-toc-cid=kpMMPDSMM1&b-toc-root-slug=metallic-materia. [Accessed 20 October 2015].

[18] "AISI 1025," 31 January 2003. [Online]. Available: http://app.knovel.com/web/view/pdf/show.v/rcid:kpMMPDSMM1/cid:kt003INPK1/viewerType:pdf/root_slug:metallic-materials-properties-3/url_slug:aisi-1025?cid=kt003INPK1&b-toc-cid=kpMMPDSMM1&b-toc-root-slug=metallic-materials-properties-3&b-toc-url-slug=aisi-10. [Accessed 20 October 2015].

[19] "Ti-6Al-2Sn-4Zr-2Mo," 31 January 2003. [Online]. Available: http://app.knovel.com/web/view/pdf/show.v/rcid:kpMMPDSMM1/cid:kt003INT3L/viewerType:pdf/root_slug:metallic-materials-properties-3/url_slug:ti-6al-2sn-4zr-2mo?cid=kt003INT3L&&issue_id=kt003INSY3&b-toc-cid=kpMMPDSMM1&b-toc-root-slug=metallic-materials-prope. [Accessed 20 October 2015].

[20] "Ti-13V-11Cr-3Al," 31 January 2003. [Online]. Available: http://app.knovel.com/web/view/pdf/show.v/rcid:kpMMPDSMM1/cid:kt003INT91/viewerType:pdf/root_slug:metallic-materials-properties-3/url_slug:ti-13v-11cr-3al?cid=kt003INT91&&issue_id=kt003INT03&b-toc-cid=kpMMPDSMM1&b-toc-root-slug=metallic-materials-properti. [Accessed 20 October 2015].

[21] MatWeb, "7000 Series Aluminum Alloy," MatWeb LLC., [Online]. Available: http://www.matweb.com/search/DataSheet.aspx?MatGUID=ab9706916818406b80c22b7f39db0c78. [Accessed 20 October 2015].

[22] L. MatWeb, "Low Carbon Steel," MatWeb, [Online]. Available: http://www.matweb.com/search/DataSheet.aspx?MatGUID=aa1c987a696e42bd95ddad57e5f3e1c7&ckck=1. [Accessed 20 October 2015].

[23] MatWeb, "Medium Carob Steel," MatWeb LLC., [Online]. Available: http://www.matweb.com/search/DataSheet.aspx?MatGUID=a2fe6ff24cf44bf1bdebf35b1b2b6259. [Accessed 20 October 2015].

[24] MatWeb, "Alpha/Near Alphat Titanium Alloy," MatWeb LLC., [Online]. Available: http://www.matweb.com/search/DataSheet.aspx?MatGUID=0626279b487341b386352fae80ba0574. [Accessed 20 October 2015].

[25] "AISI 4330 Alloy Steel," AZO Materials, [Online]. Available: http://www.azom.com/article.aspx?ArticleID=6670 . [Accessed 20 October 2015].

[26] MatWeb, "Titanium Ti-6Al-2Sn-4Zr-2Mo (Ti-6-2-4-2), Sheet," MatWeb LLC., [Online]. Available: http://asm.matweb.com/search/SpecificMaterial.asp?bassnum=MTA642. [Accessed 20 October 2015].

[27] M. Tuttle, Structural Analysis of Polymeric Composite Materials, New York: Marcel Dekker, 2004.

[28] B. Gryba, "The Design and Analysis of a Fibre Reinforced Polymer Wheel Assembly for use in an FSAE Vehicle," Mech 4162, Winnipeg.

[29] Hexcel, "Honeycomb Sandwich Design Technology," London, 2000.

[30] W. C. Young and R. G. Budynas, Roark's Formulas for Stress and Strain, New York: McGraw-Hill, 2002.

[31] Solid Creativity, "TRIZ 40," [Online]. Available: http://www.triz40.com/TRIZ_GB.php. [Accessed 10 October 2015].

[32] MatWeb, "6000 Series Aluminum Alloy," MatWeb LLC., [Online]. Available: http://www.matweb.com/search/DataSheet.aspx?MatGUID=b92d6bd5c3c24f58bcbe76c46ff0f496. [Accessed 20 October 2015].

[33] MatWeb, "AISI 4340 Steel, normalized, 100 mm (4 in.) round," MatWeb LLC., [Online]. Available: http://asm.matweb.com/search/SpecificMaterial.asp?bassnum=M434AE. [Accessed 20 October 2015].

[34] Dassault Systems, "SOLIDWORKS," 2015.

[35] CSA, "Welded Steel Construction (Metal Arc Welding)," 2008.

THIS PAGE WAS INTENTIONALLY LEFT BLANK

APPENDIX

Table of Contents

List of Figures

List of Tables

A.1 Material Selection

Each material has different combinations of mechanical properties that can be advantageous to loading devices. This section outlines which properties are most important to our design. Using decision matrices, properties can be weighted and prioritized. Materials can then be selected based on further weighted decision matrices. The materials considered and properties important to the design are listed in the Table I below.

Table I: PROPERTIES OF METAL MATERIALS SUITIBLE FOR LIFTING DEVICES

	Material		Yield (KSI)	Ultimate (KSI)	Shear (KSI)	Youngs Modulus (KSI)	Poisson Ratio	Hardness (Brinell)	Density (lb/in^3)	Cost (USD/kg)
1*	Steel	AISI 1025*	53.7 [1]	63.8 [1]	35 [2]	29700 [1]	0.29 [1]	126 [1]	0.284 [1]	0.436 [3]
2		AISI 4130	66.7 [4]	81.2 [4]	54 [2]	29700 [4]	0.32 [4]	217 [4]	0.284 [4]	0.515 [3]
3		AISI 4340	103 [5]	161 [5]	132 [2]	29700 [5]	0.29 [5]	321 [5]	0.284 [5]	0.841 [3]
4	Aluminum	T6-6061	40 [6]	45 [6]	30 [6]	10000 [6]	0.33 [6]	105 [6]	0.0975 [6]	2.228 [3]
5		T7451-7010	61 [7]	71 [7]	41 [7]	10200 [7]	0.33 [7]	135 [8]	0.102 [7]	2.3 [3]
6	Titanium	Ti-6Al-2Sn-4Zr-2Mo	132 [9]	130 [9]	100[13]	16500 [9]	0.32 [9]	318 [4]	0.164 [9]	11.92 [3]
7		Ti-13V-11Cr-3Al	120 [10]	125 [10]	92 [10]	14500 [10]	N/A	400 [11]	0.174 [10]	14.86 [3]

* Benchmark Material

After all the material properties are gathered, a numerical analysis is done to determine the best material for our design. To establish the weighting criteria for the material properties, each property is compared to one another, as shown in TABLE II. From this it is found that the density of the material is the most important need, accounting for 25% of the weight. It is followed closely by the material yield strength at 21%. All though the ultimate shear strength property is considered as the least important it

is given 3% of the weight. This 3% is added after the other 6 properties are rounded totaling only 97% weight.

TABLE II: MATERIAL WEIGHTING MATRIX IN % FOR MATERIALS BASED ON CUSTOMER NEEDS

		Yield Strength	Ultimate Strength	Ultimate Shear Strength	Modulus of Elasticity	Density	Cost	Hardness	Manufacturability
	Criteria	A	B	C	D	E	F	G	H
A	Yield Strength		A	A	A	E	A	A	A
B	Ultimate Strength			B	D	E	F	G	H
C	Ultimate Shear Strength				D	E	F	G	H
D	Modulus of Elasticity					E	D	G	D
E	Density						E	E	E
F	Cost							G	H
G	Hardness								G
H	Manufacturability								
	Total Hits	6	1	0	4	7	2	5	3
	Weightings	0.21	0.03	0.03	0.14	0.25	0.07	0.17	0.1

The rating of each material property was normalized by dividing the property in question by the highest rated property in the same category. This results in the highest rating possible of 1. For example, to rate the yield strength of 66.7 ksi for AISI 4130 it was divided by 132 ksi, which is the highest yield strength of

all the materials considered. This results in a rating of 0.51. For density and cost the minimum value was divided by the property of the material in question because density and cost are to be minimized, while all other properties are to be maximized. The results and overall rating for each material are shown in Table III.

Table III: RATINGS OF EACH MATERIAL BASED ON WEIGHTED AND A NORMALIZED RATING.

Materials

		1*		2		3		4		5		6		7	
Criteria	**Weight**	**Rating**	**Score**	**Rating**	**Score**	**Rating**	**Score**	**Rating**	**Score**	**Rating**	**Score**	**Rating**	**Score**	**Rating**	**Score**
Yield Strength	0.21	0.41	0.09	0.51	0.11	0.78	0.16	0.30	0.06	0.46	0.10	0.97	0.20	0.91	0.19
Ultimate Strength	0.03	0.40	0.01	0.50	0.02	1.00	0.03	0.28	0.01	0.44	0.01	0.78	0.02	0.75	0.02
Ultimate Shear Strength	0.03	0.35	0.01	0.54	0.02	0.50	0.02	0.30	0.01	0.41	0.01	1.00	0.03	0.90	0.03
Modulus of Elasticity	0.14	1.00	0.14	1.00	0.14	1.00	0.14	0.34	0.05	0.34	0.05	0.54	0.08	0.47	0.07
Density	0.25	0.35	0.09	0.35	0.09	0.35	0.09	1.01	0.25	0.96	0.24	0.58	0.14	0.54	0.14
Cost	0.07	1.00	0.07	0.85	0.06	0.52	0.04	0.20	0.01	0.19	0.01	0.04	0.00	0.03	0.00
Hardness	0.17	0.32	0.05	0.54	0.09	0.80	0.14	0.26	0.04	0.34	0.06	0.80	0.14	1.00	0.17
Manu-facturability	0.1	1	0.10	1	0.10	1	0.10	0.8	0.08	0.8	0.08	0	0.00	0	0.00
Total Score		0.56		0.62		0.71		0.52		0.56		0.61		0.61	
Rank		6		2		1		7		5		4		3	

* Benchmark Material

A.2 Concept Generation

Using the research and the client's needs, general concepts can now be developed. The main focus of these concepts is to improve the bottom clamp of the lifting device. As mentioned in the background, this has caused previous safety incidents. To reduce the risk of constraining concepts, general brainstorming is performed. TRIZ analysis is used as a primary tool in generating a first set of designs. Screening these designs is then performed using a plus minus decision matrix against the benchmark/current design. The results from this preliminary screening gave 3 primary designs. Weighted design matrices rank these 3 primary designs that are further analyzed in this report.

A.2.1 Preliminary Designs with TRIZ Analysis

From analyzing the client's needs we came up with 5 initial designs that focused primarily on reducing the weight of the device and making the device safer to use in operation. Using a house of quality there are several correlations and contradictions within the needs. An example is decreasing the weight also decreases the strength. To properly analyze these contradictions TRIZ principles have been used.

TRIZ analysis is a set of 40 inventive principles that set up a 39 X 39 matrix. Rows of the matrix indicate the 39 system features that one typically wants to improve, such as speed, weight, accuracy of measurement and so on. Columns refer to typical undesired results. Each matrix cell points to principles that have been most frequently used in patents in order to resolve the contradiction. The TRIZ solutions for decreasing weight while maintaining strength are as follows [12]:

1. Change the material type
2. Change the curvature or shape of the design
3. Segmentation or break the object into multiple segments
4. Remove material where stresses do not occur

All of the relevant TRIZ solutions, for the contradictions of the priority 5 needs, are shown below. Green boxes represent an improvement from a solution, while red boxes represent a negative outcome from a solution. Blank boxes represent no change from a solution.

Table IV: ANALYSIS OF TRIZ SOLUTIONS VS. NEEDS.

Solution #	Solution	Weight	Strength	Safety	Simplicity
1	Change the material				
2	Change the shape of the design				
3	Segmentation				
4	Remove not needed material				
5	Make objects flexible				

The following concept designs are based on the TRIZ solutions that focus on improving the importance 5 needs all simultaneously without contradicting each other.

Design 1: Composite Material

The first design is a composite model that uses a carbon wafer base, with metal insert components. This design uses composites to significantly decrease the weight of the object. Some drawbacks are it is expensive and analysis of composite models is much more complicated and less defined than metals.

Design 2: Cut Out

Design 2 is a cut out version of the original design. This design uses different geometries as well as removed material where stress concentrations are low. The main drawback from this design is it will be tougher to manufacture and therefore more expensive.

Design 3: Hinge

Design 3 is the same design as the current design, but a hinge is attached to the rods in between the top and bottom clamp. The bottom clamp is now hinged and then attached to the other rod. This design focuses on ease of operation for the crewmembers installing the device. The primary drawback is the rod, where the hinge is attached, must still fit in the air gap to remove the field pole. Also, the bottom clamp is still very heavy during use.

Design 4: Multi Component

Design 4 is a multi-component design. It focuses on segmentation by using smaller pieces of lesser weight to increase safety. The primary drawback is that it is more complicated than the original design.

Design 5: Bend

Design 5 makes the bottom component's main face curved upward. This feature allows the design to be made out of less material and maintain its strength. The main drawback from this design is it will be tougher to manufacture and therefore more expensive.

A.2.2 Concept Screening

To properly screen these designs 2 screening matrices have been made. The first is a simple plus minus matrix ruling out some of the more undesirable designs. The second matrix weights each need and then ranks the designs based on their weighted matrix score.

The plus minus matrix shown below gives a plus or minus score compared to a benchmark. In this case, the benchmark is the current lifting device.

TABLE V: PLUS/MINUS DESCISION MATRIX FOR 5 INITIAL DESIGNS AND THE BENCHMARK

	Designs					
Needs	**1**	**2**	**3**	**4**	**5**	**Benchmark**
Light weight	+	+	0	0	+	0
Simple to use	0	0	0	-	0	0
Safe to use	+	+	+	+	0	0
Lifting device is reusable	-	0	0	-	0	0
Easily maintained	-	-	-	+	0	0
Does not damage surroundings	+	0	0	+	0	0
Maneuverable	+	+	0	0	0	0
Total plus	4	3	1	3	1	0

Total minus	2	1	1	2	0	0
Total	2	2	0	1	1	0

From this decision matrix there are two designs that are more favourable: the composite design and the cut out design. We use the needs from our needs statement as selection criteria. Certain needs are eliminated because they are not important to the overall design. All of the 1 importance level needs are removed as well as well as the strength to lift the field pole. Even though strength is given a 5 importance level in the customer needs, all of these designs will have to meet the strength requirement.

To further analyze which design is the most desirable, based on the client's needs, a standard weighted design matrix must be created. This matrix is more accurate because the needs or selection criteria are weighted from most important to least important. To weigh each need properly, the needs are compared against each other directly in a simple weight matrix as shown below.

TABLE VI: WEIGHTING MATRIX FOR CONCEPTS IN % BASED ON CUSTOMER NEEDS.

		Light weight	Simple to use	Strength	Safe to use	Lifting device is reusable	Easily maintained	Does not damage surroundings	Maneuverable
		A	B	C	D	E	F	G	H
A	Light weight		A	A	A	A	A	A	A
B	Simple to use			B	D	B	B	G	B
C	Strength				D	E	F	G	H
D	Safe to use					D	D	D	D
E	Lifting device is reusable						F	G	H
F	Easily maintained							G	F
G	Does not damage surroundings								G
H	Maneuverable								
	Total Hits	7	4	0	6	1	3	5	2
	Weightings (%)	25	14	0	21	4	11	18	7

As expected, the weight of the device is the most prominent need. Also, the strength of the device does not come up at all in the matrix. The reason for this, as stated before, is that the device only needs to meet the strength criterion, not surpass it. Therefore, the strength of the device is removed from the weighted design selection matrix.

With the weight of each need generated a complete weighted design selection matrix can be completed. Based on the plus minus matrix our team is evaluating 3 designs. They are the composite, multi component, and cut out designs. Using the weighted criteria, from TABLE VI, the following design matrix is generated:

TABLE VII: WEIGHTED NEED BASED DESIGN MATRIX WITH TOTAL SCORE AND RANK.

Concepts

		Composite Design		Cut Out Design		Component Design	
Needs	**Weight**	**Rating**	**Score**	**Rating**	**Score**	**Rating**	**Score**
Light weight	**25**	5	125	5	100	4	100
Simple to use	**14**	4	56	5	42	2	28
Safe to use	**21**	4	84	4	84	5	105
Lifting device is reusable	**4**	1	4	5	20	2	8
Easily Maintained	**11**	1	11	3	33	5	55
Does not damage surroundings	**18**	4	72	3	54	5	90
Maneuverable	**7**	5	35	4	28	4	28
Total Score		387		414		414	
Rank		2		1		1	

Using the weighted decision matrix, the component design and the cut design are the clear favourites.

To determine which design we will use moving forward, we must examine the matrix that define the client's needs. The importance level 5 metrics are as follows:

TABLE VIII: METRICS TABLE INCLUDING MARGINAL AND IDEAL VALUES

Metric #	Need #	Metric	Units	Imp	Marginal value	Ideal value
1	1, 7, 8, 9	Total weight	lbs	5	70	35
3	2, 4, 8	Number of workers to install	# of people	5	3	2
9	1, 7, 8, 11	Minimum width poles	in	5	5	1/2
12	1, 7, 8, 11	Minimum width of top and bottom clamps	in	5	7.5	5

Looking at the following metrics and their importance factor, it is clear that the cut out design is the most advantageous for this project. Using the cut out design we are able to meet all of the importance factor five metrics. The design will weigh around 35 pounds, require 2 workers to install, have a decrease in set up time and meet all constraints for this project. Using decision matrices, hand calculations, and quantifiable metrics our design moving forward for the bottom clamp is the cut out design. Hand calculations and FEA Optimization is completed to prove the feasibility of our design.

A.3 Hand Calculations Methodology

Our final design must meet the constraints set for them by the client. The constraint that requires the most analysis, because of the lifting device's complex shape, is the 1/3 yield criterion. To ensure the bottom clamp meets this constraint, large amount of hand calculations and FEA modelling must be completed. All other components of the device are considered to meet the 1/3 yield criterion because their geometry, material and loading have remained unchanged. The three most common loading scenarios that the bottom clamp will experience are:

1. Vertical loading of the clamps main plate experienced from field pole removal
2. Vertical loading of the rounded edges experienced from field pole storage
3. Vertical loading of the lifting devices forks during field pole storage

Four standard preliminary loading solutions are tested against all of the models to ensure that the design can accurately represent the three common loading scenarios. The four loading solutions are as follows:

1. A distributive load test with the full weight of the pole distributed across the bottom clamp
2. A concentrated load test of the holes in the bottom clamp to simulate the poles effect in the concentrated area
3. A concentrated load test on the bottom clamps rounded edge to simulate storing the poles
4. A concentrated load test on the bottom clamp supporting forks to simulate a worst case horizontal loading

Hand calculations are necessary to ensure that FEA solutions provide reasonable answers that are similar to the basic loading solutions in this section. It also must be noted that solutions 1 and 2 are super imposed to ensure a more accurate loading case.

A.3.1 Distributive Load Case

The simplest loading the lifting device can experience under vertical loading is a perfect distribution of the weight of the pole across the bottom clamp.

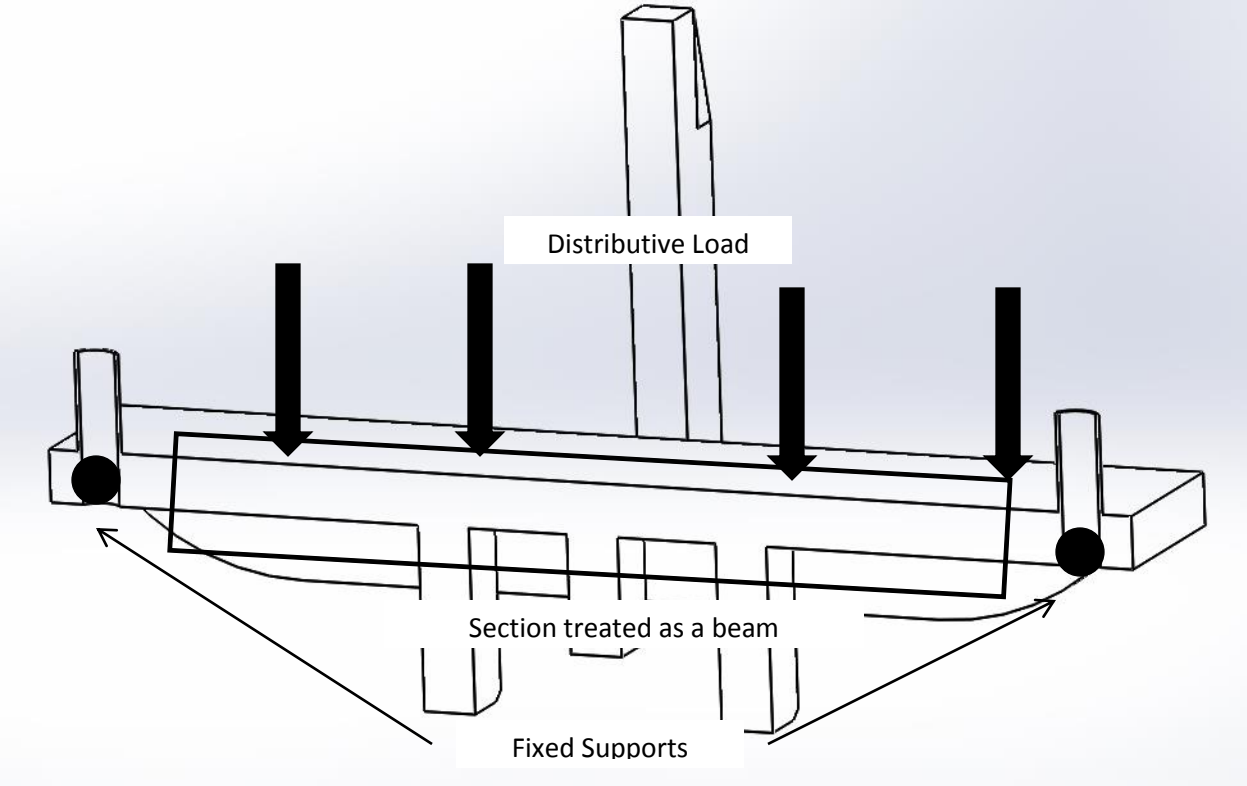

Figure 1: Cross section of view of the bottom clamp and the simplified loading scenario.

To simulate this loading, the clamp is modeled as a fixed beam with a perfectly distributed load.

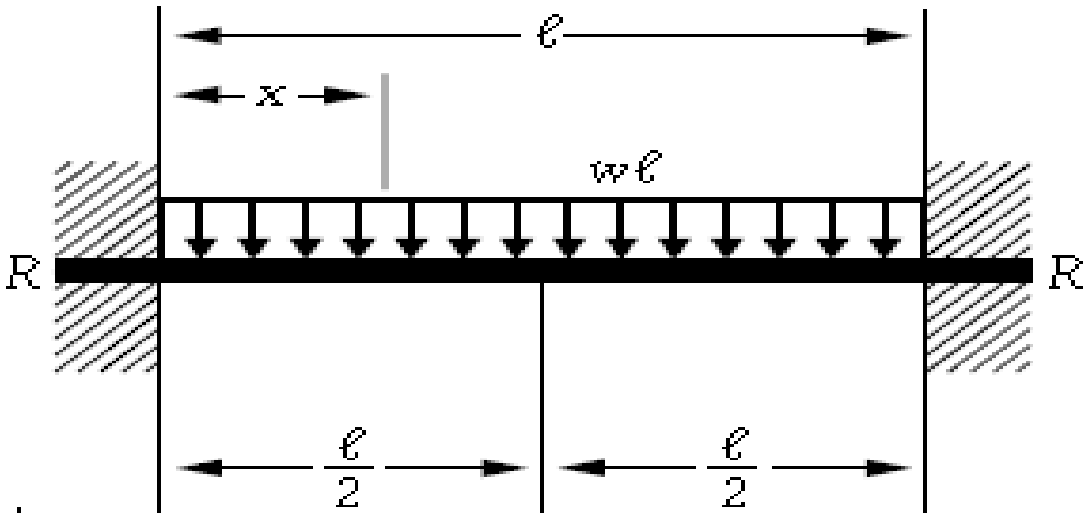

Figure 2: Simplified loading scenario of the bottom clamp during vertical lifting

This is an accurate representation of the loading happening in the middle of the device because the poles are symmetric and always supported near the middle of the device. The ends of the beam are considered fixed because the screws that support them resist both angle deformation and deflection. The maximum stress in the beam at the ends and the maximum in the centre can be governed by the following equations:

$$\sigma_{\text{at point x}} = \frac{W*l}{2*Z}\left(\frac{1}{6} - \frac{x}{l} + \left(\frac{x}{l}\right)^2\right) \quad \textit{Equation 1}$$

$$\sigma_{\text{ends}} = \frac{W*l}{12*Z} \quad \textit{Equation 2}$$

$$\sigma_{\text{centre}} = -\frac{W*l}{24*Z} \quad \textit{Equation 3}$$

In these equations, $\sigma_{at\ point\ x}$ is the stress at any point along the beam at a location x (ksi), σ_{ends} is the stress at the ends of the beam (ksi), σ_{centre} is the stress at the centre of the beam (ksi), W is load (lbs), l is the length (in), x is the location of where the stress is being analyzed (in), and Z is the section modulus of the cross section of the beam (in^3). Calculating Z is determined separately for each design concept and each geometry. These standard equations are used to calculate and compare to the stresses given by the FEA models.

A.3.2 Concentrated Hole Case

Analysing the stress concentration of the lifting rods on the bottom clamp is the second load scenario we have considered. The reasoning behind this is during vertical loading the stresses in this area are much higher than in the middle of the clamp. To ensure that the device meets the 1/3 yield criterion it must be able to withstand these loads.

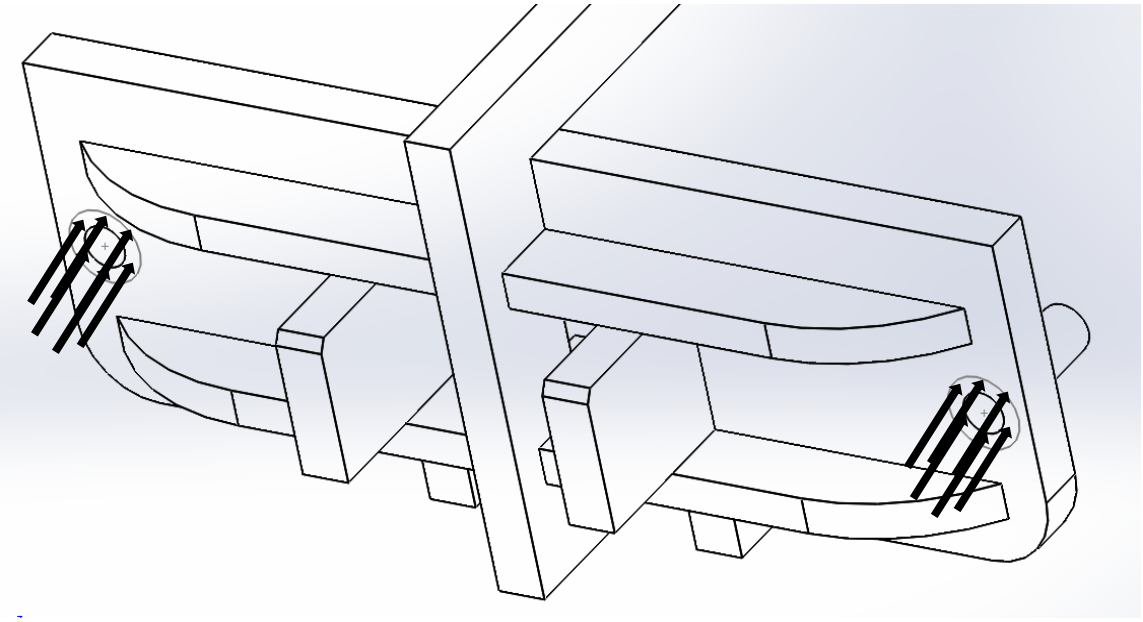

Figure 3: Simplified concentrated load scenario of the bolt's concentrated load during vertical loading.

The bolts apply compressive stress to an annular section of the clamp's plate, shown in the next figure.

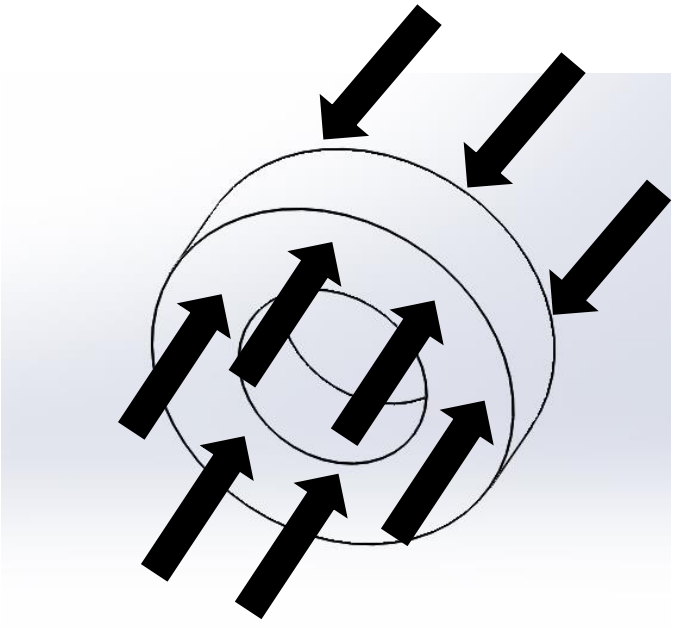

Figure 4: Simplified concentrated loading scenario is a 1D compression load of half the field poles weight.

To simplify this loading for hand calculations the nut that holds the bottom clamp in place applies the half of the full distributive load in the concentrated area. It becomes a simple 1D compression problem governed by the equation

$$\sigma_{\max} = \frac{F}{A} \qquad \textit{Equation 4} \text{ [13]}$$

where σ_{max} is the maximum stress (ksi), F is the load (lbs), and A is the area (in^2). These standard equations are used to calculate the state of stress analytically and to compare the FEA results.

A.3.3 Concentrated Round Edge Case

Analyzing the stress concentration of the rounded edges on the bottom clamp is the third load scenario we have considered. The reasoning behind this is that when the poles are stored, the full weight of the pole runs through the rounded edges to the ground, as shown in Figure 5 below. The stresses in this area are much higher than in the middle of the clamp. To ensure that the device meets the 1/3 yield criterion, it must be able to withstand these loads.

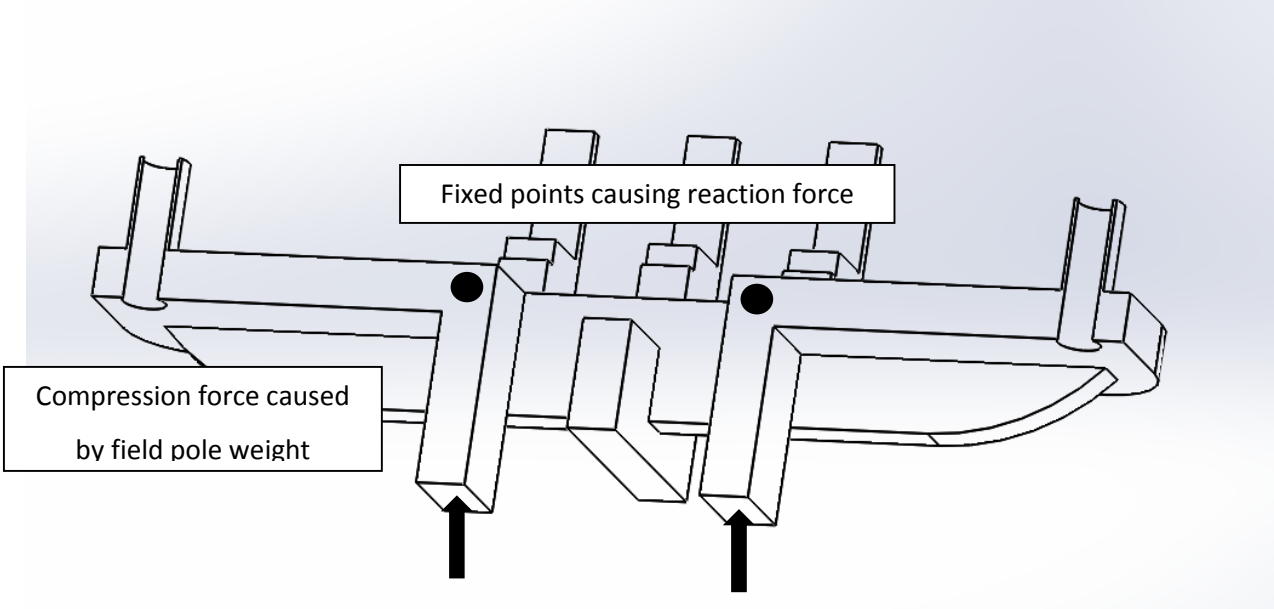

Figure 5: Simplified loading of the bottom clamp during storage of the field pole.

To simplify this loading for hand calculations the bottom clamp is considered to be a stepped flat plate with a known thickness. The load is considered to be a compressive load that is equally divided among the rounded edges. The gussets prevent the edges from buckling. The following equations define the loading of the device.

$$\sigma = \frac{F}{A_{min}} \qquad \textit{Equation 5}$$

$$A_{min} = d * h \qquad \textit{Equation 6}$$

In these equations, σ is the maximum stress in the edge (ksi), F is load (lbs), and h is the thickness (in). These standard equations are used to calculate and compare the stresses given by the FEA models.

A.3.4 Concentrated Fork Case

Analyzing the stress concentration of the forks on the bottom clamp during pole storage is the third load scenario. The reasoning behind this analysis is that when the poles are laid down, the full weight of the pole is distributed through the forks, as in Figure 6 below. The stresses in this area are much higher than in the middle of the clamp. To ensure that the device meets the 1/3 yield criterion it must be able to withstand these loads.

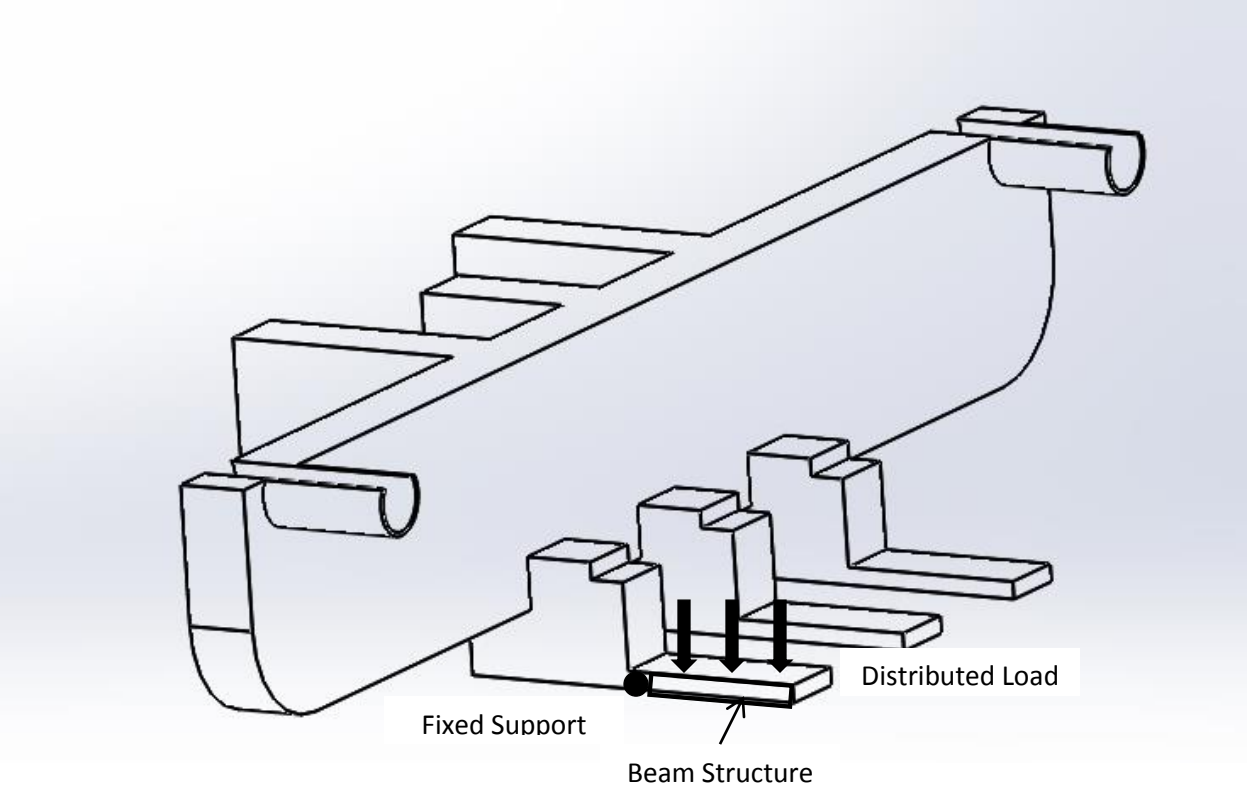

Figure 6: Cross section view of bottom clamp with simplified loading.

To simplify this loading for hand calculations, the forks are considered to be cantilever beams. The load is considered to be a distributive load on the thin portion of the fork. The weight of the pole is equally

divided among the forks on the top and bottom clamp. The left side of the beam is considered fixed and the left side's deflection angle is zero.

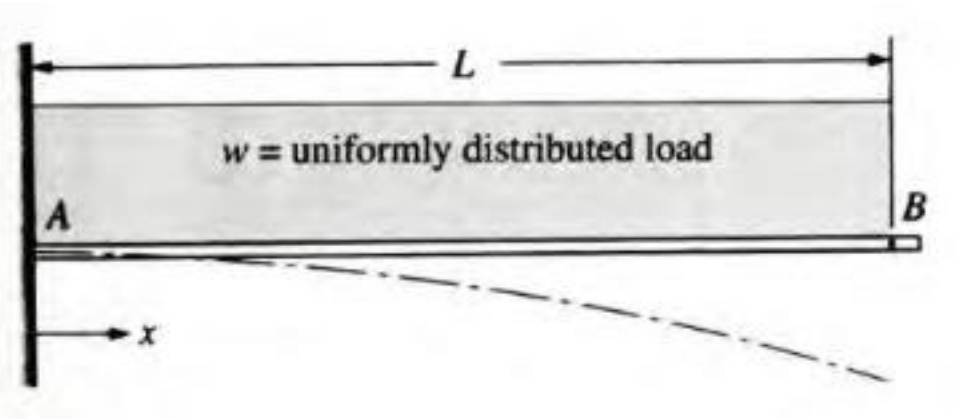

Figure 7: Simplification of the concentrated load for the forks on the bottom clamp [13].

The maximum normal stress, shear stress is determined by the following equations:

$$\sigma_{\text{norm max}} = \frac{\text{L}*\text{W}}{2*\text{Z}} \qquad \textit{Equation 7} \text{ [13]}$$

$$\tau_{\text{max}} = \frac{\text{V}*\text{Q}}{\text{I}*\text{t}} \qquad \textit{Equation 8} \text{ [13]}$$

$\sigma_{norm\ max}$ is the maximum normal stress (ksi), τ_{max} is the maximum shear stress (ksi), W is the load (lbs), L is the length (in), t is the thickness of the fork (in), Z is the section modulus of the cross section of the beam (in3), and I is the second moment of inertia of the fork (in4). Z and Q are determined separately for each design concept and are calculated in those sections. These standard equations are used to calculate and compare to the stresses given by the FEA models. For beams in distributive loading the maximum possible stress is the normal stress at the end of the beam as shown in the equation above.

To improve the original lifting device a proper analysis of the current device's stress distribution must be made. Using the calculations established in the prelim calculations general maximum stresses and geometries can be determined. These are expanded in preliminary FEA solutions for 3 different loading scenarios that the device experiences. Using the FEA calculations we are able to determine how much stress the current device experiences and what the current yield criteria is. The new designs incorporate this analysis decrease the over built yield criteria from the current design to our desired number of 1/3.

A.3.5 Old Design Hand Calculations

Using the four different loading conditions in section 8, the stress distribution can be calculated. The material of the existing device can assumed to be AISI 1025 [ref]. The maximum stresses are determined from the known geometries of the existing device and are shown below:

Case 1 using Equation 1 to determine the maximum stress:

Where Wis 2715 lbs, l is 19.5 in and $Z = \frac{bh^2}{6}$ where b is 7 in and h is 1 in.

$$\sigma_{\text{ends}} = \frac{\text{W}*\text{l}}{12*\text{Z}} = \frac{2715*19.5}{12*Z} = \frac{2715}{12*\frac{7}{6}} = 3782 \text{ PSI}$$

Case 2 using Equation 4 to determine the maximum stress:

Where F is half of 2715 lbs because the load is equally distributed. $A = \pi * \left({R_{outer}}^2 - {R_{inner}}^2\right)$; where R_{outer} is determined by the hex nut size 7/8 in which has an outer diameter of 1 1/8 in and R_{inner} is 7/8 in.

$$\sigma_{\text{max}} = \frac{\text{F}}{\text{A}} = \frac{2715}{2*\pi*(1.125^2 - .75^2)} = 614 \text{ PSI}$$

Case 3 using Equations 5-7 to determine the maximum stress:

Where F is half of the weight 2715 lbs and t is 1 in and h is 7.375 in.

$$\sigma_{norm} = \frac{F}{A_{min}} = \frac{2715}{2*7.375} = 184 \text{ PSI}$$

$$A_{min} = t * h = 1 * 7.375 = 7.375 \ in^2$$

Case 4 using Equation 8 to determine the maximum stress:

Where Wis 2715 lbs split between the six forks on the top and bottom clamp, l is 1.5 in and $Z = \frac{bh^2}{6}$ where b is 1 in and h is .75 in.

$$\sigma_{\text{norm max}} = \frac{L * \text{W}}{2 * \text{Z}} = \frac{1.5 * \frac{2715}{6}}{2 * \frac{1 * .75^2}{6}} = 2899 \text{ PSI}$$

Using all of the calculated stress the relative yield criteria for all of the different components of the bottom clamp can be calculated. The yield criteria of each component is shown below.

Table IX: YIELD CRITERIA OF EACH COMPONENT BASED ON PRELIMINARY CALCULATION LOADING SCENARIOS

Case #	Component	σ_{max} (PSI)	σ_{yld} (PSI)	Yield Criteria
1	Middle Plate (worst case)	3782	53700	7/100
2	Middle Plate	614	53700	1/100
3	Rounded Edges	184	53700	3/1000
4	Horizontal Forks	2899	53700	6/100
5	Middle Plate Combined	4396	53700	8/100

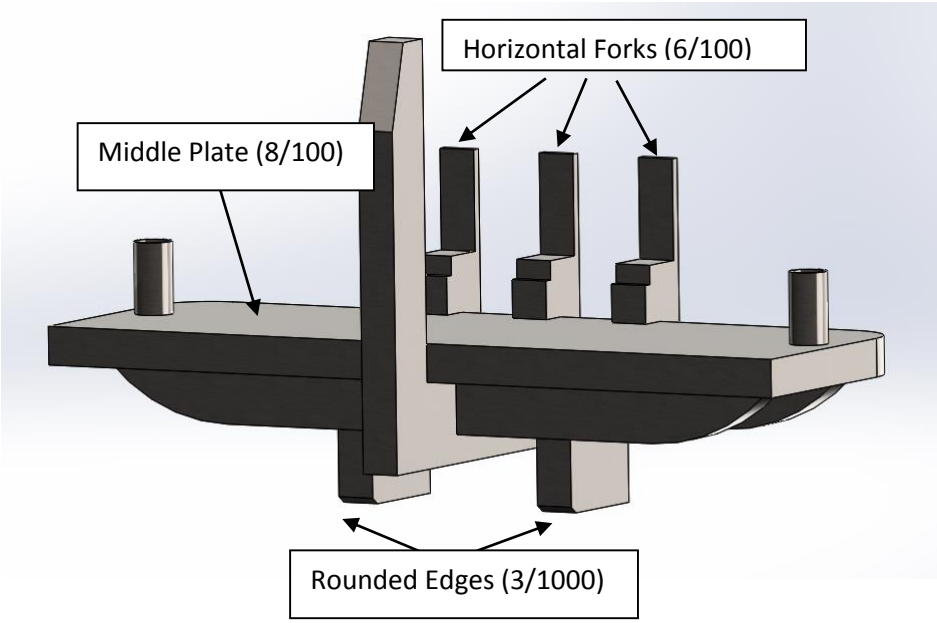

Figure 8: Location of components and corresponding yield criteria.

Since the yield criteria is much lower than 1/3 there are many modifications that can be made to the old device that will lower its weight. The design is over built and a material with less strength or removing material in over built is a possible solution and is further explored in several of our concept designs. The yield criteria generated from these calculations must be verified with FEA solutions.

A.4 Conceptual Design Carbon Fiber

The first conceptual design strives to improve on the existing lifting device design by drastically changing the material used. The goal is to utilize a material that has a much higher strength to density ratio than the low carbon steel used currently. While conventional materials where investigated in section 8, a more extreme approach will be undertaken with conceptual design 1. This design utilizes the extremely high strength to density ratio of carbon fiber. Carbon fiber presents a host of short comings when used by itself but when combined with a polymer it forms a composite (Carbon Fiber Reinforced Polymer [CFRP]) which has optimal structural properties. The biggest complication in using CFRP in design is its anisotropic material properties. In this section the CFRP material properties will be investigated as well as a simplified Composite Laminate Theory (CLT) analysis for the purposes of this conceptual design. Furthermore, the limitations of implementing a CFRP material for the design of the lifting device will be investigated.

A.4.1 Carbon Fiber Reinforced Polymer (CFRP) Material Properties

For this conceptual design, the unique material properties of Hexcel-W3T282-F155 must be identified, as the properties are required in order to complete the analysis of the CFRP design concept 1. These properties include E_{11}, E_{22}, v_{12}, v_{21}, and G_{12} and are summarized in TABLE X. It is to be noted that temperature and moisture effects will not be considered. This is because the possible range of these effects is very large and the calculations being performed for the preliminary concept design are to be simplified. This being considered the moisture and temperature effects will be included in the case that this design is chosen moving forward into the final design.

TABLE X: HEXCEL - W3T282-F155 MATERIAL PROPERTIES **Invalid source specified.**

Material Properties – Hexcel-W3T282-F155

E_{11}	E_{22}	v_{12}	G_{12}	α_{11}	α_{22}	β_{11}	β_{22}
5.11E+10	5.11E+10	6.00E-02	2.91E+09	0	0	0	0

For this conceptual design it must be understood that the CFRP is a anisotropic material and as such the properties listed will change drastically depending on the orientation of the fibers. A detailed

explanation of how these calculations are performed is included in APPENDIX A2. For our analysis Figure 9 to Figure 17 illustrate the required material properties and their dependence on the fiber orientation.

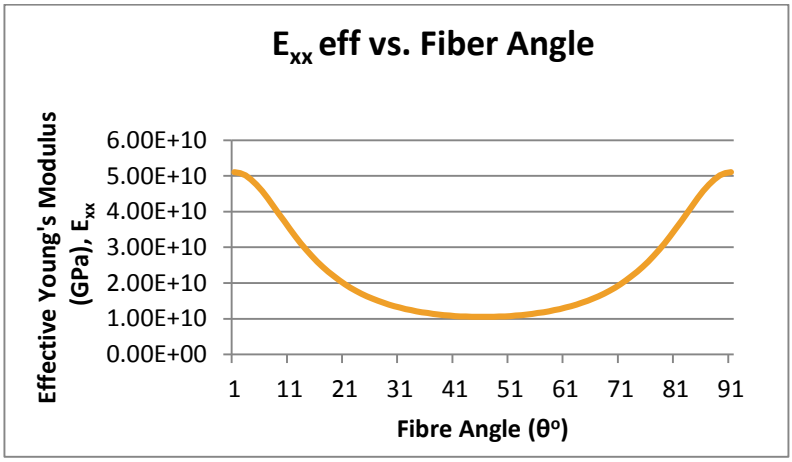

Figure 9: E_{xx} eff vs. Fiber Angle

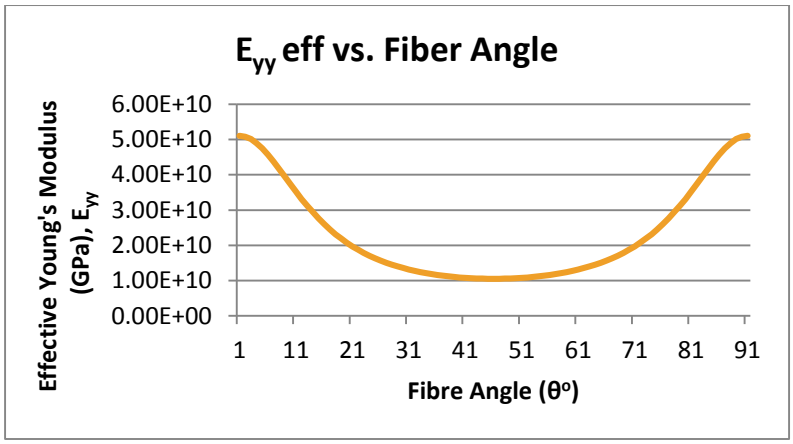

Figure 10: E_{yy} eff vs. Fiber Angle

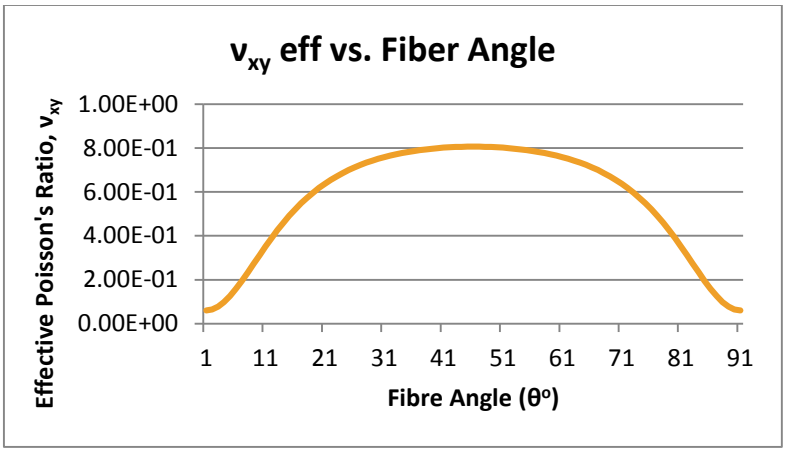

Figure 11: v_{xy} eff vs. Fiber Angle

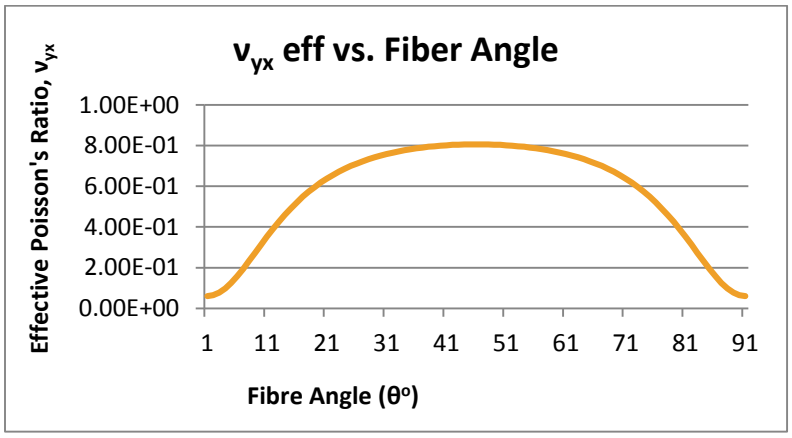

Figure 12: v_{yx} eff vs. Fiber Angle

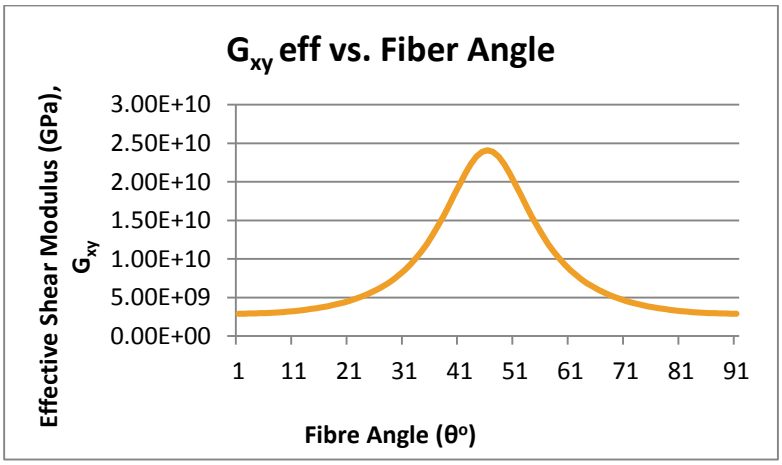

Figure 13: G_{xy} eff vs. Fiber Angle

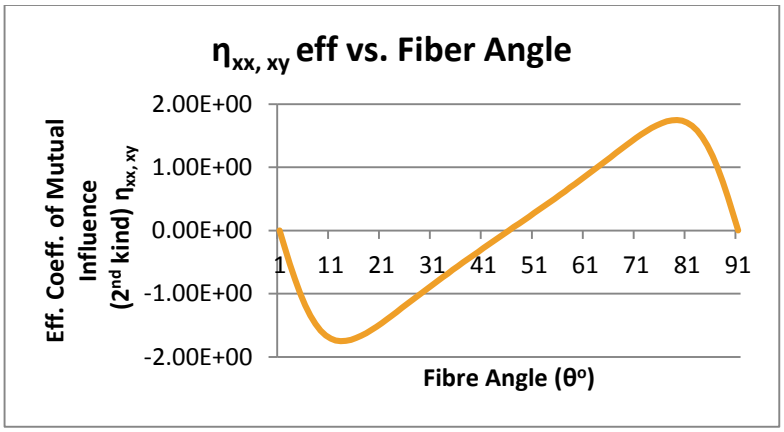

Figure 14: $\eta_{xx,\,xy}$ eff vs. Fiber Angle

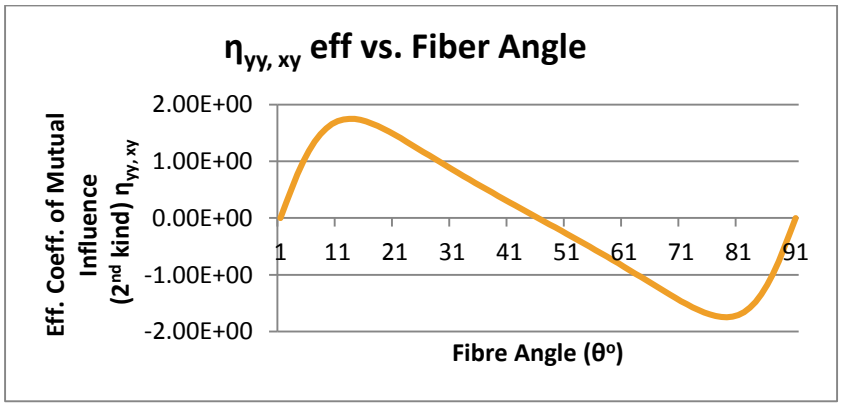

Figure 15: $\eta_{yy,\,xy}$ eff vs. Fiber Angle

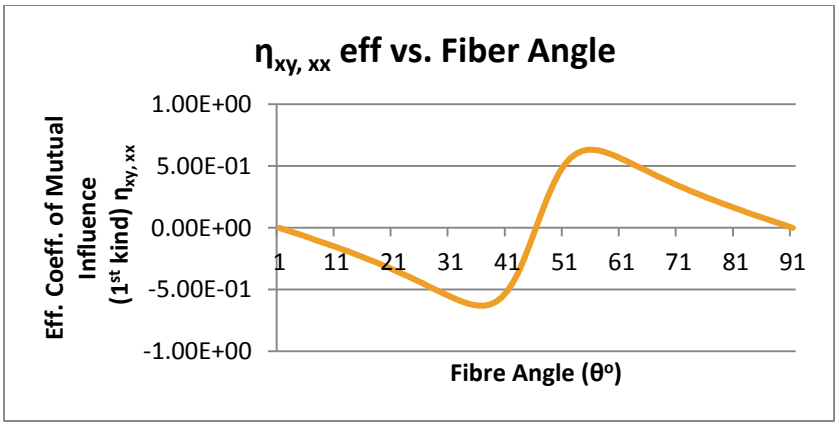

Figure 16: $\eta_{xy,\,xx}$ eff vs. Fiber Angle

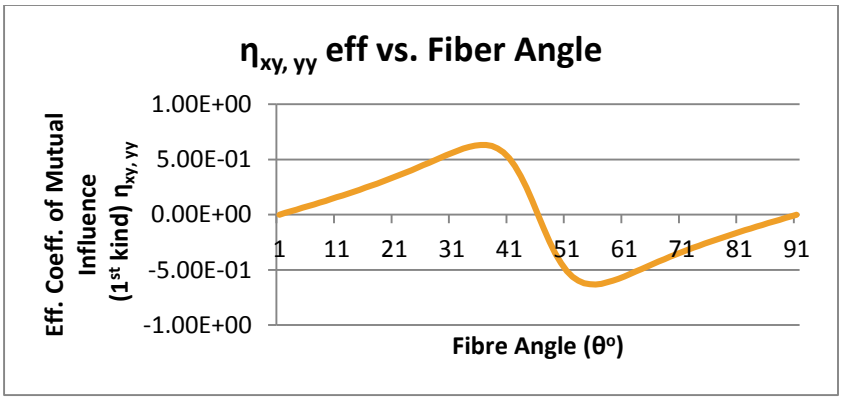

Figure 17: $\eta_{xy,\,yy}$ eff vs. Fiber Angle

A.4.2 CORRITE Structural Foam Core Material Properties

The basic principal of introducing a core material to the CFRP is to spread out the very stiff composite material by adding a very lightweight material between the plies. By classical beam theory this effectively increases the stiffness of the panel without increasing he weight substantially. The material properties for the proposed structural foam core can be seen in TABLE XI.

TABLE XI: CORRITE STRUCTURAL CORE MATERIAL PROPERTIES

200 Grade CORRITE Structural Foam	Units	
Nominal Density	Lb/ft3	20
	Kg/m3	320
Shear Strength	psi	740
	MPa	5.1
Shear Modulus	psi	9572
	MPa	66
Shear Elongation at break	%	19
Compressive Strength	psi	1247
	MPa	8.6
Compressive Modulus	psi	34519
	MPa	238
Flexural Strength	psi	1450
	MPa	10
Flexural Modulus	psi	42786
	MPa	295
Tensile Strength	psi	960
	MPa	6.6
Tensile Modulus	psi	7650
	MPa	52.7

A.4.3 Composite Laminate Theory (CLT) Geometric Simplification

By simplifying the geometry to a sandwich panel beam, as seen in Figure 18 with the L direction is at least three times longer than the "b" direction, The CLT analysis can be simplified from the calculations presented in APPENDIX A2. More specifically a sandwich panel is made up of two "skins" located on the outside of the structure that are made out of composites, in our case CFRP, and a central core material. The function of the composite skins is to support the tension and compression loads from bending and the function of the core material is to support the shear force that flows through the structure. In this aspect a sandwich panel functions very similarly to an I-beam.

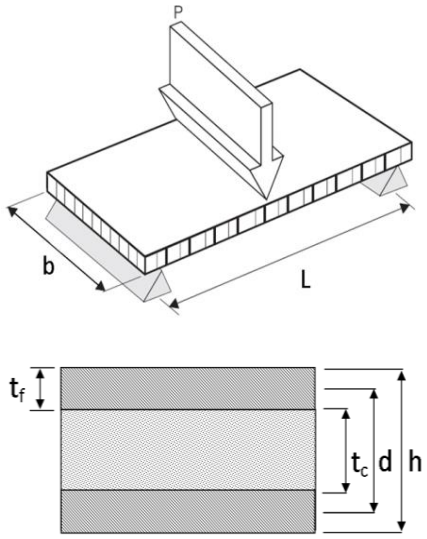

Figure 18: Simplified sandwich panel beam geometries.

The beams flexural rigidity is one of the first simplifications and is denoted by "D". The following equation can be used to calculate the flexural rigidity of a sandwich beam.

$$D = \frac{E_s b t_f{}^3}{6} + \frac{E_s b t_f d^2}{2} + \frac{E_c b t_c{}^3}{12}$$

Shear Stiffness can be calculated using the following equation. It should be noted that the shear stiffness is a property of the structure, while the shear modulus is a property of the specific material.

$$S = \frac{b d^2 G}{t_c}$$

Using the flexural stiffness and the shear stiffness of the sandwich beam the deflection can be calculated from the following equation.

$$\delta = \frac{k_b PL^3}{D} + \frac{k_s PL}{S}$$

k_b and k_s are deflection coefficients that have been calculated experimentally for different test geometries[9]. For the analysis of a simply supported beam in a three point bend, k_b and k_s are equal to 1/48 and 1/4 respectfully.

The stress in the face of the skin, or the facing stress for short, can be calculated using the following equation. Where "M" is the maximum bending moment and for a centrally loaded simply supported beam, as illustrated in Figure 18, is equal to PL/4.

$$\sigma_s = \frac{ME_s h}{2D}$$

The shear stress supported by the core can be calculated from the following equation.

$$\tau_c = \frac{Q}{D}\left(\frac{E_s t f_d}{2} + \frac{E_c}{2}\left(\frac{{t_c}^2}{4} - y^2\right)\right)$$

E_c must be taken as the in-plane core modulus, that is in the same direction as L. Q is the maximum shear force and for a centrally loaded simply supported beam is equal to P/2. Calculating the core shear stress can also be simplified when E_c is small and the skins are thin by using the following equation.

$$\tau_c = \frac{Q}{bd}$$

Using these equations we can analyze conceptual design 1. The results from these calculations are shown in TABLE XII. From adding into this table the material properties of both the Hexcel - W3T282-F155 CFRP as well as the 280 grade CORRITE Structural Foam core material it is possible to analyze the simplified geometry's maximum load as well as the expected failure type (core failure or skin failure). Emphasise is put on the failure loads both for skin tension (highlighted in blue) and core crushing (highlighted in orange) as well as the overall weight of the design (highlighted in green).

TABLE XII: SIMPLIFIED CLT ANALYSIS OF CONCEPT DESIGN 1

Simple Support Sandwich Beams	**Hexcel - W3T282-F155**	**Corrite Structural Foam**
Sandwich Panel Dimensions		
Width of Beam (b)	7	[in]
Length of Beam (L)	21.375	[in]
Number of Plys (per Side)	11	
Ply Thickness	0.0087	[in]
Skin Thickness (tf)	0.0957	[in]
Core Thickness (tc)	0.75	[in]
C-C Skin Thickness (d)	0.8457	[in]
Total Thickness (h)	0.9414	[in]
y	0.42285	[in]
Applied Load	2715	[lbs]
Calculated Peak Loads	**Max Skin Load (M)**	**Max Core Load (Q)**
Max Load (P) [lbsf]	8358.03195	8761.452
Max Bending Moment (M)	44663.23323	[lbsf-in]
Max Shear Force (Q)	4380.726	[lbsf]
Load Magnitudes (M/Q)	10.19539529	
Material Properties		
Skin Modulus (Es)	8.00E+06	[psi]
Core Modulus (in plane) (Ec)	34519.00	[psi]
Core Shear Modulus (G)	9572	[psi]
Skin Stress (sigma_s)	87000	[psi]
Core Shear Stress (tau_c)	740	[psi]
Bending Deflection(kb)	0.020833333	
Shear Deflection (ks)	0.25	
Deflection (delta)	0.512808804	[in]

Governing Equations for Panel		
Flexural Rigidity (D)	1933147.943	[lbs-in^2]
Shear Stiffness (S)	63895.77289	[lbsf]
Weight Calculations		
Density (skin)	0.05780367	[lbs/in^3]
Density (core)	0.0115607	[lbs/in^3]
Area	149.625	[in^2]
Volume (skin)	28.638225	[in^3]
Volume (core)	112.21875	[in^3]
Weight Total	2.95272181	lbs

A.4.4 Further Design Aspects

The CFRP sandwich panel has a very high strength to weight ratio and performs very well under bending but the CFRP is known to perform poorly under a crushing load. To combat these poor compression properties metal inserts and teeth are added to withstand the crushing loads. The inserts are integrated into the core of the sandwich panel and support the crushing and bearing load experienced where the clamping rods are secured. The metal teeth are integrated onto the surface of the sandwich panel and serve multiple roles. The first is to withstand the compression load incurred when the field pole is lowered onto the power house floor and the second is to hold the field pole in place at all stages of the lifting procedure. To better understand conceptual design one a computer aided design model was constructed and is shown in Figure 19.

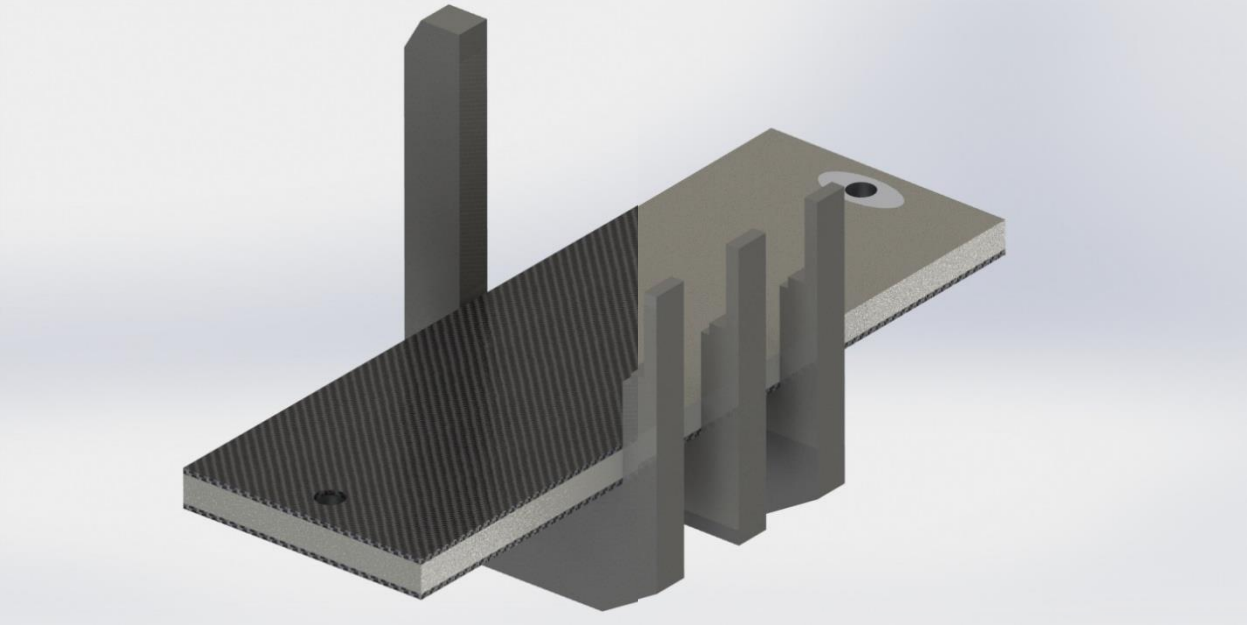

Figure 19: Conceptual design One CFRP sandwich Panel with cut out to show inserts and internal geometry

A.4.5 Limitations

While CFRP introduces a lot of positive design aspects they don't come without their drawbacks. The first drawback has already been discussed in the previous sections as the anisotropic material properties can create design challenges as well as directional dependencies and coupling. Other limitations include moister absorption, oil contamination, fracture propagation, impact failure, delamination, complexity and difficulty to inspect. This long list of short comings is difficult to overcome but a few of them are very impactful to the situation of the design. Moisture and oil absorption will be very detrimental to the design as it will be utilized in a hydro generating station where moisture is very prevalent and oil will get on the device at one point in the devices life. He moisture absorption will cause the structural properties of the design to change as well as the weight savings achieved will be slowly mitigated by the added weight of both the oil and moisture. Additionally the nature for the CFRP to fail due to impact will detrimental as the design will not be handled overly cautiously.

A.5 Concept Design 2 Analysis

Our final consists of the same features of the existing device but with smaller geometries. Since the existing device has very low stresses we can lighten the design by removing material while making sure the design still meets the ⅓ yield criterion. This device weights 36.4 lbs, very close to the target value of 35 lbs. However, this design is not optimized for the stress requirement, so the factor of safety is much larger than necessary.

The figure below shows the shape of the design. The design keeps all the geometric features of the existing device, including the tusks, ribs, and stiffeners, but reduces their size to lower the overall weight. The sizes of these geometries are based on hand calculations as well as an effort to use standard sizes and to avoid slender or non-compact sections.

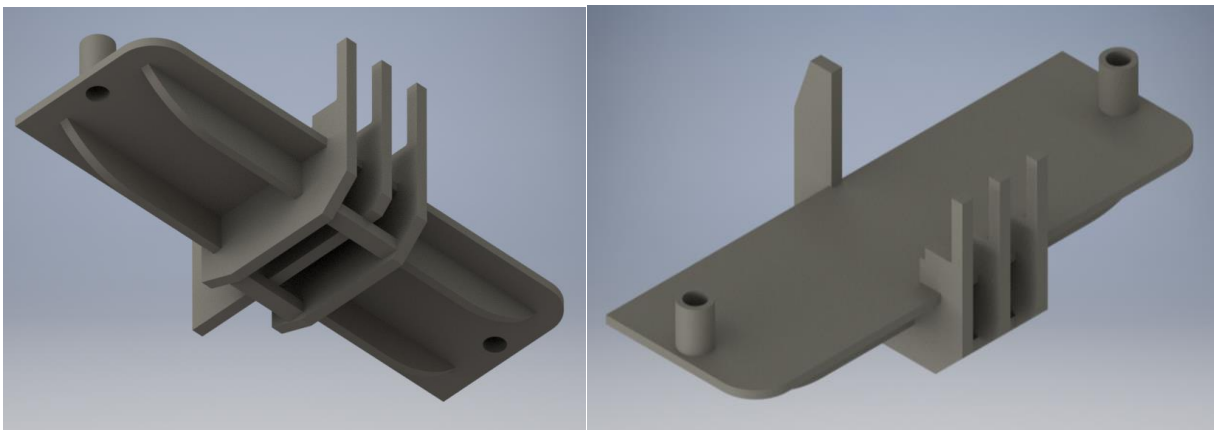

Figure 20: Two views of concept design 2

We can do hand calculations for several loading scenarios: the distributive load case, where the clamp is taken to be in bending, the concentrated hole case, where bending and compression act near the rod holes, the round-edge case, where the full weight of the pole is supported by the tusk ribs, and the fork case, where the forks are loaded with the full weight of the field pole. The bending analysis will ignore the effects of the ribs that protrude below the plate.

A.5.1 Distributive load case

In this case the clamp is loaded in bending with both ends fixed. For a beam of constant cross-section, the highest bending moment and stress occur in the middle. This design, however, has two different cross-sections. Ignoring the ribs, the middle of the clamp is a top plate with two stiffening bars. Beyond

the outer ribs, the cross-section becomes a pi-shaped beam due to the webs, which run along the length of the clamp.

The figure below shows the cross-section of the middle portion of the clamp. The stiffeners and the top plate are connected by the tusk ribs, but the bending resistance of the ribs are ignored in this analysis.

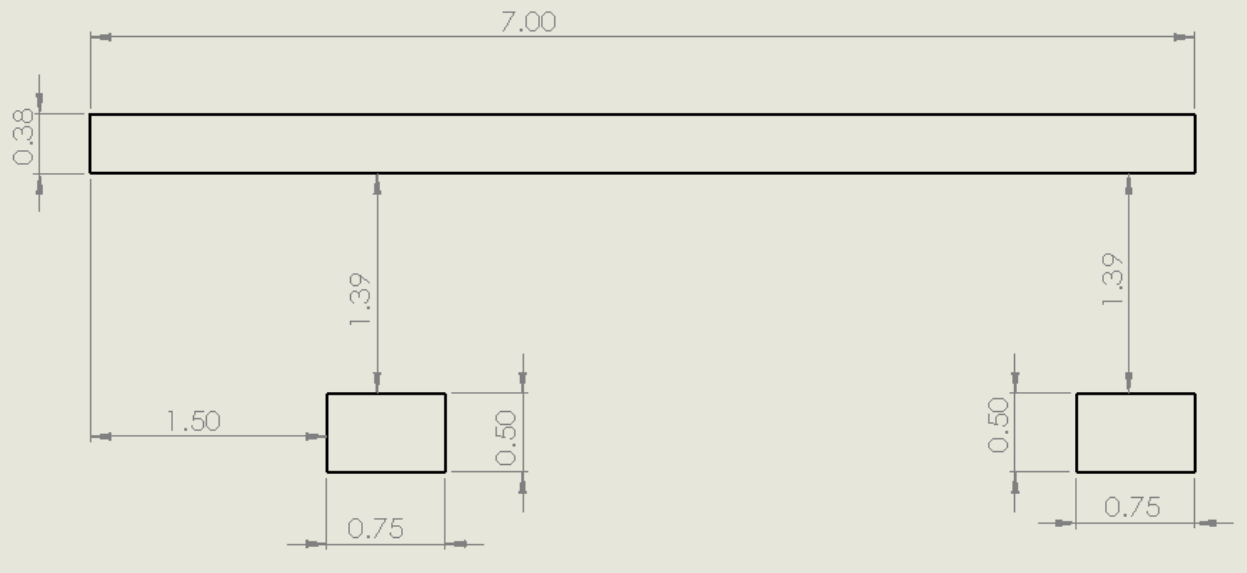

Figure 21: Cross-section of the middle portion of the clamp with dimensions in inches.

For the middle of the beam, equation 3 can be rewritten to find the section modulus in terms of allowable stress:

$$Z_{centre} = -\frac{\mathrm{Wl}}{24\sigma_{\mathrm{centre}}} \qquad \text{Equation 3a}$$

Using the properties of AISI 4130, we can calculate the minimum allowable section modulus to be

$$Z_{min,centre} = 0.0945\ \mathrm{in}^3$$

We can use this result to calculate the minimum dimensions for the stiffeners. This section modulus, however, results in a very small stiffener size. Since these stiffeners are useful for other loading scenarios and are so short that increasing their size makes little difference to the weight of the clamp, they will be given a larger, stock, size. Using the dimensions in Figure 21, the section modulus of this clamp section becomes

$$Z_{centre} = 0.682\ \mathrm{in}^3$$

which is well above the minimum required value.

The pi-shaped beam sees a different moment than the centre of the beam. The cross-section with dimensions is shown below:

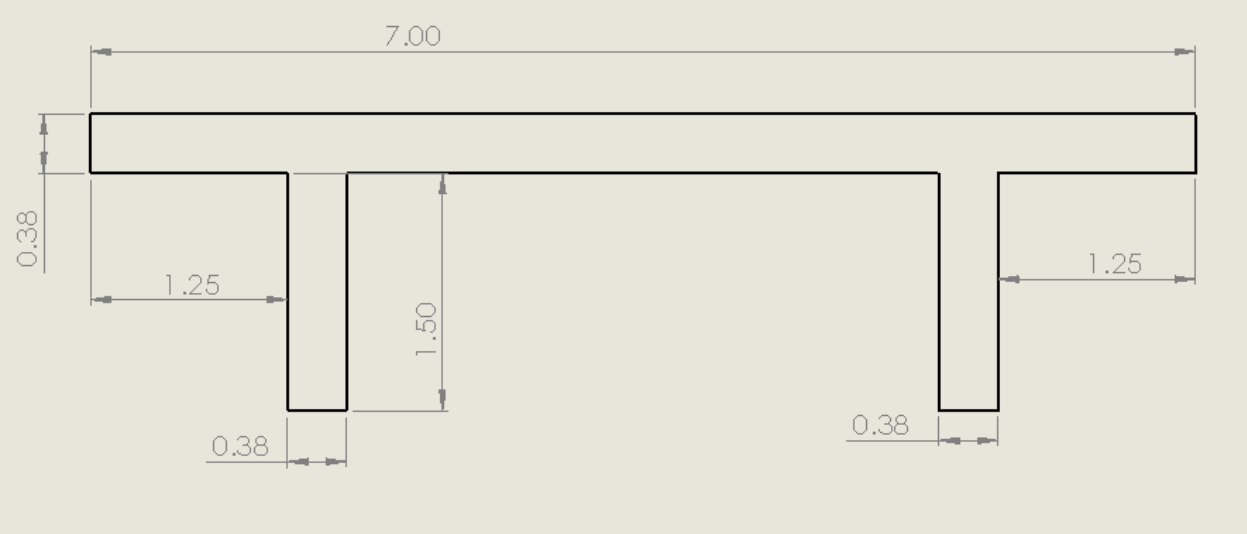

Figure 22: Dimensions in inches of the pi-shaped cross-section

Equation 1 can be rewritten in terms of allowable stress to yield the minimum required section modulus:

$$\mathrm{Z} = \frac{Wl}{2\sigma_{at\ point\ x}}\left(\frac{1}{6} - \frac{x}{l} + \left(\frac{x}{l}\right)^2\right) \qquad \text{Equation 3a}$$

The outer tusk ends 2¼" from the centre of the clamp, so

$$x = \frac{(19.5)}{2} - 2.25 = \ 7.5 \text{ in}$$

$$\mathrm{Z(x)} = \frac{Wl}{2\sigma_{at\ point\ x}}\left(\frac{1}{6} - \frac{x}{l} + \left(\frac{x}{l}\right)^2\right)$$

$$\mathrm{Z}_{min.pi-shape} = 0.0700 \text{ in}^3$$

Keeping the same plate size of ⅜" × 7" from the previous calculation and the existing web depth of 1½", the minimum web thickness is

$$t_{web,min} = 0.003\ in$$

This result is unrealistically small, indicating that the web thickness is limited by another factor. We instead choose a thickness of ⅜", giving the member a height-to-thickness ratio of four and leaving any

optimization to FEA results. This dimension avoids buckling and gives some useful torsion resistance in other loading scenarios. The associated section modulus is

$$Z_{pi-shape} = 0.644 \text{ in}^3$$

which is comfortably above the calculated minimum. The result is also similar to the section modulus in the centre of the clamp, so the stresses will be similar in both of those sections. The maximum bending stresses in both sections occur at the bottom of the clamp, in the stiffeners and the web, since these areas are the furthest from the neutral axis. These stresses can be calculated from Equations 3 and 3a to be

$$\sigma_{max,centre} = 3.23 \; ksi$$

$$\sigma_{max,pi-shape} = 2.88 \; ksi$$

These stresses are well below even the ⅓ yield criterion. More material reductions could be made here using a more detailed analysis, but since the dimensions are already small the weight reductions would also be small. In addition, structural failure modes like buckling may become important if more material is removed, and these geometries may be structurally significant in other loading scenarios.

A.5.2 Concentrated hole case

This loading case examines the stresses near the end of the clamp around the hole through which the rods pass. The stress in this scenario is the sum of the bending moment and the compressive force of the bolt head. The stress is given by

$$\sigma_{hole} = \frac{Wl}{12Z} + \frac{F}{A}$$

With a plate thickness of ⅜", section modulus of Z = 0.22 in^3, and a bolt head outer diameter of 1⅛",

$$\sigma_{hole} = \frac{(2715)(19.5)}{12(0.2)} + \frac{0.5(2715)}{2\pi(1.125^2 - 0.75^2)}$$

$$\sigma_{hole} = 20.36 \; ksi$$

This stress is relatively close to the design limit and is much higher than the rest of the clamp. This particular geometry will be important to model carefully, since the calculated stresses are very dependent on the model and the applied fixtures used to calculate stress.

A.5.3 Concentrated round edge case

This loading case is concerned with the buckling failure of the tusk ribs under the crushing load of the field pole, when the lifting assembly contacts the ground but is still vertical. Due to the effects of the stiffeners between ribs and the webs that run along the length of the clamp, the ribs will not fail in buckling. The stiffening elements will also avoid stress concentrations that would occur at the welds. This distribution of stress is too complicated for hand calculations, so FEA is needed to calculate it.

The stresses in the bottom of the ribs, then, are simply from the weight of the field pole. Ignoring stiffening elements, and assuming half the weight of the pole passes through one rib,

$$\sigma_{rib} = \frac{F}{A}$$

$$\sigma_{rib} = \frac{0.5(2715)}{(0.375)(7)}$$

$$\sigma_{rib} = 517\ psi$$

This is a very low stress, but FEA is needed to get the full picture of stress in this loading scenario.

A.5.4 Fork loading case

The maximum load on the forks is specified in the concentrated fork loading case. The only dimension that can be changed is the fork width, since the forks fit with the field pole geometry. The unchangeable dimensions are shown in the following figure:

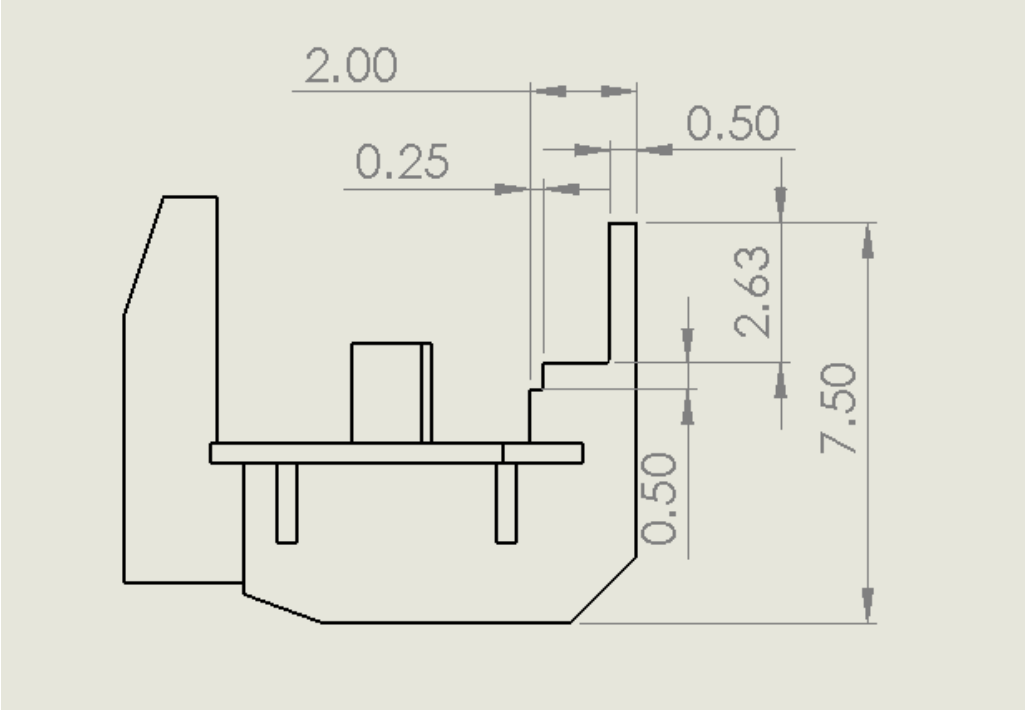

Figure 23: Bottom clamp tusk dimensions in inches.

To find the minimum allowable width of the tusks we follow a similar procedure as for the cross-section in bending. Each tusk sees 1/6th of the field pole weight and we assume all the weight is applied to the thin portion of the tusk. This tusk can fail in either bending or shear so we calculate the minimum width for each failure mode and choose the larger size.

For bending, the required section modulus can be found using Equation 8, where L is the length of the thin portion of the tusk:

$$Z_{min} = \frac{L^2 P}{3\sigma_{all}}$$

$$Z_{min} = 0..0124\ in^3$$

Since

$$Z = \frac{bh^2}{6}$$

With h = ½",

$$b_{min} = 0.54\ in$$

The tusks can also fail due to shear. The shear strength of AISI 4130 is 11 ksi. Equation 9 gives the maximum shear stress for a beam. For a rectangular beam, the equation becomes

$$\tau_{max} = \frac{3V}{2A}$$

Where A is the cross-sectional area. Setting A = bh, the minimum allowed width becomes

$$b_{min} = \frac{3W}{2h\tau_{all}}$$

$$b_{min} = 0.37\ in$$

Since the minimum required width to resist bending is larger we will base our design that value, rounding up to 5/8" for ease of manufacturability. These dimensions yield a section modulus of 0.0326 in^3 and a stress of 18.3 ksi.

A.5.5 Summary of Results

The calculated stresses are tabulated below:

Table XIII: SUMMARY OF CALCULATED STRESS IN MATERIAL REMOVAL DESIGN

Case #	Component	σ_{max} (ksi)	Yield Criterion
1a	Middle Plate (worst case) stiffeners	3.23	1/20
1b	Middle Plate (worst case) pi-beam	2.88	1/25
2	Middle Plate (hole)	20.4	1/4
3	Rounded Edges	0.517	1/135
4	Horizontal Forks	18.3	1/4

These results show that the stress is close to ideal in some areas but very small in others. This implies that there are geometries that are overdesigned, and that more cut outs at these points could yield even more weight savings.

A.6 Concept Design Multi Component

The final concept aims to break the lower clamp of the lifting device into 3 smaller pieces therefore making the device easier to handle. This will increase assembly time by adding 4 extra fasteners but greatly reduces the weight of any single lift. The concept is broken into 2 mounts which attach to the clamping rods of the lifting device and a plate attaching each mount, the field pole will sit on this plate. To verify the validity of this concept detailed hand calculations along with a preliminary CAD model and FEA will be provided in this section.

A.6.1 Detailed Hand Calculations

This section of the report gives a detailed overview of the simplified hand calculations done on concept 3. These calculations are done for the four loading scenarios the device may encounter in application.

A.6.1.1 Distributive load case

The stresses at each end of the plate in the multi component design, as shown in Figure 24, is represented by the equation below. For this calculation only the plate and plate supports were included in the section modulus while the any contribution from the forks was neglected.

$$\sigma_{ends} = \frac{W*l}{12*Z} = \frac{2715*15.876}{12*1.181} = 3041.4\ PSI$$

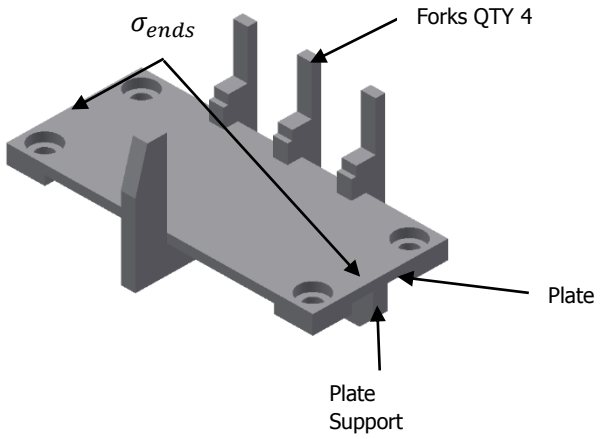

Figure 24: Location of center stress and end stress on plate of multi component concept

A.6.1.2 Concentrated hole case

The mounting plate that is connected between the connecting poles and the plate have 3 locations where it is secured with fasteners. From Figure 25 it is clear that that mounting hole 1 would have the largest stresses, as the full load is transferred through it. The stresses at this locations are represented by equation 4, as shown below.

$$\sigma_{max} = \frac{F}{A} = \frac{{}^{2715}/_{2}}{2*\pi*(1.125^2-.75^2)} = 307.3\ PSI$$

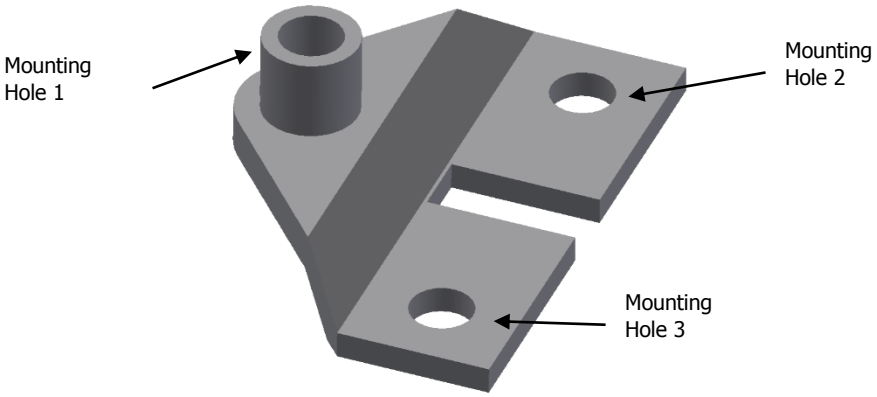

Figure 25: Location of high stress on component plate mounts

A.6.2.3 Concentrated round edge case

The third case of loading considered is when the lifting device is used to lower the field pole and all the weight is placed on plate support shown in Figure 24.

$$\sigma_{\text{norm}} = \frac{\text{F}}{\text{A}_{\text{min}}} = \frac{2715}{2*17.838} = 75.7\ PSI$$

A6.2.4 Fork loading case

The final loading condition is when the lifting device is being used to lay the field pole and all the weight is on the 3 common forks shown in Figure 24. The stress in the 3 common forks is outlined below.

$$\sigma_{\text{norm max}} = \frac{L*\text{W}}{3*\text{Z}} = \frac{2.625*450}{3*0.03125} = 12600\ \text{PSI}$$

A.6.2 Summary of Results

A summary of all the calculated stresses are listed below in Table XIV, showing the concept is viable can further be refined at a later stage. According to the calculations above the design is feasible and can further be optimized, as the maximum stresses did not meet or exceed 1/3 yield strength.

Table XIV: SUMMARY OF CALCULATED STRESSES IN COMPONENT CONCEPT DESIGN

Case #	Component	σ_{max} (PSI)	Yield Criterion
1	Middle Plate (worst case)	3041.4	6/100
2	Middle Plate	307.3	6/1000
3	Rounded Edges	75.7	1.5/1000
4	Horizontal Forks	12600	1/4
5	Middle Plate Combined	3348.7	6/100

A.7 Fracture Analysis

Given the relatively thin steel plate design used, fractures could become a problem. Because of this we used Paris and Tada's "The Stress Analysis of Cracks Handbook" to obtain crack geometries that would be most likely to cause failure. The three crack geometries considered are depicted in Figure 26 and Figure 27.

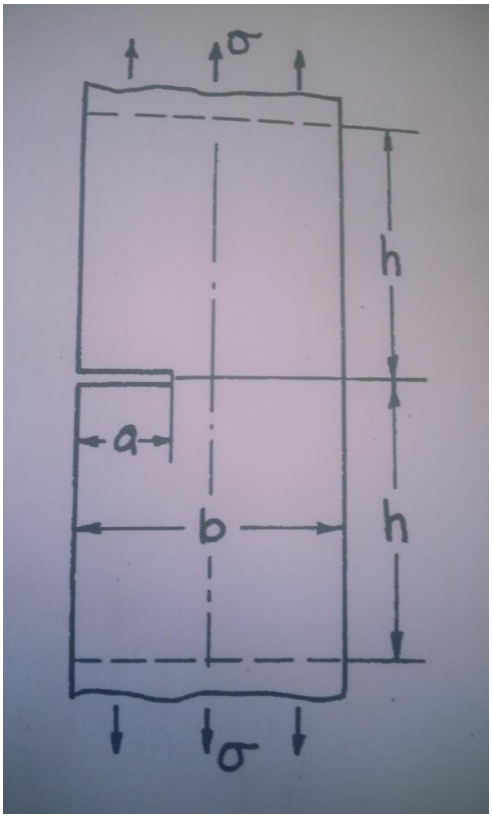

Figure 26: Tension crack geometry

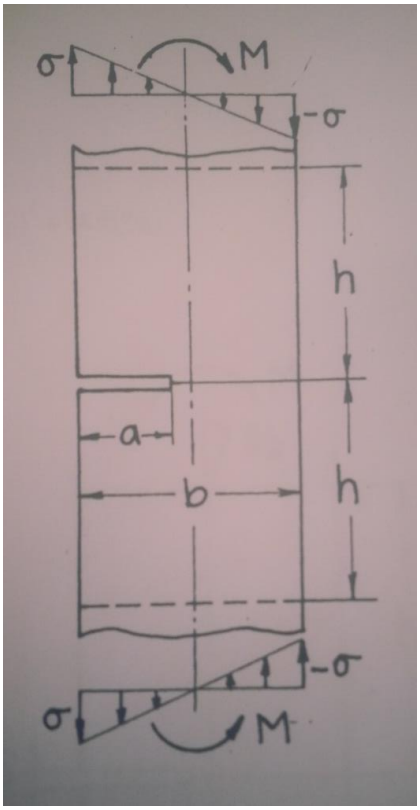

Figure 27: Bending crack geometry

These geometries were chosen because of the loads being applied to the plate will cause bending stress distribution acting along the length of the design. Because of the stiffeners and the resulting T-beam cross section therein, the neutral axis will be moved towards the top of the design and will experience both a bending load as well as an axial load as seen in Figure 28. When considering the location of potential fracture the area that experiences the maximum amount of tensile stress is inspected, in this case it will be at the bottom of the stiffeners.

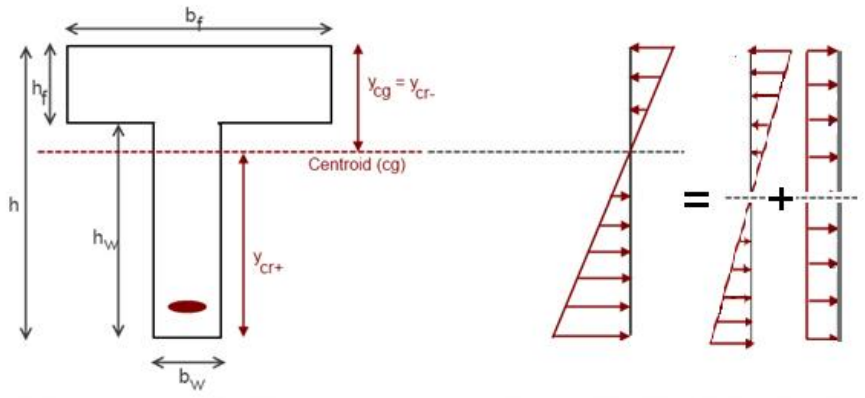

Figure 28: T-beam bending distribution

Assuming a crack forms on the bottom of the stiffeners and a 2D slice where the crack starts, we can see from Figure 29 that the cracks geometry closely resembles that in Figure 26 & Figure 27. This is assuming that the crack is very small and has propagated linearly in just one plane. Knowing the location of the crack and the orientation of the loads we can predict the loading scheme the slice of material located at the crack.

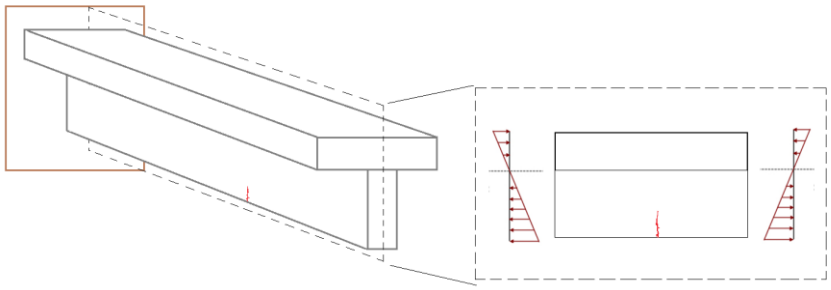

Figure 29: Stiffener simplification and crack positioning

Looking again at the 2D slice at the crack it can be seen that this load applies a both an axial stress, and bending stress as seen in Figure 29 and by the principal of superposition we can decompose this stress distribution into a bending stress and an axial stress Figure 30.

Figure 30: Crack loading scenario

These two load distributions contribute to mode 1 fracture and thus by the principle of superposition they can be calculated separately and then added together.

At this point it must be noted that all the following equations were presented in metric units and as such all values will be converted to metric for this analysis.

From Figure 30 and using Paris and Tada's "The Stress Analysis of Cracks Handbook", the stress intensity factor can be found using Equation 9. Where K_1 is the stress intensity factor, σ is the stress, a is the crack length and b is the thickness, and F(a/b) is a function of a and b.

$$K_1 = \sigma\sqrt{\pi a} \cdot F\left(\frac{a}{b}\right) \qquad \text{Equation 9}$$

The function F(a/b) is defined using a multitude of different methods including; Boundary Collocation Method (Gross, 1964), Mapping Function Method (Bowie 1965), Green's Function Method (Emery 1969, 1972), Weight Function Method (Bueckner, 1970, 1971), Asymptotic Approximation (Benthem, 1972), and Finite Element Method (Yamamoto, 1972). Using Least squares fitting (Gross 1964; Brown 1966) we can define the F(a/b) function using Equation 10. The accuracy of this method is 0.5% for an a/b less than or equal to 0.6.

$$F\left(\frac{a}{b}\right) = 1.122 - 0.231\left(\frac{a}{b}\right) + 10.550\left(\frac{a}{b}\right)^2 - 21.710\left(\frac{a}{b}\right)^3 + 30.382\left(\frac{a}{b}\right)^4 \qquad \text{Equation 10}$$

Alternatively the F(a/b) function can be found using Tada's work from 1973 resulting in Equation 11. This method has an accuracy of better than 1% for an a/b of less than 0.2 and 0.5% for an a/b greater than or equal to 0.2.

$$F\left(\frac{a}{b}\right) = 0.265\left(1-\frac{a}{b}\right)^4 + \frac{0.857 + 0.265\left(\frac{a}{b}\right)}{\left(1-\frac{a}{b}\right)^{\frac{3}{2}}} \qquad \text{Equation 11}$$

Finally there is Equation 12 also obtained from Tada's 1973 work, this results in an accuracy of better than 0.5% for any a/b. Because this method gives us such reliable results and for any a/b it is the method used for this case of fracture analysis.

$$F\left(\frac{a}{b}\right) = \sqrt{\frac{2b}{\pi a}\tan\left(\frac{\pi a}{2b}\right)} \cdot \frac{0.752 + 2.02\frac{a}{b} + 0.37\left(1-\sin\left(\frac{\pi a}{2b}\right)\right)^3}{\cos\left(\frac{\pi a}{2b}\right)} \qquad \text{Equation 12}$$

By substituting K_1 with K_{1c} in Equation 9it is possible to calculate the maximum allowable stress the crack can withstand at a given length. These values are plotted in Figure 31.

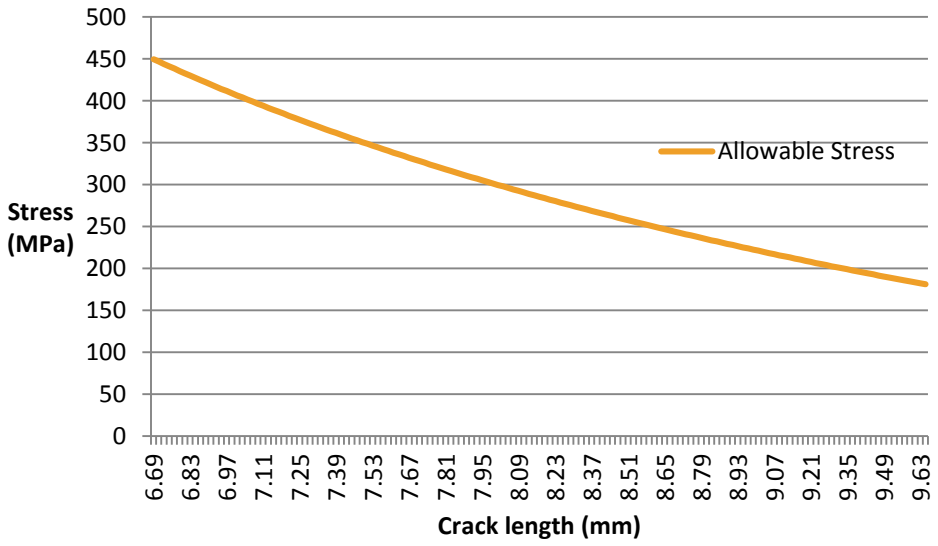

Figure 31: Allowable stress for tensional loading

Using our design constraints and material properties of CSA G40.21 70w grade steel it is know that the maximum Von Mises stress experienced by the design is 83MPa in the membrane found through the

finite element analysis performed in Section 6. The maximum stress possibly applied to the design is not the maximum stress applied to the crack but if we use it as such then we err on the side of caution as the stress should still be relatively close to this value. Using this maximum stress and Equation 9 it is possible to calculate the stress intensity factors at varying crack length. The stress intensity factors are plotted against the crack length and the critical fracture toughness of the material in Figure 32.

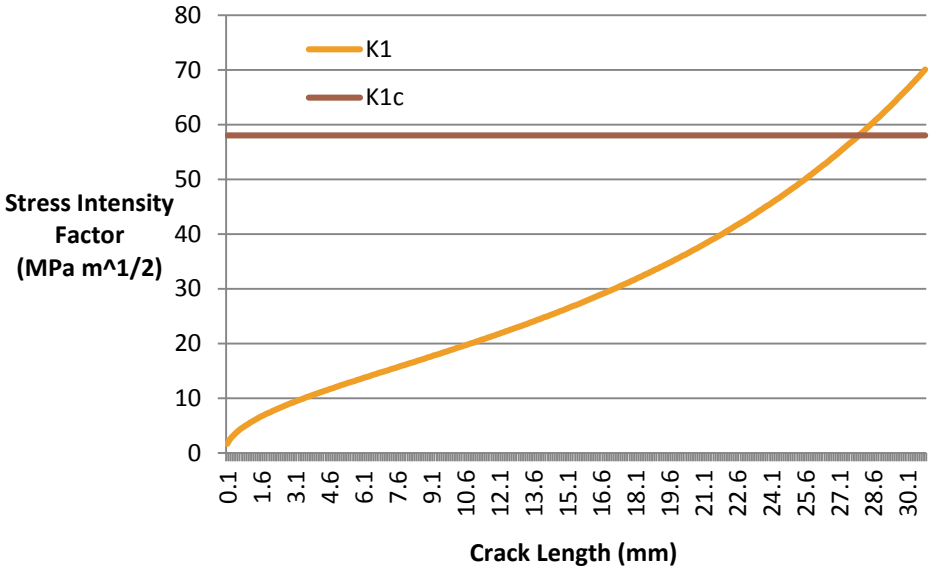

Figure 32: Stress intensity for varying crack length for tensional loading

The other loading orientation seen in Figure 27 is also included in Paris and Tada's "The Stress Analysis of Cracks Handbook". The base equation is the same as the other case but σ is defined by Equation 13.

$$\sigma = \frac{6M}{b^2} \qquad \text{Equation 13}$$

The F(a/b) is also obtain using different equations. The first method is derived using least squares fitting (Brown, 1966) and gives use Equation 14. This equation has an accuracy of 0.2% for an a/b less than or equal to 0.6.

$$F\left(\frac{a}{b}\right) = 1.122 - 1.40\left(\frac{a}{b}\right) + 7.33\left(\frac{a}{b}\right)^2 - 13.08\left(\frac{a}{b}\right)^3 + 14.0\left(\frac{a}{b}\right)^4 \qquad \text{Equation 14}$$

The other equation given for F(a/b) was found using Tada's 1973 work and is depicted in Equation 15This results in an accuracy of 0.5% for any a/b. Because of the accuracy and ability to be used for any a/b Tada's method was used for the fracture analysis.

$$F\left(\frac{a}{b}\right) = \sqrt{\frac{2b}{\pi a}\tan\left(\frac{\pi a}{2b}\right)} \cdot \frac{0.923 + 0.199\left(1 - \sin\left(\frac{\pi a}{2b}\right)\right)^4}{\cos\left(\frac{\pi a}{2b}\right)} \qquad \text{Equation 15}$$

Using the same method as with load case 1 the K_1 was replaced with K_{1c} and the total allowable stress was plotted against crack length in Figure 33.

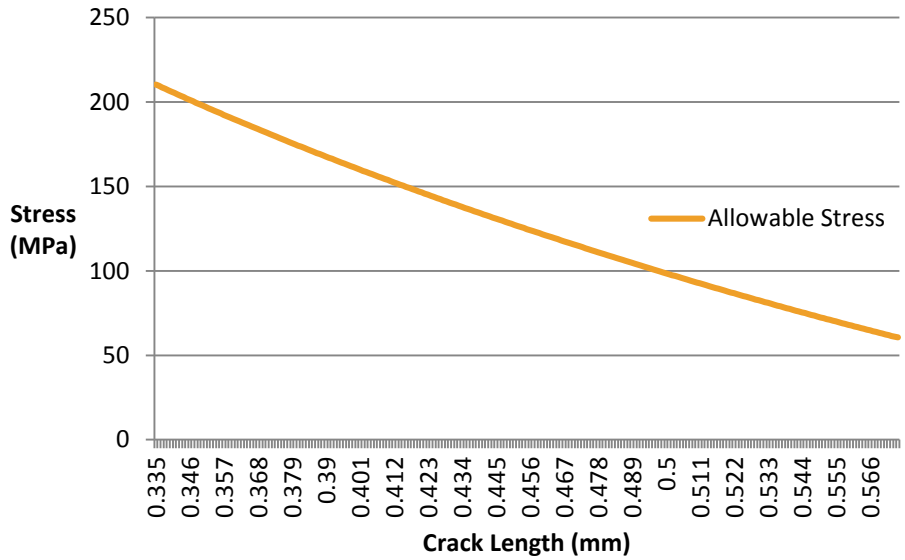

Figure 33: allowable stress for bending loading

Again if we assume that this load type sees the maximum possible bending load applied to the model, while not 100% accurate should give us a reasonable conclusion as well as err on the side of caution. Thus using this maximum stress of 80MPa and Equation 13 it is possible to calculate the stress intensity factors at varying crack length. The stress intensity factors are plotted against the crack length in Figure 34.

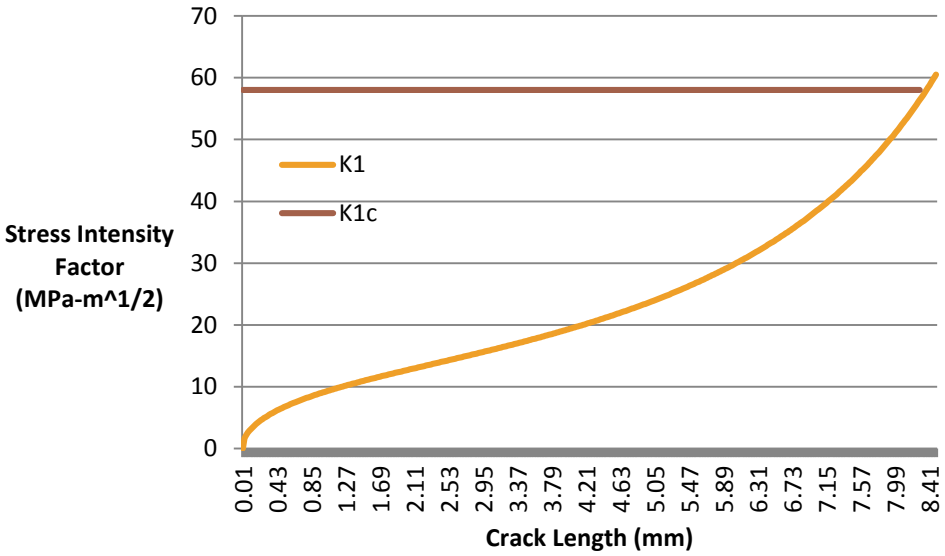

Figure 34: Stress intensity for varying crack length for bending loading

By adding the results from both loading orientations the stress intensity factor for mode 1 fracture can be found for this fracture case, seen in Figure 35.

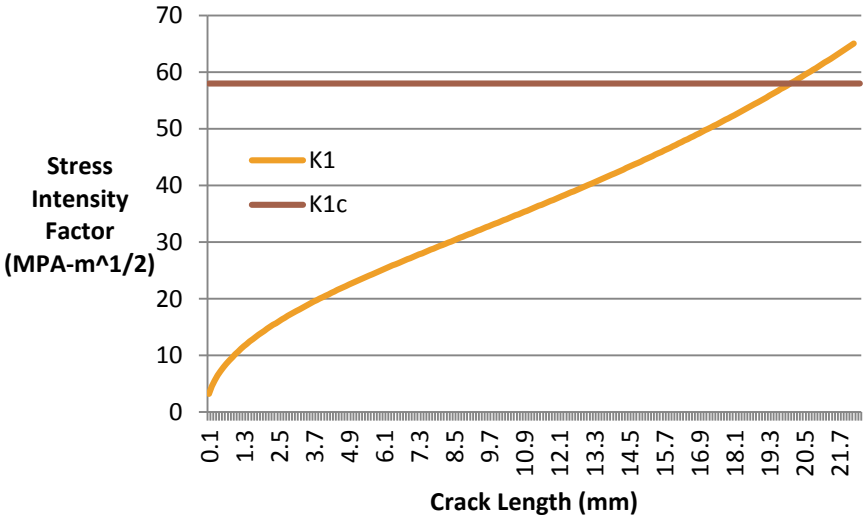

Figure 35: Stress intensity for varying crack length for tensional and bending loading

It can be seen that from this analysis the critical crack length found in the stiffeners is 20mm, propagating directly into the bottom of the stiffener. This critical crack length is substantially larger than the minimum visible crack length of 1mm.

The same analysis is performed for the teeth as analyzed previously. The teeth geometry will see only the bending load seen in Figure 27 and as such the 155mpa bending stress is used as the stress, σ. Following the same methodology as before the stress intensity is graphed against crack length and fracture toughness of the material and presented in Figure 36.

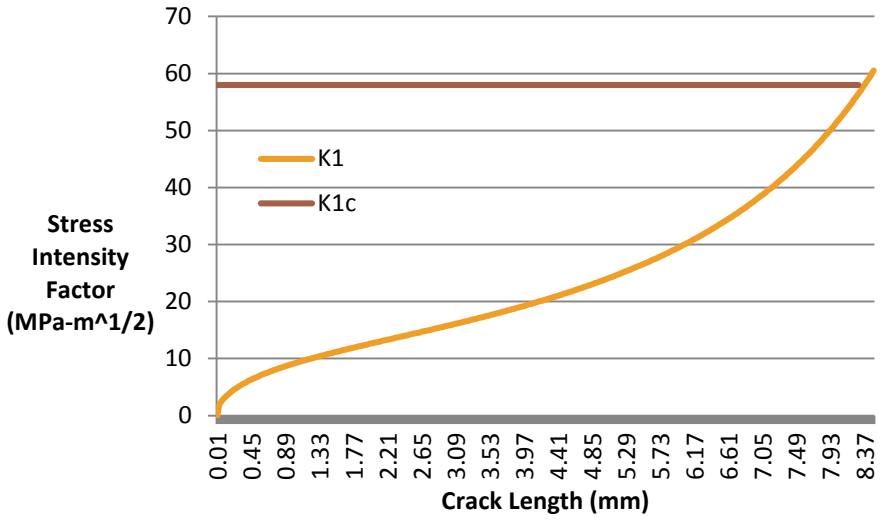

Figure 36: Stress intensity for varying crack length for tooth

It can be seen from Figure 36 that the critical crack length in the teeth is 8mm which exceeds our minimum visible crack length of 1mm.

A.8 Works Cited

[1] L. MatWeb, "Low Carbon Steel," MatWeb, [Online]. Available: http://www.matweb.com/search/DataSheet.aspx?MatGUID=aa1c987a696e42bd95ddad57e5f3e1c7&ckck=1. [Accessed 20 October 2015].

[2] "AISI 1025," 31 January 2003. [Online]. Available: http://app.knovel.com/web/view/pdf/show.v/rcid:kpMMPDSMM1/cid:kt003INPK1/viewerType:pdf/root_slug:metallic-materials-properties-3/url_slug:aisi-1025?cid=kt003INPK1&b-toc-cid=kpMMPDSMM1&b-toc-root-slug=metallic-materials-properties-3&b-toc-url-slug=aisi-10. [Accessed 20 October 2015].

[3] Dassault Systems, "SOLIDWORKS," 2015.

[4] MatWeb, "Medium Carob Steel," MatWeb LLC., [Online]. Available: http://www.matweb.com/search/DataSheet.aspx?MatGUID=a2fe6ff24cf44bf1bdebf35b1b2b6259. [Accessed 20 October 2015].

[5] MatWeb, "AISI 4340 Steel, normalized, 100 mm (4 in.) round," MatWeb LLC., [Online]. Available: http://asm.matweb.com/search/SpecificMaterial.asp?bassnum=M434AE. [Accessed 20 October 2015].

[6] MatWeb, "6000 Series Aluminum Alloy," MatWeb LLC., [Online]. Available: http://www.matweb.com/search/DataSheet.aspx?MatGUID=b92d6bd5c3c24f58bcbe76c46ff0f496. [Accessed 20 October 2015].

[7] "3000 Series Wrought Alloys," 31 January 2003. [Online]. Available: http://app.knovel.com/web/view/pdf/show.v/rcid:kpMMPDSMM1/cid:kt003INR1P/viewerType:pdf/root_slug:metallic-materials-properties-3/url_slug:3000-series-wrought-alloys?cid=kt003INR1P&&issue_id=kt003INPI2&b-toc-cid=kpMMPDSMM1&b-toc-root-slug=metallic-materia. [Accessed 20 October 2015].

[8] MatWeb, "7000 Series Aluminum Alloy," MatWeb LLC., [Online]. Available: http://www.matweb.com/search/DataSheet.aspx?MatGUID=ab9706916818406b80c22b7f39db0c78. [Accessed 20 October 2015].

[9] "Ti-6Al-2Sn-4Zr-2Mo," 31 January 2003. [Online]. Available: http://app.knovel.com/web/view/pdf/show.v/rcid:kpMMPDSMM1/cid:kt003INT3L/viewerType:pdf/root_slug:metallic-materials-properties-3/url_slug:ti-6al-2sn-4zr-2mo?cid=kt003INT3L&&issue_id=kt003INSY3&b-toc-cid=kpMMPDSMM1&b-toc-root-slug=metallic-materials-prope. [Accessed 20 October 2015].

[10] "Ti-13V-11Cr-3Al," 31 January 2003. [Online]. Available: http://app.knovel.com/web/view/pdf/show.v/rcid:kpMMPDSMM1/cid:kt003INT91/viewerType:pdf/root_slug:metallic-materials-properties-3/url_slug:ti-13v-11cr-3al?cid=kt003INT91&&issue_id=kt003INT03&b-toc-cid=kpMMPDSMM1&b-toc-root-slug=metallic-materials-properti. [Accessed 20 October 2015].

[11] MatWeb, "Titanium Ti-6Al-2Sn-4Zr-2Mo (Ti-6-2-4-2), Sheet," MatWeb LLC., [Online]. Available: http://asm.matweb.com/search/SpecificMaterial.asp?bassnum=MTA642. [Accessed 20 October 2015].

[12] Solid Creativity, "TRIZ 40," [Online]. Available: http://www.triz40.com/TRIZ_GB.php. [Accessed 10 October 2015].

[13] R. B. A. S. Warren Young, Roark's Formulas for Stress and Strain, McGraw Hill Publication, 2011.

[14] B. Gryba, "The Design and Analysis of a Fibre Reinforced Polymer Wheel Assembly for use in an FSAE Vehicle," Mech 4162, Winnipeg.

[15] W. C. Young and R. G. Budynas, Roark's Formulas for Stress and Strain, New York: McGraw-Hill, 2002.

[16] M. Tuttle, Structural Analysis of Polymeric Composite Materials, New York: Marcel Dekker, 2004.

[17] R. L. Mott, Machine Elements in Mechanical Design Fourth Edition, Colmbus: Pearson Prentice hall, 2004.

[18] MatWeb, "Alpha/Near Alphat Titanium Alloy," MatWeb LLC., [Online]. Available: http://www.matweb.com/search/DataSheet.aspx?MatGUID=0626279b487341b386352fae80ba0574. [Accessed 20 October 2015].

[19] V. Campbell, "Risk Assessment and Mitigation: Failure Modes and Effect Analysis (FMEA)," Winnipeg, 2015.

[20] J. Bunkowsky, "Rotor Pole Removal Powerpoint," unpublished.

[21] CSA, "Welded Steel Construction (Metal Arc Welding)," 2008.

[22] Manitoba Hydro, "Weld Design Using FEA," Unpublished.

[23] Rubber Cal inc., "Skirtboard - SBR Rubber - 70A," 2014. [Online]. Available: http://www.rubbercal.com/industrial-rubber/rubber-shock-absorbers/skirtboard-sbr-rubber-70a.html. [Accessed 15 November 2015].

[24] ANSYS, "Release Documentation for ANSYS," 1 September 2015. [Online]. Available: http://www.ansys.com/Products/Simulation+Technology/Fluid+Dynamics/Specialized+Products/ANSYS+Polyflow/Features/Online+Help+&+Documentation. [Accessed 12 Octorber 2015].

[25] Manitoba Hydro, "Producing Electricity," [Online]. Available: https://www.hydro.mb.ca/corporate/facilities/gi_producing_electricity.shtml. [Accessed 18 September 2015].

[26] Manitoba Hydro, "Powerhouse Rotor Pole Lifting Device As-Built Asembly & Details, 1-00112-DE-76730-0003," unpublished.

[27] Manitoba Hydro, "Power House Rotor Pole Lifting/ Handle, 1-00112-DC-76730-0004," unpublished.

[28] Manitoba Hydro, "Mechnical Stress Analysis Standard Revsion 00," December 2, 2013. Unpublished.

[29] Hexcel, "Honeycomb Sandwich Design Technology," London, 2000.

[30] ESAB Welding and Cutting Products, "ESAB Waterjet Knowledge centre," 6 August 2013. [Online]. Available: http://www.esabna.com/us/en/education/blog/how-much-does-waterjet-cutting-cost.cfm. [Accessed 15 November 2015].

[31] "CSA G41.21," Portland Bold & Mfg. Co., 2015. [Online]. Available: http://www.portlandbolt.com/technical/specifications/csa-g40-21/. [Accessed 11 November 2015].

[32] Manitoba Hydro, "Cross-Sectional View General Arragement, 1-00112-DE-40000-0004".

[33] ASME, "Below-The-Hook Lifting Device Design," 2014.

[34] ESAB Welding and Cutting Products, Basic Welding Filler Metal Technology, 2000.

[35] "AISI 4330 Alloy Steel," AZO Materials, [Online]. Available: http://www.azom.com/article.aspx?ArticleID=6670 . [Accessed 20 October 2015].

[36] 3M, "3M Neoprene High Performance Rubber & Gasket Adhesives 1300, 1300L," March 2015. [Online]. Available: http://multimedia.3m.com/mws/media/66251O/neoprene-hi-perf-rubber-gasket-adh-1300-1300l.pdf. [Accessed 15 November 2015].

A.9 Technical Drawings

All technical drawings are meant for A0 size paper, but have been compressed for this report.

BILL OF MATERIALS

ITEM	QTY	DESCRIPTION	MATERIAL	SPECIFICATION
1	2	Outside Teeth	Steel 70WT	CSA G40.21
2	1	Middle Tooth	Steel 70WT	CSA G40.21
3	4	Stiffiners	Steel 70WT	CSA G40.21
4	1	Lifting Plate	Steel 70WT	CSA G40.21
5	2	Cross Beams	Steel 70WT	CSA G40.21
6	2	Clamping Rod Alignment Tubes	Steel 70WT	CSA G40.21
7	1	Rubber Cushioning	NEOPRENE HIGH PERFORMANCE RUBBER	

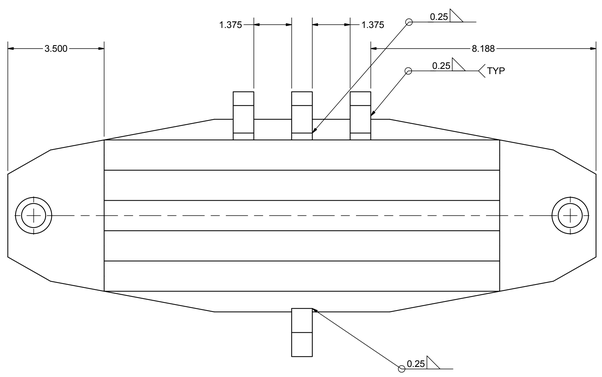

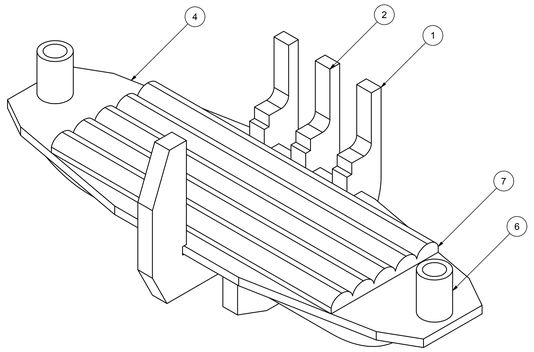

NOTE:

- REMOVE ALL SHARP EDGES
- PAINT STEEL PARTS YELLOW AS SPECIFIED BY MHS 217
- ATTACH RUBBER CUSHIONING WITH GASKET ADHESIVE 1300L OR EQUIVALENT

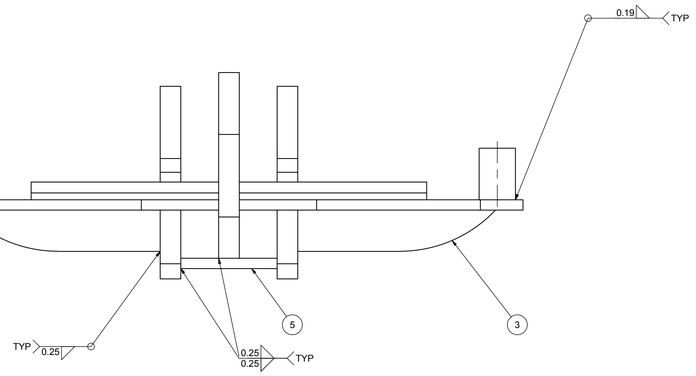

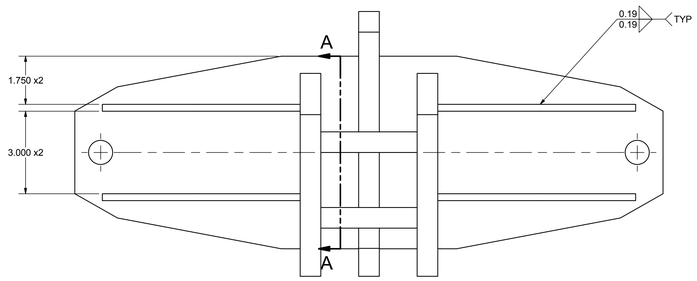

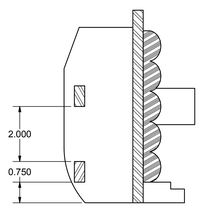

Detail A-A

UNLESS OTHERWISE SPECIFIED	REV.	DATE	DESCRIPTION	BY	CKD.	APP.
DIMENSIONS ARE IN INCHES TOLERANCES: FRACTIONAL ± 1/16 X DECIMAL ± 0.03 XX DECIMAL ± 0.03 XXX DECIMAL ± 0.03 ANGLES/DEG ± 2 BREAK ALL SHARP EDGES 0.030 MAX FINISH 125						

Manitoba Hydro

AUTHENTICATION FOR CURRENT REVISION

DRAWN: TSS	DRAWING CHECK:	MANAGER:
DESIGNED:	DESIGN CHECK:	DATE:

GRAND RAPIDS

BOTTOM CLAMP WELDMENT

DRAWING NUMBER	SHEET	REVISION
	1	

SCALE: 1/2

SIZE: A0

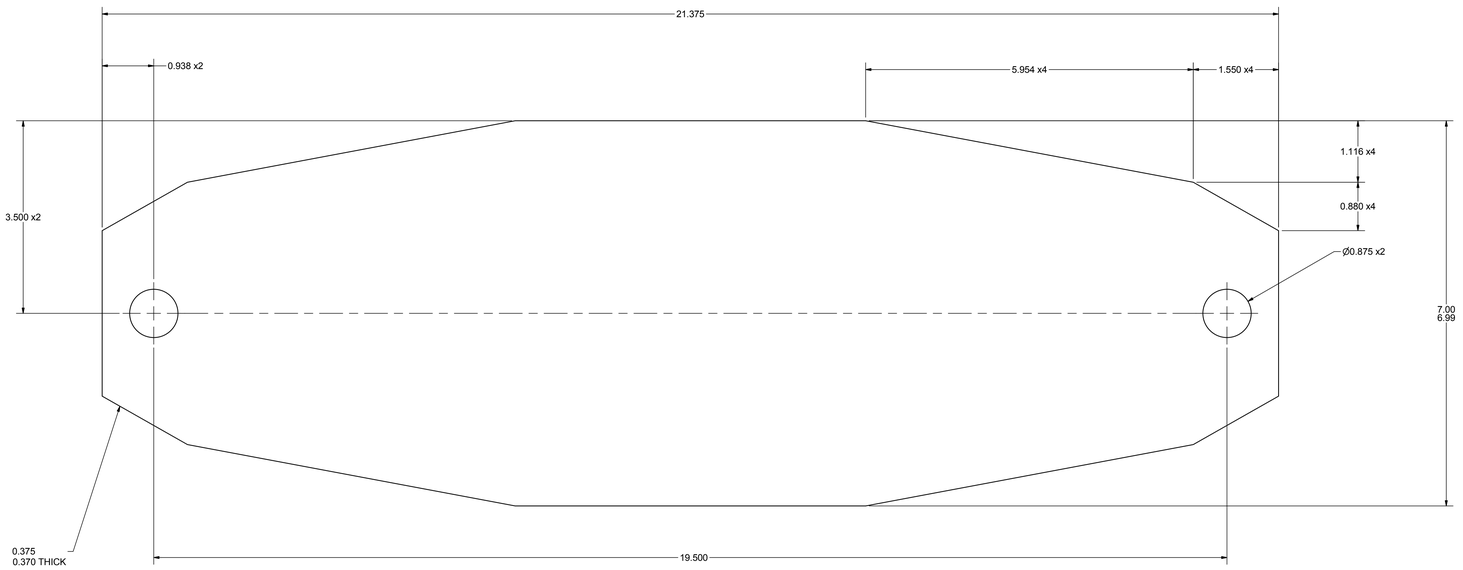

LIFTING PLATE

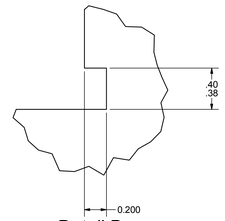

Detail B

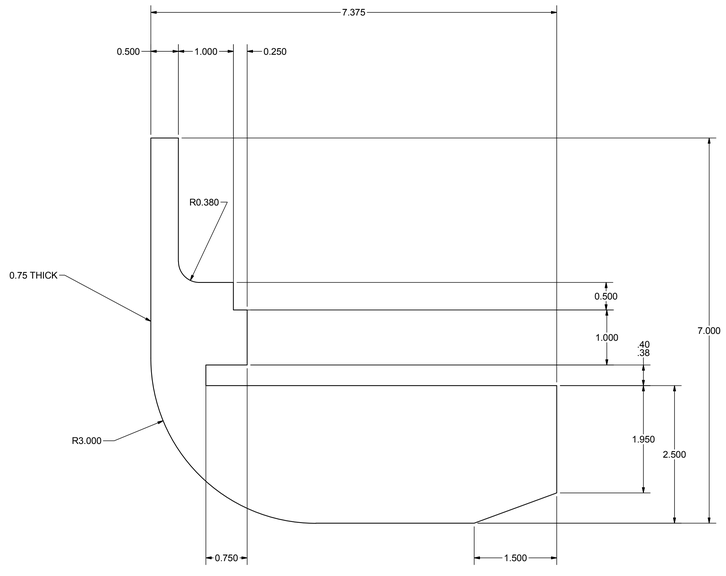

OUTSIDE TEETH

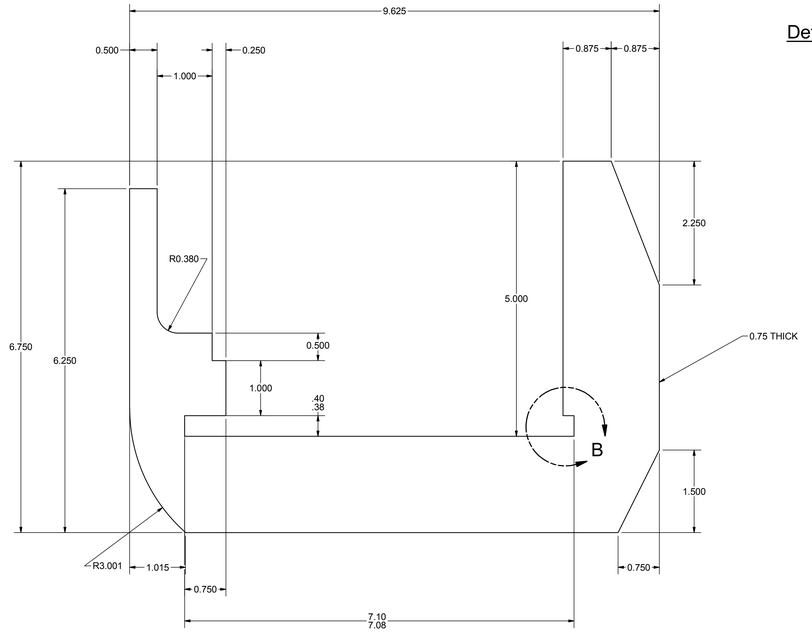

MIDDLE TOOTH

UNLESS OTHERWISE SPECIFIED	REV.	DATE	DESCRIPTION	BY	CKD. APP.
DIMENSIONS ARE IN INCHES TOLERANCES: FRACTIONAL ± 1/16 X DECIMAL ± 0.03 XX DECIMAL ± 0.03 XXX DECIMAL ± 0.03 ANGLES/DEG ± 2	Manitoba Hydro	DRAWN: TSS	DRAWING CHECK:	MANAGER:	
		DESIGNED:	DESIGN CHECK:	DATE:	
		GRAND RAPIDS			
BREAK ALL SHARP EDGES 0.030 MAX	AUTHENTICATION FOR CURRENT REVISION	BOTTOM CLAMP WELDMENT			
FINISH 125		DRAWING NUMBER		SHEET 2	REVISION
SCALE: 1:1					

SIZE: A0

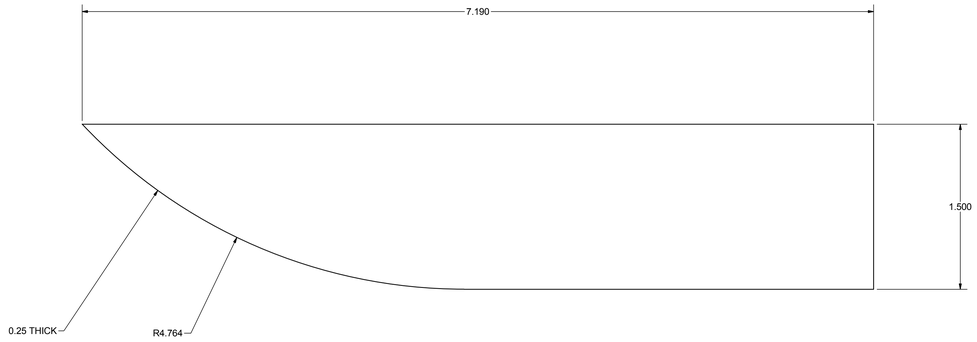

STIFFENER

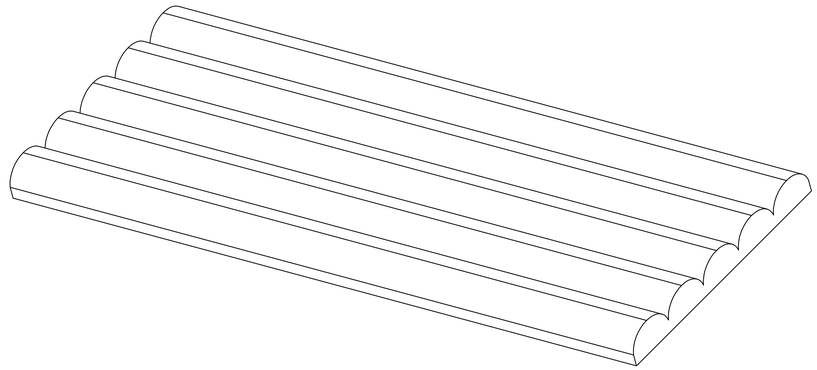

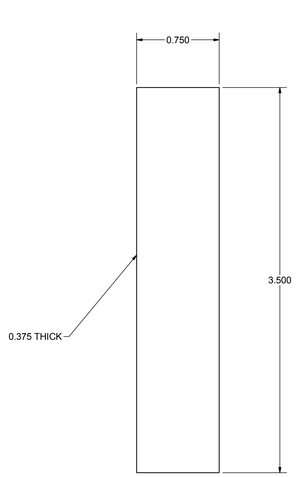

CROSS BEAM

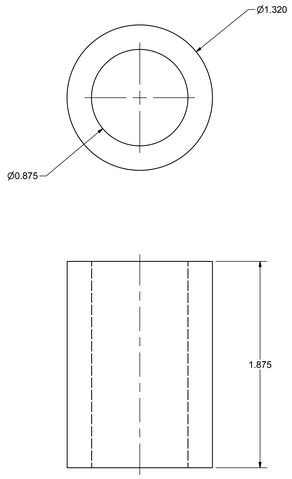

CLAMPING ROD
ALIGNMENT TUBE

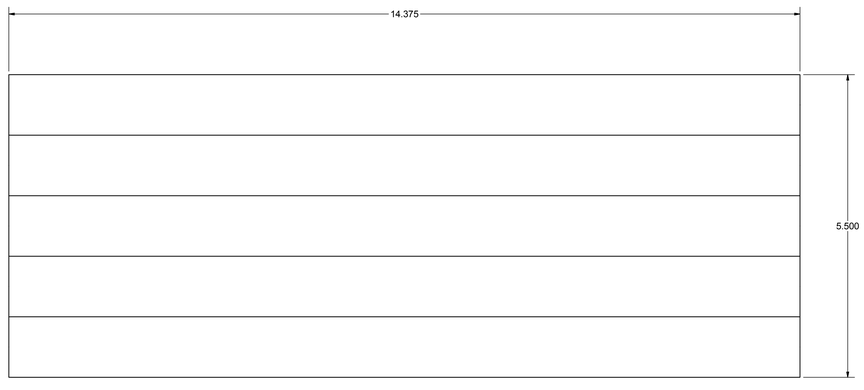

RUBBER CUSHIONING

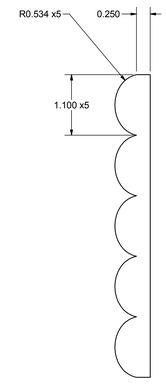

UNLESS OTHERWISE SPECIFIED	REV.	DATE	DESCRIPTION	BY	CKD.	APP.
DIMENSIONS ARE IN INCHES TOLERANCES: FRACTIONAL ± 1/16 X DECIMAL ± 0.03 XX DECIMAL ± 0.03 XXX DECIMAL ± 0.03 ANGLES/DEG ± 2						
BREAK ALL SHARP EDGES 0.030 MAX						
FINISH 125						

Manitoba Hydro

AUTHENTICATION FOR CURRENT REVISION

DRAWN: TSS	DRAWING CHECK:	MANAGER:
DESIGNED:	DESIGN CHECK:	DATE:

GRAND RAPIDS

BOTTOM CLAMP WELDMENT

SCALE: 1:1	DRAWING NUMBER	SHEET	REVISION
		3	

SIZE: A0